KU LEUVEN

FACULTEIT BIO-INGENIEURSWETENSCHAPPEN

Modelling and controlling blood flow by active cooling of the fingers to prevent nail toxicity

Modelleren en controleren van bloeddoorstroming door actieve koeling van de vingers met als doel het voorkomen van nageltoxiciteit

Promotoren:
Prof. Jean-Marie Aerts
Departement Biosystemen
Afdeling M3-BIORES: Meet, Modelleer &Manage Bioresponsies

Dr. ir. Guido De Bruyne

Masterproef voorgedragen
tot het behalen van het diploma van
Master of science in de bio-ingenieurswetenschappen:
biosysteemtechniek

Maarten D'Haene

juni 2015

Foreword

First, I would like to thank my supervisors, Prof. Jean-Marie Aerts, Prof. Guido De Bruyne and Dr. Ali Youssef, for giving me the opportunity to perform this research work and especially for their support and guidance during this last year of my education. I very much appreciated your input, advice, stimulating discussions, critical questions and feedback.

I am also very grateful to the technicians of the University of Antwerp for their technical support and for repairing the experimental device.

I also want to take this opportunity to gratefully acknowledge the 11 test persons who participated voluntarily on the experiments.

Finally, also a big “thank you” to all my friends and family for their continuous support, the unforgettable moments of relaxation, exciting football matches, and fantastic time we have had together!

Executive summary/Samenvatting

Chemotherapie-geïnduceerde nageltoxiciteit is een wijdverspreid fenomeen. De meest ernstige vorm van nageltoxiciteit is onycholyse, wat de complete afscheuring van de nagelplaat van het nagelbed is. Nageltoxiciteit is vooral gelinkt aan behandelingen die gebruik maken van taxanen, zoals bijvoorbeeld bij de behandeling van borstkanker. Het koelen van de handen en voeten van de patiënt tijdens deze behandelingen reduceert tijdelijk de bloeddoorstroming doorheen de vingers en vermindert de hoeveelheid chemische stoffen die het nagelbed bereiken. Deze studie tracht de dynamische respons van de huidtemperatuur van de vingers op gecontrolleerde lokale koeling van de vingers te modelleren. The uiteindelijke doel is het ontwikkelen van een 'real-time model-based control system' die in staat is de bloeddoorstroming doorheen de vingers van de patient te controleren. De ontwikkelde modellen voor huidtemperatuur en bloeddoorstroming zijn gebaseerd op data verkregen uit 65 experimenten uitgevoerd op elf vrouwen tussen 35 en 55 jaar. Tijdens deze experimenten werd een toestel gebruikt dat in staat is de vingers actief en lokaal te koelen. Dit 'onycholyse-toestel' werd ontwikkeld aan de Universiteit Antwerpen.

Voor bijna al de testpersonen was een tweede-orde model ($R^2 = 0.9120 \pm 0.1178$) het meest geschikt om de huidtemperatuur te modelleren. Het ontwikkelde tweede-orde model kon worden gevalideerd in (bijna) alle gevallen voor de wijsvinger door parameter-betrouwbaarheidsintervallen op te stellen, de polen in het complexe z-vlak te bepalen en de auto- en crosscorrelatiefuncties af te leiden. Op basis van de verkregen modellen werd dan een 'Proportional-Integral-Plus (PIP-)' controller ontwikkeld. Deze controller werd getest voor een wijde parameter-range van tweede orde-modellen met 2 b-parameters (b1 en b2) en een time-delay van 1. De controller was in staat de gewenste respons nauwkeurig te volgen voor alle geteste modellen, al was de controller enkel stabiel voor een beperkte range van b2-parameters (=limiterende factor), nl. $-0.1518 \leq b1 \leq -0.0394$. Dit resultaat illustreert de noodzaak van on-line bepaling van de parameters en de real-time retuning van de controller.

Verder werd in deze studie de model parameters van de ontwikkelde modellen vergeleken met elkaar en met model parameters die werden bepaald uit data van gelijkaardige experimenten met Elasto-Gel® frozen gloves, welke nu worden gebruikt ter preventie van nageltoxiciteit, in plaats van het onycholyse-toestel. De belangrijkste resultaten hiervan zijn dat er een significant verschil is tussen de a-parameters van dezelfde vingers van verschillende personen en dat de a-parameters van de handschoen-modellen globaal gezien significant verschillen van de a-parameters van het onycholyse toestel.

Tenslotte werd een mechanistisch model ontwikkeld dat, op basis van ‘a priori’ kennis van het systeem, het verloop van de huidtemperatuur aan de vingertip tijdens koeling modelleert. Dit model bevestigt de hypothese dat initieel de temperatuur van de vingertip daalt en vasoconstrictie optreedt. Na verloop van tijd treedt ‘Cold-Induced VasoDilation’ op. Dit gaat vrijwel onmiddelijk gepaard met een stijging van de vingertip-temperatuur. Ook werd een mechanistisch model van de opwarming door conductie en convectie van de Elasto-Gel® frozen glove opgesteld. Hier werd uit bepaald dat conductie langs de tafel initieel de voornaamste reden van warmteverlies is.

List of abbreviations and symbols used

a	Radius blood vessel	m
A	Area	m^2
ACF	Auto-correlation function	
AVA	Arterio-venous anastomoses	
c	Heat capacity	J/kg °C
CCF	Cross-correlation function	
CFD	Computational Fluid Dynamics	
CIA	Chemotherapy-induced alopecia	
CITD	Complex, Individual, Time variant, Dynamic	
CIVD	Cold-induced vasodilation	
c_p	Specific heat	J/kg K
De	Dean number	
g	Acceleration due to gravity	m/s^2
h	Heat transfer coefficient	W/m^2 °C
H_0	null-hypothesis	
k	Thermal conductivity	W/m °C
L	Characteristic length	m
LASCA	Laser speckle contrast analysis	
PET	Positron Emission Tomography	
MRI, PC-MRI	Magnetic Resonance Imaging; Phase-contrast Magnetic Resonance Imaging	
Nu	Nusselt number	-
P	Pressure	Pa

Pr	Prandtl number	-
Q	Volumetric heat generation	W/m^3
q	Heat Flux	W/m^2
r, R	Radius	m
Ra	Rayleigh number	-
Re	Reynolds number	-
R_g	Universal gas constant	8,314 J/mol.K
T	Temperature	K
t	Time	s
TF	Transfer Function	
u, v	velocity	m/s
α	Thermal diffusivity	m^2/s
β	Coefficient of thermal expansion	1/K
μ	Dynamic viscosity	Pa.s (kg/m.s)
	Kinematic viscosity	m^2/s
ρ	Density	kg/m^3
ΔP	Pressure difference	Pa
ΔT	Temperature gradient	K

Table of Contents

I. Foreword I

II. Executive summary/Samenvatting II

III. List of abbreviations and symbols used IV

IV. Table of Contents VI

V. Context and aims 1

1. Literature review 5

1.1. Introduction 5

1.2. Cytotoxic chemotherapy and its adverse side effects 6

1.3. Chemotherapy-induced nail toxicity 12

1.4. Cryotherapy 18

1.5. Blood flow measurements 28

1.6 modelling and controlling of biosystems 30

2. Materials and Methods 33

2.1.Introduction 33

2.2. Description of the active cooling system 33

2.3. Test subjects 35

2.4. Experimental conditions 35

3. Model identification and model-based controlling 39

3.1. Introduction 39

3.2. Theoretical basis and Methods used 39

3.3. Results and discussion 43

4. Statistical analysis 51

4.1. Introduction 51

4.2. Material and methods 51

4.3. Results and discussion 52

5. Mechanistic model 59

5.1. Introduction 59

5.2. Theoretical basis and methods used 59

5.3. Results and discussion 64

6. General Conclusion 75

Bibliography 79

APPENDIX A – Graphs 85

Popularised Summary 89

Context and aims

Globally, there were more than 14 million new cancer cases in 2012, of which lung, breast and colorectal cancer are the most commonly diagnosed cancers. In Belgium, as well as in Europe, breast cancer is by far the most common cancer for women, with an estimated 464.000 new cases diagnosed each year (28,8% of all cancers in women) in Europe (Ferlay et al., 2013). Especially in the Western European countries and in Northern Europe, the highest incidence rates were estimated, notably in Belgium (147 per 100.000), Denmark (143), France (137), Iceland and The Netherlands (131). In Flanders, 6094 breast cancer patients were reported by the Belgian Cancer Registry in 2012. (Kankerregister)

The main types of treatment for (breast) cancer are surgery, radiation therapy (both are local therapies), and chemotherapy, hormone therapy, immunotherapy and targeted therapy (systemic therapies). Cytotoxic chemotherapy is one of the most common treatments. It is used to treat all stages of breast cancer, before and after surgery or radiation therapy, and for advanced-stage/metastatic disease. However, none of the cytotoxic drugs has the ability to distinguish between normal cells and cancer cells, causing severe adverse side effects as well. A large number of chemotherapeutic agents can be responsible for the development of nail changes (colouring, brittleness,…) of which the most severe and painful change is onycholysis. Onycholysis is the detachment of (a portion of) the nail plate from the nail bed, often preceded or accompanied by severe pain. Minisini et al. (2003) reported that 44% of the patients treated with taxanes, an effective chemotherapeutic agent for the treatment of many cancers including breast, lung, ovarian, bladder and prostate cancer, developed nail toxicities.

To prevent nail toxicity and onycholysis, cryotherapy is often applied by the use of frozen gloves and socks (Elasto-Gel®), or ice baths. By cooling the extremities, local vasoconstriction occurs, resulting in a reduction of the blood flow towards the fingers (and toes). Hence, the drugs cannot reach the nail bed that easily. However, the currently applied techniques are uncomfortable, unpractical and often refused by the patients involved. Another important drawback of the cooling devices (ice bath or frozen gloves) is the fact that the temperature cannot be controlled and increases rapidly after putting on. There is no way to control or improve the applied temperature profiles to minimize the blood flow.

The problem is even more complicated since the localised cooling of the extremities temporarily decreases the blood flow through the fingers'/toes' blood vessels, but as a counter reaction to prevent cold-induced damages to the fingers/toes, cold induced vasodilation will occur. This will

result in a sudden increase of the blood flow through the fingers/toes and consequently an increase of the skin temperature of the fingers/toes. A cyclic pattern of vasodilation and vasoconstriction will occur, which is called the Lewis reaction (Lewis, 1930).

The main aim of this study is to develop a model to determine the optimal cooling conditions to prevent nail changes. Hence, it is the aim to model the dynamic responses of the fingers' skin temperature, as a function of the blood flow through the fingers, to controlled localised cooling of the fingers. The ultimate goal is the development of a real-time model-based control system to control the blood flow to the patient's fingers.

In previous work, a new device has been developed by the University of Antwerp (Steckel et al., 2013) to allow active and local cooling of the fingers. More specifically, the device measures the skin temperature and blood flow using temperature sensors and Laser-Doppler flowmetry after local cooling of the fingers. This research platform will be used in this thesis for the experimental part of the work.

The research work presented in this thesis consists of the following parts:

An extended literature review is presented in Chapter 1 introducing the adverse effects of cytotoxic chemotherapy. A review of previous studies on the efficacy of cryotherapy for prevention of nail toxicities is made.

Chapter 2 describes the materials and methods used. The experiments have been performed on a homogeneous test group of 11 healthy women (35-55 years old). This age interval has been chosen because of the high incidence rates of breast cancer in this group in combination with the fact that chemotherapy is often applied for younger patients (premenopausal women). Measurements have been performed with the new cooling device, as well as with the frozen gloves to compare the performance of both techniques. The data obtained in 65 experimental runs form the input for the modelling work.

In chapter 3, all data were statistically analyzed and a second order discrete time transfer function mode has been developed. For each model obtained for the index fingers of the test persons, a suitable PIP-controller has been developed. The controllers were tested for their stability and the model parameter perturbations.

In Chapter 4, a statistical comparison was made between the model parameters of the models developed from the data of the experiments with the frozen gloves and the experiments with the device.

Besides this, in Chapter 5, a first attempt has been made to develop a mechanistic model to describe the temperature decrease during cooling of the fingers, using ANSYS Fluent® software.

The overall conclusions and suggestions for future work are summarized in Chapter 6.

1. Literature review

1.1. Introduction

Worldwide, many people are coping with cancer, of which lung, breast and colorectal cancer are the most commonly diagnosed cancers. In Belgium, as well as in Europe, breast cancer is by far the most common cancer for women, with an estimated 464.000 new cases diagnosed each year (28,8% of all cancers in women) in Europe (Ferlay et al., 2013). The Belgian Cancer Registry reported 6.094 breast cancer patients in the Flemish region in 2012. The age specific incidence rates are shown in Figure 1: (Kankerregister)

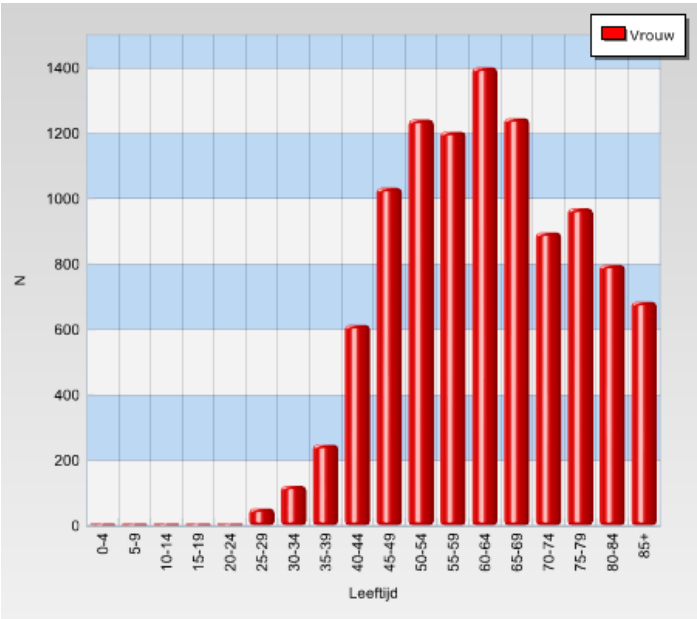

Figure 1: Age-specific absolute numbers of new breast cancer cases in Flanders in 2012 (www.kankerregistratie.be)

The main types of treatment for (breast) cancer are surgery, radiotherapy (both are local therapies), and chemotherapy, hormone treatment, immunotherapy and new targeted treatments (systemic therapies). Sometimes a combination of different treatments is required.

In this literature review, a brief introduction is given about chemotherapy and its adverse side effects, thereby focusing on nail toxicities. The nail anatomy, the role of taxanes inducing nail toxicity and the different nail abnormalities caused by chemotherapeutic drugs are described.
Next, an overview is given of previous work reported on cryotherapy to prevent nail toxicity. The Lewis cycle (or Hunting phenomenon) is explained. Since the aim of cryotherapy is the reduction of the blood flow towards the nail bed, a brief description of possible blood flow measurement techniques is given at the end of this chapter.

1.2. Cytotoxic chemotherapy and its adverse side effects

Cancer is a collective name for a variety of diseases that have one element in common: a continuous increase of sick cancer cells (a tumor) that infect healthy cells and organs. The sick cells can expand themselves locally and distribute themselves through the blood stream towards other organs (metastasis). They begin as the result of an abnormality of the genes in one or more cells in the body. The abnormality can be inherited or acquired by damage or mutation of a normal gene. The damaged genes are normally in control of the regulation of the process of cell replication. After a mutation, the regulation is lost and uncontrolled cell division occurs. When the disease is not treated, the disease will evolve and will cause death by the affected patient. There are many different types of cancer (e.g. breast cancer, lung cancer, prostate cancer…), with each its own characteristics. As a consequence, different cancers have to be treated in a different way.

Cytotoxic chemotherapy is one of the most common treatments. It is used when the tumor has become too big to remove surgically or when there is metastasis.

1.2.1. Chemotherapeutic drugs

Cytotoxic chemotherapy operates by inhibiting the process of (uncontrolled) cell division, by disrupting the process of mitosis. Mitosis is the multiplication of the nuclear genetic material on the chromosomes of the mother cell and the subsequent formation of two new identical daughter cells. Cytotoxic chemotherapy drugs, evolved from the discovery of nitrogen mustard, use a variety of ways to break down the process of mitosis. Based on this, the classification of these kinds of drugs is made (Table 1).

Alkylating agents Bendamustine, Cyclophosphamide, Dacarbazine , Melphalan, Mitomycin, Nitrogen mustard …
Platinum analogues Carboplatin, Cisplatin, Oxaliplatin
Antimetabolites Capecitabine, Fluorouracil, Hydroxyurea, Mercaptopurine, Methotrexate, Pemetrexed…
Topoisomerase I inhibitors Irinotecan, Topotecan
Topoisomerase II inhibitors Daunorubicin, Doxorubicin, Etoposide, Idarubicin, Mitoxantrone…
Cytotoxic antibiotics Bleomycin, Mitomycin, Dactinomycin
Anti-microtubule drugs Docetaxel, Paclitaxel, Vincristine, Vinorelbine…

Table 1: Classification of chemotherapeutic drugs

Alkylating agents

Alkylating agents contain an alkyl group (e.g. CH_2) and uses this group to combine with other compounds by covalent bonds. The general formula for an alkylating reaction or alkylation is:

$$R - CH_2 - X + Y \rightleftharpoons R - CH_2 - Y + X$$

Mostly the alkyl groups of the alkylating agents attack the nitrogen atoms at the N-7 position on the purine base guanine, in nuclear DNA and RNA. In this way, the alkylating agents will prevent the DNA/RNA to act as templates for the formation of new DNA. As a result, DNA replication and subsequent cell division are inhibited.

Platinum analogues

Cisplatin forms cross-linkages between DNA strands in the helix after intracellular activation, mainly by attacking the N-7 position on the purine guanine base. In this way, it will prevent separation of the strands during the DNA replication process prior to cell division. Carboplatin and oxaliplatin are analogues derived from cisplatin.

Antimetabolites

There are three different types of antimetabolites. The first group inhibits the conversion of folic acid to folinic acid. Folinic acid is the biologically active form of the vitamin folic acid. It is an essential co-enzyme in the synthesis of purines and pyrimidines (e.g. Methotrexate). The second group of antimetabolites interferes with purine synthesis (e.g. Mercaptopurine) while the third group interferes with pyrimidine synthesis (e.g. Fluorouracil).

Topoisomerase inhibitors

Topoisomerase I and II are enzymes that are responsible for the regulation of the DNA structure. Inhibition of these enzymes leads to single, or double, strand breakages in the nuclear DNA chains. Some of the topoisomerase II inhibitors, i.e. Daunorubicin, Doxorubicin, Epirubicin and Idarubicin, are anthracyclines and act also by intercalating with the nuclear DNA. This means that they are incorporated within various parts of the DNA double helix where their presence distorts the DNA template preventing the duplication of the DNA.

Cytotoxic antibiotics

Dactinomycin was the first cytotoxic antibiotic that was produced from cultures of the soil bacteria actinomycetes. It can bind to DNA and prevent DNA transcription. It also forms free radicals

damaging the existing DNA. Later on, other cytotoxics were produced from bacterial cultures, for example Bleomycin. Bleomycin also causes DNA damage by the formation of free radicals.

Anti-microtubule drugs

Taxanes are the most common used anti-microtubule drugs. They include Docetaxel and Paclitaxel which are derived from the needles of the European yew tree and the bark of the Pacific yew tree, respectively. They are called anti-microtubule drugs because they interact with microtubules, which are made up of microtubulin heterodimers (molecules of tubulin coupled with a partner molecule) by polymerization. There is a continuous dynamic equilibrium between tubulin dimers and microtubules in each eukaryotic cell, i.e. a continuous balance between polymerization and depolymerization. In the process of mitosis, the newly formed daughter chromosomes organize themselves at the cell spindle, formed by microtubules, before the cell division occurs. Microtubules are constantly reshaped through lengthening or shortening of the unstable bonds at their ends. When taxanes are bond to the dynamic ends of the microtubuli, they freeze the disassembly of the microtubule and prevent the formation of the cell spindle and hence the mitotic cell division (Priestman, 2008) (toxipedia, Gilbert, 2014).

1.1.2. Adverse side effects of chemotherapy

None of the cytotoxic drugs have the ability to distinguish between normal cells and cancer cells. Many of the side effects of chemotherapy are due to the direct damage of normal cells, although there is a difference in the speed of repairing injury between normal cells and the biologically abnormal cancer cells. In order to reduce the side effects of cytotoxic therapy, consecutive chemotherapies are spread in time. The time between two treatments is chosen in a way that the normal cells will be able to recover while the cancer cells are still struggling to repair the damage done by the drugs.

Patients often react differently to the same treatment. Even if the same chemotherapy, for the same type of cancer, is applied on several people with a similar age and a similar level of fitness, they may react completely different on the therapy. Also the type of drugs and the doses used have influence on the (amount of) side effects. Despite all the precautions to reduce side effects, they are inevitable. Some of the most common side effects are bone marrow suppression, nausea and vomiting, tiredness, alopecia (hair loss), and damage on skin and nails.

Bone marrow suppression

Bone marrow suppression is normally a temporary effect that is induced by cytotoxic inhibition. The production of white blood cells in the bone marrow is the most sensitive to cytotoxic inhibition. Since

white blood cells are part of the immune system and help our body fight infections, a reduction of white cells increases the risk on infections. The combination of an infection with neutropenia is called febrile neutropenia or neutropenic sepsis (more severe). Some chemotherapy regimens are more likely than others to cause profound neutropenia. For example the combination of Docetaxel and breast cancer is well-known to have a high risk (> 20%) of febrile neutropenia. After treatment of the febrile neutropenia, mostly with antibiotics, the aim is to continue the planned chemotherapy with no dose reduction.

Another downside of bone marrow suppression can be Anaemia, i.e. when the haemoglobin level falls below 10 g/dl. Treatment can be performed by blood transfusion or erythropoetic agents such as epoetin alfa. These agents are related to the hormone erythropoietin in the kidneys, which stimulates red blood cell production. Recently, questions raised about the safety of these agents, whether or not they could lead to an increase in cancer growth, which has led to the policy that these agents can only be ministered under specific conditions. (HowStuffWorks, 2014)

Nausea and vomiting

Nausea is a common side effect of cytotoxic treatment, sometimes accompanied with vomiting. Some drugs have a higher chance to cause emesis (vomiting) than others. It is also approved that some people are more vulnerable to chemotherapy-induced nausea and vomiting than others: women are more at risk than men and younger people are more at risk than elderly. Nowadays, there are several measures taken to reduce the risk of emesis (e.g. drugs that block 5HT3-receptors (antagonists), neurokinin-1 (NK_1) inhibitors).

Tiredness (or fatigue)

Tiredness is a problem four out of five people have to deal with during chemotherapy. It is usually present during the first two weeks of treatment and it often gets more apparent as the course of treatment continues. It can take to more than a year after the last chemotherapy to completely lose the feeling of fatigue; especially older people need more time to recover their stamina. The feeling of fatigue can be made worse by other factors like anaemia, feeling clinically depressed and infections. To reduce the feeling of fatigue, it is important to prevent/cure these other factors by for example blood transfusions, antibiotics and/or antidepressants.

Hair loss or alopecia

Different studies have reported that chemotherapy-induced alopecia (CIA) is one of the most common and distressing side effects of cancer therapy. The presence of CIA is strongly related to the kind of cytotoxic drugs that is given (see Table 2). Hair loss usually starts three-four weeks after

starting chemotherapy and once it has started, it can progress very fast, with almost complete hair loss within a few days. Hair loss caused by drugs with 'medium risk of noticeable hair loss' is mostly a process of gradual thinning of the hair over several months.

High risk of total alopecia Cyclophosphamide, Dactinomycin, Daunorubicin, Docetaxel, Doxorubicin, Paclitaxel …
Medium risk of noticeable hair loss Bleomycin, Fluorouracil, Idarubicin, Melphalan, Topotecan, Vincristine, Vinorelbine …
Very low risk of hair loss Carboplatin, Cisplatin, Cacarbazine, Mercaptopurine, Methotrexate, Mitoxantrone, Oxaliplatin …

Table 2: Drugs inducing alopecia

Chemotherapy can affect hair on all parts of the body (scalp hair, eyebrows, eyelashes, under-arm hair and pubic hair) but scalp hair is the most sensitive for chemotherapy because it grows more rapidly than hair on the other parts of the body. About one month after the treatment has stopped, hair starts growing back and it will completely be restored between three to six months after treatment. This is possible because in most cases, the stem cells of the hair follicles are protected against the effects of cytostatic agents, presumably by their slower growth rate. CIA can be prevented, or reduced, by different mechanisms. These mechanisms include pharmacological agents (folic acid and a liposomal alternative of Doxorubicin), tourniquets (to reduce blood flow to scalp hair follicles), electrotrichogenesis and scalp cooling. Scalp cooling is the most common used and effective method to prevent CIA. Several studies showed a significant increase in hair preservation when scalp cooling was used. Scalp cooling induces vasoconstriction and slows down the metabolism. Vasoconstriction reduces the blood flow, and so the flow of cytotoxic agents, towards the hair follicles. The reduced biochemical activity makes hair follicles less vulnerable to the damage by cytotoxic agents. The last years, the method of scalp cooling has been developed from simple bags with crushed ice to precooled caps (Figure 2). In previous years, cooling systems have been developed that cool continuously instead of the conventional caps which have to be replaced frequently (Breed et al., 2011).

Figure 2: Scalp cooling to prevent hair loss

The success rate of scalp cooling depends on several factors. First the dosage and type of chemotherapy play an important role. Better results are achieved at lower dosage chemotherapies. The best results were obtained with chemotherapies using taxanes or anthracyclines schedules. However, when taxanes and anthracyclines are combined and given together, the results of scalp cooling are very poor. Also scalp temperature during the cooling period influences the success rate of CIA-prevention. Despite its importance, optimal scalp hypothermia for various chemotherapy schemes is unknown. The reasons are that it is difficult to carry out scalp temperature measurements during cooling and that the heat gradient from cold cap to scalp is different for each individual. Moreover, cold-induced heat production by the body has to be taken into account. It is supposed that wetting of the hair in advance of scalp cooling increases the success rate. Other factors to be taken into account are the half-time of the used cytostatic drugs and the duration of infusion. These determine the cooling time after infusion of chemotherapy. Also previous chemotherapy, hair characteristics and haircare may influence the success rate of scalp cooling. Scalp cooling can have some unpleasant side-effects like headaches, irritation due to the heaviness of the cap and coldness, dizziness and transient lightheadedness. Mostly these side-effects are 'well tolerable' and they can sometimes even be prevented by other drugs.

Nail toxicity

In this work, the main focus will be on nail toxicity as a result of chemotherapy. There are different forms of nail toxicity which can be induced by different chemical agents. The continuously dividing nail matrix cells are easily perturbed by the cytotoxic activity of most chemotherapeutic agents (Piraccini et al., 2006). These nail changes, possibly induced in all twenty nails, are cosmetically distressing to many patients and can be very painful. Incidence and severity of nail changes can vary widely among different cases. In literature, a grading scale is used to determine the severity of nail

toxicities (Table 3), according to version 3.0 of the National Cancer Institute Common Toxicity Criteria (2006).

Grade	Description
1	Discoloration; ridging (koilonychias); pitting
2	Partial or complete loss of nail(s); pain in nail bed(s)
3	Interfering with activities of daily living

Table 3: Classification of nail changes (Institute, 2006)

1.3. Chemotherapy-induced nail toxicity

1.3.1. Nail anatomy

The human nail has more functions than someone would think. It can be seen as an ornament of the hand but it also has a protective value against trauma of the underlying distal phalanx, a counterpressure effect important for walking and tactile sensation, a scratching function and the manipulation of small objects. The nail unit consists of several different components (Figure 3a): the nail plate, the nail matrix, the proximal and lateral nail fold, the nail bed and the hyponychium. The nail plate is an epidermal structure which is continuously formed by maturation and keratinization of the nail matrix cells. During this process, matrix cells mature and lose their nuclei and organelles and become cemented in a thick mortar. This process is known as onycholemmal keratinization. The nail plate emerges from underneath the proximal nail fold and grows distally. This plate remains adherent to the nail bed to the level of the hyponychium where there is a natural release of the nail plate. The nail plate allows visualization of nail bed blood vessels which results in a pink color. The free edge starting from the hyponychium has a white color. The nail matrix is mostly located under the proximal nail fold and its distal end can be detected by a convex white area, the lunula (Figure 3b).

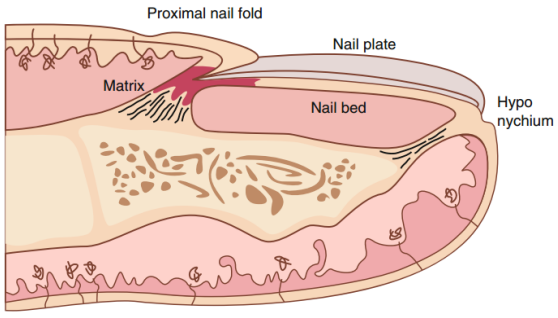

Figure 3a : schematic cross section of the fingertip

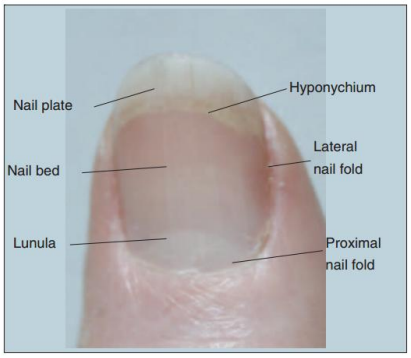

Figure 3b: nail structure

The nail matrix contains two types of cell lines: keratinocytes, which form the nail plate, and melanocytes, which form melanin. The proximal nail fold contains a dorsal and a ventral part. The dorsal part continues distally with the skin of the dorsal digit, from which it differs from the absence of sebaceous glands and hair. The ventral part is continuous with the nail matrix and cannot be seen from the outside. The interface between dorsal and ventral part of the proximal nail fold is formed by a thin band of horny layer, the cuticle. The cuticle forms a barrier to infections and external insults by avoiding penetration of water and environmental particles. The lateral nail fold surrounds the nail plate. The nail bed grows together with the nail plate and is made of keratinizing epithelium. Its function is allowing nail plate longitudinal growth keeping it strongly attached.

In the nails, many capillaries are present oriented in different ways according to the location. The capillaries of the proximal nail fold are oriented in longitudinal lines parallel to the skin surface. The capillaries of the nail bed run parallel to the nail plate surface in a longitudinal direction (Figure 4). The capillaries of the nail matrix and hyponychium are similar to skin capillaries.

The capillaries are responsible for transporting chemical agents coming from chemotherapy towards the nails, which induces nail toxicity. The most frequent problems are due to taxanes, Docetaxel and Paclitaxel, but also other chemical agents, like anthracyclines, can induce severe problems (Piraccini et al. 2013).

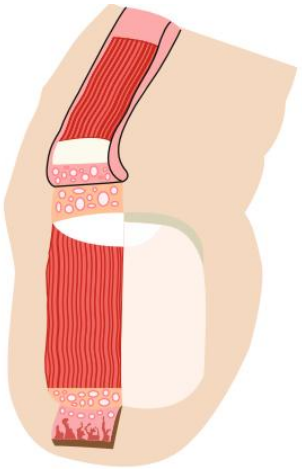

Figure 4: capillaries in the fingertip

1.3.2. Taxanes inducing nail toxicity

Paclitaxel ($C_{47}H_{51}O_{14}$) and Docetaxel ($C_{43}H_{53}O_{14}$) (Figure 5) are administered intravenously during chemotherapy and their kinetics show a large volume of distribution and a rapid elimination from the plasma with a short terminal half-life of respectively 5h and 12h. They work by enhancing the polymerization of tubulin into stable microtubules and inhibiting the depolymerization of microtubules. This disrupts the equilibrium in the cell between tubulin dimers and microtubulin and ultimately leads to cell death. Docetaxel is more effective in inhibiting microtubule depolymerization than Paclitaxel because of its higher affinity for microtubules. Both taxanes are especially used in the treatment of ovarian cancer and breast cancer, but to a lesser extent also in the treatment of non-small cell lung cancer, head and neck cancer, gastric cancer, etc. (Verweij et al., 1994; Wildiers et al., 2004).

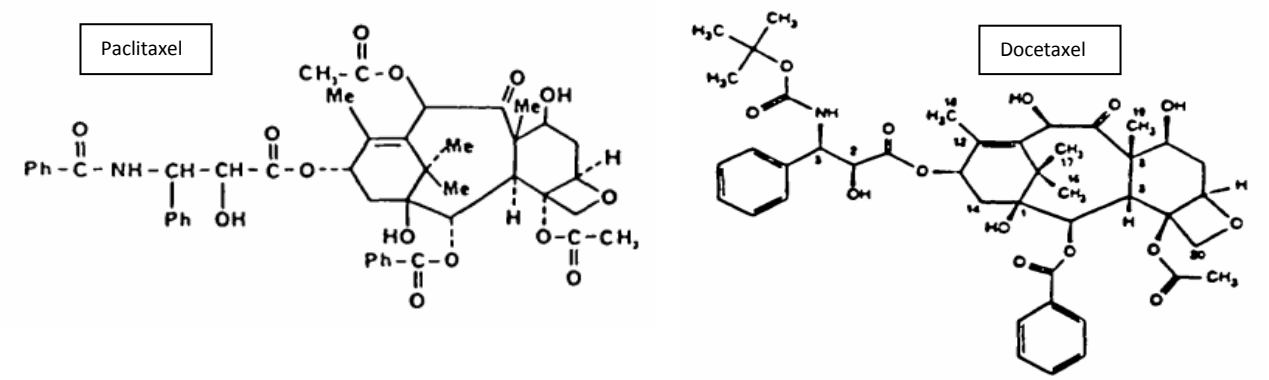

Figure 5: Chemical structure of Paclitaxel (left) and Docetaxel (right)

In recent years, the efficacy of the administration schedules of taxanes has been intensively investigated: generally, weekly schedules show less acute toxicities (e.g. neutropenia) than 3-weekly-schedules while the efficacy is comparable. On the other hand, cumulative toxicities like fatigue, alopecia and nail changes are much more prominent (Ghetti et al., 2003, Gilbar et al. 2009).

In the literature, different case reports reporting nail toxicity after treatment with Docetaxel and Paclitaxel are present. The incidence of nail changes reported in early studies ranges from 0% to 44% (Minisini et al., 2003). For breast cancer patients, who receive higher doses of taxanes, even more than 60% of the patients show clinically significant nail toxicities. The majority of studies citing nail changes among drug induced toxicity are related to the use of Docetaxel, mentioning a wide variety of nail toxicities. Docetaxel was deemed to be the likely causative agent in the cases where combination therapy with Cisplatin, Carboplatin, Epirubicin, etc was applied. In 2006, Hong et al. (2007) investigated 84 patients who were treated against non-small cell lung cancer with Docetaxel combined with Cisplatin. Forty-one patients were treated with every-3-week schedules Docetaxel plus Cisplatin, whereas 43 patients were treated with weekly Docetaxel plus Cisplatin. Six cases (14.6%) from the 3-weekly schedule suffered from nail toxicity while nail toxicity occurred in sixteen cases (37.2%) from the weekly schedule group. In total, thirteen patients (15.5%) had grade 1 or 2 nail changes and nine patients (11%) had grade 3 nail changes. 7 out of 9 patients with grade 3 nail toxicity received weekly Docetaxel. The difference in the hazard between the 3-weekly and weekly Docetaxel is significant which supports the general assumption that nail changes are more prevalent in weekly schedules. Treatment with oral antibiotics only resulted in sustained improvement in 1 case out of 7 after one week. The other six cases had persistent nail changes, resulting in nail extraction. Furthermore the number of chemotherapy cycles given and the cumulative dose were strongly associated with the development of nail toxicity. In this study, the patients with grade 3 nail

toxicity had to interrupt their chemotherapy because of the nail toxicity. Winther et al. (2007) studied between June 2004 and July 2005 fifty-five patients with metastatic breast cancer, who were all treated with Docetaxel every three weeks. Thirty-two patients (58.1%) showed some degree of nail toxicity after first contact with Docetaxel. After three additional cycles of Docetaxel, the number of patients with nail changes was increased to thirty-one out of thirty-five (88.5%). A literature review performed by Hussain et al. (2000) showed that out of 140 cases of chemotherapy-induced onycholysis, 75 were the result of treatment with only Docetaxel as chemotherapeutic agent.

Hussain et al. (2000) observed that ultraviolet radiation worsens chemotherapeutically-induced nail changes, which might indicate that inflammatory processes are on the basis of nail toxicity. To explain the interaction between the integrity of peripheral neural fibers and the development of nail abnormalities after treatment with Docetaxel, two neurotropic mechanisms may be postulated. The first hypothesis is that Docetaxel might activate nociceptive C-fibers that cause neurogenic inflammation contributing to onycholysis. Stimulation of neurogenic C-fibers causes the release of vasoactive substances, namely calcitonin gene related peptide (CGRP) and substance P (SP). These neuropeptides induce cutaneous vasodilation and plasma-extravasation. The combination of both events has been termed 'neurogenic inflammation'. The other hypothesis is that Docetaxel elicit a release of prostaglandines from sympathetic terminals in the distal extremities, including the nail bed. These prostaglandines cause an inflammation in the surrounding tissue contributing to onycholysis.

Paclitaxel is not commonly associated with dermatologic reactions like nail alterations, although isolated reports of tissue necrosis following extravasation and localized skin reactions have been reported. An estimated 2% of patients who receive Paclitaxel have nail toxicity. Although, nail toxicity is more prevalent if Paclitaxel is administered weekly rather than every three weeks. Spazzapan et al. (2002) started a phase II trial of weekly Paclitaxel in metastatic breast cancer: Paclitaxel administered weekly (4 weeks, 1 cycle) without rest periods. Fifty-eight patients were administered into this trial. Nail toxicity occurred in 16 patients (27.6%), mostly of grade 2 and 3 toxicity (75%). In 2 cases, chemotherapy delay was required in order to manage nail disorders. Lüftner et al. (1998) observed various forms of nail toxicity in 6 out of 39 patients (15.4%) treated weekly with Paclitaxel. Hussain et al. (2000) evaluated 21 patients who received 6 to 32 weekly courses of Paclitaxel. Thirteen of the 21 patients were treated during the late spring and summer. Five patients (24%), all treated during the summer months, developed onycholysis (grade 2/3 nail toxicity). Paclitaxel generally is administered intravenously as Taxol together with Cremophor EL and dehydrated ethanol USP. Minutilli et al. (2006) suggested that Cremophor EL plays an important role in Paclitaxel-induced nail changes. Cremophor EL is - among others - responsible for augmented neurotoxicity. This Cremophor EL –

induced peripheral neuropathy seems to be involved in the development of nail toxicity by causing neurogenic inflammation with the release of neuropeptides by activation of nociceptive C-fibers, as described by Wasner et al. (2002). (Winther et al., 2007) (Kishner S, Consuelo T. L., 2013) (Farlex, 2014), (Swenson et al. 2014)

1.3.3. Nail Abnormalities

Damage to the nail matrix

Damage to the nail matrix is the result of the interference of the drugs with the normal kinetics and keratinization of nail matrix keratinocytes. This can result in the appearance of Beau's lines, onychomadesis (Figure 6), nail thinning or fragility and nail plate color changes. Beau's lines are deeply grooved transverse lines in the nail plate. They are caused by temporary decrease in nail plate production because of a decrease of the mitotic activity of the nail matrix keranocytes. The depth of the depression indicates the amount of damage to the matrix, while the length corresponds to the duration of chemotherapy administration. The distance between the lines is proportional to the interval between the treatment cycles. Beau's lines move distally with nail growth and eventually disappear without specific treatment. If the inciting event results in full matrix toxicity, onychomadesis may be seen. The nail matrix is then divided into two parts by a sulcus or groove leading to the shedding of the nail. All drugs causing Beau's lines can cause onychomadesis, especially among patients which are treated with high-dose chemotherapy (Tosti et al. 2010).

Figure 6: Beau's lines (left); Onychomadesis (right)

When the nail matrix keratinocytes are slightly damaged, this can result in the creation of a nail plate that is thinner and more fragile than normal. Both the upper layers of the nail plate and the surface of the proximal part of the nail can be detached.

Nail plate color changes are the result of the influence of chemotherapeutic agents on melanocytes, in addition to previously discussed nail alterations where the working of keratinocytes is altered. When the melanocytes, which are normally quiescent in the nail matrix epithelium, are activated by toxins, melanin is produced, resulting in nail plate color changes. Activation of a cluster of melanocytes gives rise to the appearance of (multiple) light brown to black longitudinal or transverse band(s).

A diffuse activation of nail matrix melanocytes produces a pigmentation of the entire nail plate. This phenomenon is called Melanonychia (Figure 7). Each band in the nail corresponds to a cycle of chemotherapy.

Figure 7: Melanonychia

Damage to the nail bed

Abnormalities in the nail bed can have many different clinical presentations, but in all cases the overlying nail plate remains unchanged. The most severe and painful change resulting from damage to the nail bed is onycholysis. Onycholysis is the detachment of (a portion of) the nail plate from the nail bed with the formation of a new space that usually appears white (Figure 8). It can be the result of damage to the nail bed epithelium and the loss of adhesion of the nail plate to the nail bed below or it may follow the complete destruction of the epithelium as a result of the formation of a hemorrhagic blister. In the latter case, the onycholysis is very painful. Subungual hematoma and subungual abscesses are also complications of chemotherapy that cause nail plate separation and potential loss of the nail plate. Onycholysis and subungual abscesses are often linked with treatment therapies with taxanes (Docetaxel and Paclitaxel). Next to the pain caused by these nail changes, the separation of the nail plate from the nail bed also create a portal for infection, which increases sepsis risk in immunocompromised patients undergoing chemotherapy treatment. The pain accompanying onycholysis can result from damage to the peripheral nerves, but also other factors like a change in the peripheral blood flow play an important role. Onycholysis is dose related, which means that it may improve or even regress with dosage reduction. In most cases, it regresses spontaneously after the drug withdrawal, but healing may take several months.

Figure 8: Onycholysis

Damage to the proximal nail folds

Proximal nail fold changes include paronychia and pyogenic granulomas (Figure 9). Paronychia is an inflammation of the nail folds and results in erythematous, swollen and painful nail folds. It usually develops soon after drug intake and is frequently related to the use of taxanes. Often it is a precursor to onychomadesis, but normally it heals gradually after drug withdrawal. Pyogenic granulomas are lobular tumors of capillaries that frequently involve the nail unit, including the nail folds and the nail bed. This side effect is more common in toenails because feet are more subjected to chronic friction than hands.

Figure 9: Paronychia (left) and pyogenic granulomas (right)

Alterations to nail blood vessels

Drug-induced vascular abnormalities involving the nail include hemorrhagic changes (Figure 10). Hemorrhage is a condition in which a person bleeds too much and cannot stop the flow of blood. Splinter hemorrhages appear as multiple, longitudinal, purple-to-brown streaks most often evident in the distal nail bed. A hematoma is the result of a subungual hemorrhage and is a mass of usually clotted blood as a result of a broken blood vessel. It appears as a red-to-black discoloration of the nail that slowly migrates distally with nail growth (Tosti et al. 2010). (Gilbar et al. 2009) (Panagiotakopoulos et al. 2000) (Ciastko A.R. 2002) (De Almeida et al. 2011) (Piraccini et al. 2006)

Figure 10: Splinter Hemorrhages (left) and hematoma (right)

1.4. Cryotherapy

1.4.1. Previous studies

As already stated nail changes are usually transitory and often diminish during treatment and disappear completely after drug withdrawal. However, in some cases, they persist after discontinuation of the treatment. Although nail changes are not life threatening, they should be managed properly since they can cause huge discomfort for the patient and even can be the cause of early discontinuation of the chemotherapy. According to Can et al. (2012) management of nail

toxicity involves counseling patients regarding the potential for nail toxicity, providing practical strategies (nail cutting, avoiding potential irritants) for prevention, and instituting appropriate treatment (antibiotics) when necessary. Similar to the management of alopecia, nail toxicity can also be dealt with by cryotherapy. Cold temperatures applied to the hands and feet of the treated patients induce vasoconstriction, which reduces the amount of drug reaching the nails. Nowadays, cooling of the hands is done by Elasto-Gel© mitts (Figure 11). These gloves contain glycerin which is a polyol compound with thermal properties; this implies that it can hold longer the cold temperatures (20-40 minutes) after a few hours in the refrigerator at -25 to -30 °C. Another advantage claimed by the company is that the Elasto-Gel® mitts offer a soothing cold, which means that they gradually transfer cold to the hands. (Products, 2014)

Figure 11: Elasto-Gel© Cancer Care Hypothermia Mitts

Scotté et al. (2005) evaluated the effect of the Elasto-Gel® mitts on forty-three patients between August 2002 and September 2003. They were all treated with Docetaxel, either alone (71%) or in combination with other agents (29%), on a 3-weekly schedule. With every Docetaxel infusion, every patient wore the Elasto-Gel® frozen glove for 90 minutes (15 minutes before administration of Docetaxel, 60 minutes during Docetaxel infusion and 15 minutes after administration) on the right hand. After 45 minutes, the frozen gloves were replaced by freshly cooled ones. The left hand was unprotected and was considered as the control side. To indicate the degree of nail toxicity, Version 2.0 of the National Cancer Institute Common Toxicity Criteria (1999) was used. This slightly differs from version 3.0 indicated above as it doesn't include grade 3. Also patient's comfort level was measured using a 4-point rating system that determined whether patients were dissatisfied (0), not very satisfied (1), satisfied (2), or very satisfied (3). Patients who indicated grade 0 or 1 were eventually classified as dissatisfied and patients who indicated grade 2 or 3 were labeled as satisfied. The overall occurrence of nail toxicity was significantly lower at the frozen glove-protected hands compared to the unprotected hands (51% vs. 11%). Grade 2-toxicity (onycholysis) was reduced from

22% in the unprotected left hands to 0% in the protected right hands. Grade 1-toxicity was present in 29% of the left hands and in 11% of the right hands. Also the median time to toxicity occurrence was delayed with frozen glove protection from 58 days to 106 days (Table 4), although this difference is statistically not significant.

	Toxicity grade		Median time to toxicity occurrence
	Grade 1	Grade 2	
Protected hand	11%	/	106 days
Unprotected hand	29%	22%	58 days

Table 4: Clinical study on 43 patients (Scotté et al., 2005)

In the end, 37 patients (86%) were satisfied with the Elasto-Gel® frozen glove application, whereas 6 were dissatisfied (14%), including 5 (11%) who withdrew from the study because of cold intolerance during glove contact.

A study performed by Hayashi et al. (2009) confirmed these findings. Between September 2007 and June 2008, fifty-two patients, all treated with a combination of Docetaxel and Cyclophosphamide for four cycles on a three-weekly schedule, were treated with a frozen glove on the protected hand while the other hand (control hand) was free before, during and after administration of Docetaxel. Only forty-one patients were able to complete the planned four cycles without dose reduction or study discontinuation. Out of fifty-two, nail changes occurred in 10 cases (19,2%) of the protected hands and in 21 cases (36,5%) of the control hands. This means that nail toxicity was significantly decreased at the protected hands compared to the control hands. In this study, no (severe) adverse effects by the frozen gloves were observed.

Sakurai et al. (2009) performed a similar study to investigate the efficacy of the use of frozen gloves in preventing Docetaxel-induced onycholysis and cutaneous toxicity in breast cancer patients. One hundred twenty-two patients were evaluated between March 2006 and May 2007. Participants were divided into two groups: a case group of 70 patients where each person wore a frozen glove on both hands for 90 minutes before, during and after Docetaxel administration and a control group of 52 patients where no frozen glove therapy was applied. The results are summarized in Table 5:

	Number of patients	Toxicity grade		
		Grade 0	Grade 1	Grade 2 to 3
Case group	70	41%	54%	4,3%
Control group	52	8%	74%	18%

Table 5: Clinical study on 122 patients (Sakurai et al., 2009)

In this study, thirty-two patients (46%) suffered from the deterioration of pigmentation on hands and/or feet, regardless of wearing a frozen glove or not. Also the median time to nail toxicity was not significantly different between the case group and the control group. Although one patient (1,4%) complained about cold intolerance because of the frozen gloves, generally no adverse effects caused by the frozen gloves were reported. Based on these results, frozen gloves seem an effective auxiliary in the prevention of nail toxicity (onycholysis) because it significantly reduces nail changes associated with Docetaxel treatment without huge discomfort for the patients.

Can et al. (2012) performed a study and formulated different conclusions compared to the previously discussed studies. 200 patients treated with taxanes for different kinds of cancers, ranging from breast to lung cancer, were evaluated to determine the efficacy of frozen gloves and socks in the prevention of taxane-induced nail toxicity. All patients had received taxane-containing therapy for at least three cycles with a mean number of 5.8 ± 2.37 cycles. The test subjects were divided between a control group, with 145 patients, and a test group including 55 patients. All members of the test group were prescribed an hourly taxane infusion and elected to wear the Elasto-Gel® frozen gloves/socks during treatment. Patients who received 3-h taxane infusions or did not want cold application during treatment were assigned to the control group. Both groups showed no statistically significant difference for age, BMI, gender, cancer diagnosis, type of number of taxane cycles administered, and severity of taxane-related neuropathy. Only the incidence of diabetes history and metastatic disease was higher in the test group than in the control group. The frozen gloves/socks worn by the test group were cooled for at least 3 hours before the test at -18 to -20°C. During the cooling period of 90 minutes, they are exchanged every 20-30 minutes to maintain a consistently low temperature. In this study, version 3.0 of the National Cancer Institute Common Toxicity Criteria was used to indicate the level of nail toxicity. Table 6 shows the results of the effect of cryotherapy on nail toxicity. Both for Docetaxel and Paclitaxel, it can be seen that there are no significant differences in nail toxicity between the test group and the control group. The frozen gloves seem to have less effect on the occurrence of nail changes in this study. The median time to occurrence of nail changes showed no significant difference between the test group and the control group.

	Number of patients	Toxicity grade			
		Docetaxel		Paclitaxel	
		Grade 0	Grade 1-3	Grade 0	Grade 1-3
Control group	145	38 (26,2%)	38 (26,2%)	33 (22,8%)	36 (24,8%)
Cryotherapy group	55	17 (30,9%)	15 (27,3%)	11 (20,0%)	12 (21,8%)

Table 6: Results of the study performed by Can et al., 2012

Can et al. (2012) assumed that the administration of the frozen gloves was not long enough to prevent taxane-related nail changes because the clearance of taxanes from the body takes longer than 90 minutes. They propose to advise patients to continue to implement 20-min cryotherapy at home 4-5 times a day, for 2-3 days after treatment.

Another study performed by McCarthy et al. (2014) investigated the efficacy and safety of frozen gel gloves with respect to the prevention of Docetaxel-induced nail toxicities in cancer patients. It differs from other studies because it completely randomizes the hands and blinds the assessors and investigates the risk of cross-infection between multiple users of the gloves. In this way, the study investigates the hypothesis of right-hand dominance and nosocomial transmission of organisms between the gloves and the multiple, vulnerable users of the gloves. Two studies were performed during December 2010 and December 2012 on patients who were prescribed Docetaxel for a minimum of three cycles, as a single or multimodal treatment for any cancer diagnosis. Participants in both studies acted as their own control by wearing the frozen gloves on one randomized hand for 90 minutes and leaving the other hand free before, during and after Docetaxel infusion. The first study (pilot study) tested the feasibility of implementing the intervention and the microbial testing protocol. Thirteen patients participated in this study and the gloves were frozen at -25°C prior to use. Out of thirteen, six patients withdrew from the study due to cold intolerance. Because of the results of the pilot study, one opted to freeze the gloves in a domestic freeze with a temperature of about -4°C for at least 12 h to limit cold intolerance in the second study (main study). Fifty-three patients were enrolled in the main study. Twenty-one participants provided valuable data while the others withdrew from the study because of dissatisfaction with the glove temperature or immobility constraints. To test the risk of infection at multiple uses of the frozen gloves, a modification to the gloving procedure was tested. Usually a disposable cotton glove is worn underneath the gel glove to diminish the risk of infection. In this study also a disposable nitrile glove between the cotton and the gel glove was worn. Patients were, based on swabs of epidemiologically-significant microorganisms (for example *Staphylococcus aureus*) assigned into different groups wearing triple-layer gloves and double-layer gloves. The group with triple-gloved patients contained both multidrug-resistant organisms' negative patients and multidrug-resistant organisms' positive patients. Swabbing of the microbial load of the frozen gel gloves occurred on every tenth intervention glove at predetermined time-points. In terms of safety, referring to the risk of cross-infection, the study showed no significant difference between the double- and triple-gloved groups. There was no carriage of microbial organisms on the surface on any of the gel gloves at any time. In terms of efficacy, the studies (both the pilot and the main study) confirmed the conclusions of the study of Can et al. (2012), namely there is no significant reduction of incidence, severity and time-to-onset of

Docetaxel-induced nail toxicities by wearing the frozen gloves. Possibly, the efficacy of the cryotherapy was influenced by the higher temperatures used to cool the gloves in the main study. Also the small amount of patients that finished the study limits the generalizability of the results. Although other studies proved the positive effect of cryotherapy, the authors concluded that the value of the intervention with frozen gloves has to be seen in the right perspective. Their arguments are the fact that the patients interact with each other and potentially discuss the (negative) experience of the gloves, influencing the withdrawal rate, and encourage many patients to stop/never begin with the frozen gloves therapy. Another argument they quote are the logistic problems (workload, equipment, costs…) the therapy causes for the medical staff. Also for many patients, the nail problems are only cosmetic and not really interfere with the patients' quality of life. For these kinds of problems, the discomfort caused by the gloves, and the lack of efficiency, does not offset any potential benefit from the therapy. Finally, it is noted that the severity of nail toxicity is dependent on the total amount of Docetaxel administered. For many cases, where this cumulative amount is limited, intervention with frozen gloves is not really necessary.

Ishiguro et al. (2012) compared a different mode of preparation and protection of the Elasto-Gel© frozen gloves with the standard one used by Scotté et al. (2005). First a study was performed on 8 hospital staff volunteers where the duration of the cooling effect and skin temperatures of the hands and fingers were observed during cooling by Elasto-Gel® gloves frozen at -25 to -30°C and -10 to -20°C. No significant differences were observed although some of the volunteers had redness and increased skin temperatures due to reactive increase in blood flow at the hand wearing the frozen glove cooled at -25°C to -30°C. Furthermore 7 out of 8 participants experienced discomfort due to cold intolerance in the hand wearing the glove frozen at -25°C to -30°C. This study formed the base for a more profound study on 16 patients treated at least monthly with Docetaxel. The patients were tested to compare the cooling effects in each individual patient between one control hand (left) using a frozen glove prepared (frozen between -25°C and -30°C overnight) and used (duration of 90 minutes with replacement of the glove after 45 minutes) by the standard procedure as applied by Scotté et al.(2012); on the experimental hand (right), the patients wore a glove for 60 minutes that was frozen at -10 to -20°C for 90 minutes. The time of applying the glove was determined by the fact that the time the maximum blood concentration of Docetaxel is reached, is 60 minutes after the initiation of dosing. The patients started wearing the gloves at the right hand 15 minutes after the start of Docetaxel infusion until 15 minutes after the end of infusion. At last, 2 patients developed nail toxicity at the right hand after 7.2 and 7.3 months respectively. The first patient developed nail toxicity of grade 2 while the second patient suffered from nail tenderness, which can't be attributed exclusively to the Docetaxel therapy. None of the patients had to discontinue the study because of

cold intolerance, but 100% of the patients complained of discomfort at the left hand ranging from pain to arthritis. On the other hand, only 52% of the test subjects suffered from discomfort at the right hand. These results indicate that the experimental preparation and protection result in similar performance as the standard method while it causes less discomfort and is economically more beneficial.

1.4.2. Hunting phenomenon

The principle behind cryotherapy to prevent alopecia and nail toxicity is the 'hunting phenomenon'. This is a characteristic vascular response that occurs in the extremities of mammals following exposure to cold. It was first described by Lewis (Lewis, 1930). He discovered that the temperature of the skin of the fingers during continued immersion in water of 15-18°C or colder fell rapidly for the first few minutes, and thereafter spontaneous rewarming took place. Cyclic phases of cooling and rewarming followed as long as the cold stimulus was applied, which is known as the 'hunting reaction' or the 'Lewis reaction'. The decrease in skin temperature is because of a conductive loss of heat from the immersed tissue, as well as a decrease in delivery from heat through the blood flow due to vasoconstriction. The increase in skin surface temperature is due to vasodilation and is called 'Cold Induced Vasodilation (CIVD)'; this is again followed by a phase of vasoconstriction, etc., as illustrated in Figure 12. (Fox et al. 1962)

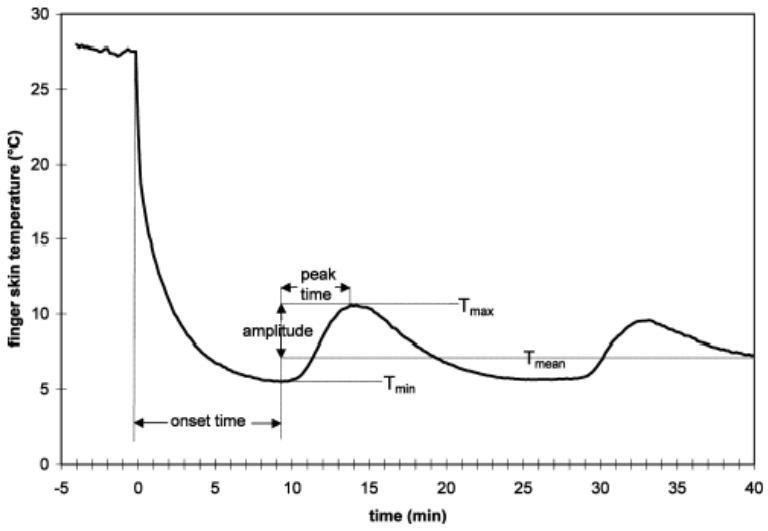

Figure 12: The changes in finger skin temperature during cold exposure (Daanen, 2003)

Peripheral vasoconstriction is a powerful mechanism to reduce the heat loss, but causes strong cooling of the extremities. According to Hoffman and Wittmers (1990), several factors appear to have a role in the initial vasoconstriction and subsequent decrease in blood flow following acute cold exposure. First of all, reflex excitation of vasoconstrictor nerve fibers causes a neurogenic constrictor response. Also direct constrictor response of vascular smooth muscles to cooling appears to have an

influence on vessel diameter. Thirdly, an increased blood viscosity caused by cooling results in a decreased blood flow without appreciable change in diameter of the vessels. At last, direct tissue cooling lowers tissue metabolism, resulting in a decreased formation of vasodilator metabolites in the vicinity of vascular smooth muscles.

The emergence of CIVD has been described as nonsystematic in the literature, hence its causative agent(s) as well as its function(s) remain unexplainable. Daanen (2003) explained the phenomenon of CIVD by a mechanism of peripheral origin to protect the extremities from cold injury. According to this study, arterio-venous anastomoses (AVAs) play a major role in CIVD. AVAs are not fixed blood vessels which may develop when necessary and disappear when no longer needed. Their formation takes about 2-3 days. They are characterized by a thick muscular wall and a lumen, measuring on average 10-30 µm (Gray, 2000), 35 µm (Roddie, 1983) or even 50 µm (Sherman, 1963). The walls of the vessels are strongly innervated by non-myelinated fibers of the sympathetic nervous system. Indirect evidence that AVAs are involved in CIVD is the fact that CIVD occurs mainly at locations where AVAs are abundant (e.g. finger tips). Also the finding that the blood flow through the capillaries is insufficient to explain the magnitude of heat transfer during CIVD strengthens the presumption of the involvement of AVAs in CIVD. Many different possible mechanisms of CIVD have been described (Daanen, 2003). The most likely hypotheses are the release of a dilating substance in the blood and a decreased release of norepinephrine from adrenergic nerve endings. A dilating substance may be formed when local temperature decreases under a certain threshold and the concentration should be dependent on the temperature. In contrast to the conclusions of Daanen (2003), Flouris et al. (2008, 2009) assumed that CIVD is a centrally originating phenomenon caused by sympathetic vasoconstrictor withdrawal instead of a phenomenon of peripheral origin. In short, CIVD is caused by inhibited vasoconstriction rather than by active vasodilation. This theory is supported by the findings of Lossius et al. (1993) who discovered a strong synchronicity in the vasomotion of AVAs in the different areas of the body. Also the strong relationship of blood flow fluctuations through all AVAs with variations in heart rate and arterial blood pressure suggests the involvement of supraspinal regions of the central nervous system in the control of CIVD (Lossius et al., 1993). Flouris et al. (2008, 2009) assumed that survival of the whole organism takes precedence over survival of individual tissues in the periphery, and as a consequence, CIVD is an aspect of a co-ordinated thermoregulatory response to cold exposure that is implemented via local and central mechanisms of vasoconstrictor control, with the goal of releasing body heat and control the thermal balance. It does so by a sympathetic vasoconstrictor withdrawal when the body temperature rises and CIVD occurs. This means that CIVD acts as a control mechanism that dissipates heat when body temperature is too high. This might seem contradictory since CIVD occurs when exposed to cold. In normal circumstances, an increased body temperature is common since 70-100% of the metabolic

energy released for muscular work is converted to heat. In cold environments, an increase of body temperature can take place because of shivering thermogenesis and changes in the metabolism, in addition to the heat obtained from the metabolic energy. In summary, according to Flouris et al. (2008, 2009), the initial vasoconstriction is intended to conserve heat. After a while, the body reacts to the cold by an increased heat production, which is slower and more adaptive than peripheral vasoconstriction. Due to the increased heat production in addition to the peripheral vasoconstriction, the body temperature rises transiently above ideal and CIVD occurs to dissipate the excess heat. Until now, there is no consensus about the origin (peripheral or central) and the function (protection of extremities against cold injuries or releasing excess heat) of CIVD.

Daanen (2003) discovered that subjects that are often exposed to local cold develop an enhanced CIVD response. Also other factors, such as gender, alcohol consumption, smoking, altitude, stress and age affect CIVD. In elderly, CIVD reaction occurs later and is less pronounced. Females tend to have lower hand blood flows than men when exposed to cold due to increased vascular reactivity, although few studies are done on this matter and further investigation of this phenomenon is necessary. Stressed persons appear to have a diminished/abolished hunting reaction. The effect of alcohol is unknown, as different studies report inconsistent results.

In general, it seems that alcohol results in vasodilation and that intoxicated subjects are less likely to suffer from severe freezing cold injuries. Tobacco smoking leads to a faster onset of CIVD and higher finger skin temperatures. It is hypothesized by Daanen (2001) that the repeated changes between peripheral vasodilation and vasoconstriction in abstinent smokers leads to desensitization of blood vessels to local vasoactive stimuli, causing an enhanced hunting response. Kramer and Schulze (1948) also discovered that the hunting reaction is more pronounced in the afternoon, than in the morning or the night. Also in the summer, CIVD is more pronounced than in the winter (Tanaka, 1971). In general, it can be assumed that the hunting reaction is more pronounced when the core temperature is relatively elevated. Sendowski et al. (1997) compared CIVD response during finger immersion and hand and forearm immersion in 5°C water. They concluded that CIVD was more pronounced after finger immersion than after immersion of a bigger area in water. Two possible explanations were quoted. First, it is possible that the arterial blood is cooler when it reaches the fingers after passing through the cooled hand/forearm. This induces a stronger vasoconstriction and less pronounced CIVD. A second explanation was that sympathetic activity was higher during hand/forearm immersion, which was illustrated by higher scores for pain sensation. Sympathetic activity causes vasoconstriction and so on inhibits vasodilation.

O'Brien (2005) performed a study to investigate the reproducibility of the CIVD response in the human finger. The within subject variability in the CIVD response under standardized conditions was

investigated and quantified. Standardized conditions imply that all tests were performed at the same time of the day (between 7 am and 9 am) and at a constant temperature (27°C) and humidity (50% relative humidity). Also test subjects were instructed to refrain from alcohol and vigorous for 24h and from caffeine and tobacco usage for 12h before each test. The core temperature from the test subjects was measured and had to be in between 0.2°C of the mean core temperature. At last, the test persons were asked to wear standardized clothing, consisting of shorts, T-shirt, shoes, and socks. Twenty-one volunteers (19 men and 2 women) completed each five tests, with exception of one subject who only completed four tests. The test consisted of a first period where the patients rested quietly for 15 minutes, then the volunteer immersed the middle finger in warm water (42°C) for 15 minutes to abolish vasoconstriction and standardize initial finger temperature before cold water finger immersion and at last the volunteer immersed the middle finger in cold water (4°C) for 30 minutes. A first conclusion was that in 15 out of 21 persons, pain was reported during finger immersion with a significant higher average pain on test 1 than on test 2 or test 4. Also pain was found to be highest on minute 4 of finger immersion. Furthermore blood flow was measured by using infrared laser-Doppler flowmetry and skin temperature was measured on the nail bed and on the pad of the middle finger on the immersed hand by a wire thermocouple. Cutaneous vascular conductance (CVC) was defined as the ratio of skin blood flow (mV, measured by laser-Doppler flowmetry) to mean arterial pressure (mmHg, 1/3 · (systolic – diastolic) + diastolic pressure). It was found that 1) reproducibility of skin temperature during CIVD was better in the nail bed than in the pad; 2) reproducibility of onset and apex times for the skin temperature was poor, although they were similar in nail bed and pad; 3) onset and apex times associated with nadir and apex CIVD had good reproducibility in both nail pad and finger pad; 4) the magnitude of CVC, expressed as percent of peak during warm water immersion, was similar between nail bed and pad for nadir, apex and overall mean, but had poor reproducibility. Compared with whole hand immersion (Daanen, 1997), it can be seen that onset of CIVD is earlier, and the amplitude was similar to nail bed amplitude but much lower than finger pad amplitude. This can indicate a greater sympathetic stimulus of whole hand immersion compared to finger immersion. This greater sympathetic response can lead to more reproducible results. In the study of *O'Brien* the differences in CIVD response and reproducibility can also be due to the measurement site. For example the location of the laser-Doppler probe may have been different during different tests (placed more or less towards regions with a higher density or depth of AVAs and capillary blood vessels). This is reflected by the fact that the reproducibility was poorer for blood flow than for skin temperature. Another disadvantage of laser-Doppler blood flow measurement is the fact that it doesn't quantify absolute blood flow. In this study, it was chosen to calculate the relative change in blood flow from a theoretically stable value, namely peak temperature elicited during warm water immersion. It was also found that warm water immersion

was not an optimal method to standardize initial finger temperature. In general, 70% of the test subjects showed a classic hunting response during cold water immersion, the remaining 30% showed a more proportional control. But possibly, the subjects with a more proportional control needed longer than 30 minutes to reach the next nadir. An interesting observation was that variability across tests within subjects was not due to a change in the pattern of the response, but especially due to a shift in period and/or amplitude. Also slight indications of acclimatization were observed. The most reproducible characteristic of CIVD response in this study was the time course of the blood flow response.

1.5. Blood flow measurements

Various techniques have been developed and are available for the measurement of blood flow and its related parameters, which can be classified in two major groups, i.e. invasive (direct) methods and non-invasive (indirect) methods of blood flow measurement.

The direct methods are indicator dilution methods, using a colored dye or injecting a bolus of cold saline as an indicator. The latter causes a drop in temperature which is measured. The end result of the dye dilution techniques is affected by errors in the blood sampling procedure, type of dye and nature of dye infusion used. In the following, only the non-invasive techniques will be discussed further.

A first class of indirect measurement methods are the plethysmography methods measuring the volumetric changes in the blood flow. One way is to place a strain gauge around e.g. the limb to be measured, which is connected to an electronically calibrated plethysmograph. Venous occlusion is achieved by inflation of a cuff: there is an arterial inflow into the limb but no venous outflow. Other plethysmography methods can be classified depending on the type of transducers involved. Capacitance plethysmography makes use of the change in capacitance of the transducer due to the volumetric changes in blood flow. The impedance plethysmograph measures small changes in electrical resistance. A constant current is applied using 4 skin electrodes and the change in the impedance is measured. The disadvantages are the relatively poor accuracy and the slow response time. The photoelectric method makes use of a beam of red/NIR-light which is directed to the part of the tissue to be measured (e.g. a finger). The blood flow modulates the attenuated/reflected light and this is recorded. The transmitted/reflected light is collected by a photo detector. This is a simple method but not well-suited for measuring changes in volume and is very sensitive to motion artifacts.

Ultrasound techniques (frequency range above 20 kHz) are based on the underlying principle that the sound undergoes a frequency (Doppler) shift when reflected due to the movement of blood. An

ultrasound of a specific frequency is transmitted into a blood vessel and the reflected sound is detected. Ultrasound contrast agents can be used to increase the echoes. The transmission and reception of ultrasound waves can be either continuous (CW) or with a Pulsed Wave (PW) Doppler system. In general, the ultrasound techniques can be applied to measure flow velocities in major blood vessels with considerable blood velocity but capillary flow measurements are difficult. As the flow velocity is lower, the analysis of the reflected spectrum from the noise spectrum is difficult. The ultrasound technique can be used to measure instantaneous values and can be beamed through the skin. However, the instrument cannot be calibrated in absolute units.

Another method to measure and visualize flow is the phase contrast magnetic resonance imaging (PC-MRI) technique (Ballinger et al.) (Luijkx T., 2013).

In PC-MRI, two gradient pulses with equal magnitude but opposite direction are applied which induce phase shifts in moving protons; the phase shift is proportional to the velocity of the spins. Stationary spins undergo no net phase change. PC-MRI can be used for high resolution measurements in any part of the circulatory system. The measured mean velocities and velocity profiles can also be used to compare with or validate CFD-simulations.

Positron Emission Tomography (MRI, PET) is a nuclear imaging technique that gives a three-dimensional (cross sectional) image of the body. A very small amount of a radiotracer is introduced in the human body, and after an appropriate uptake period, the concentration of the tracer is measured.

However, MRI and PET are expensive techniques and cannot easily be applied widely.

Besides of the before mentioned photoelectric plethysmography, other important optical techniques are the laser Doppler and laser speckle methods.

The Laser Doppler Imaging technique is based on the frequency shift of lasers (Doppler effect), similar as with ultrasound. The light scattered back is shifted in frequency because of the fact that the light is scattered by moving red blood cells. The light from the laser source reaches the surface of the skin using a fiber optical cable, and the same or another cable is used to collect the scattered light from the skin, and is returned to a detector. The advantages are the non-invasive character, very simple in use, giving a continuous or near continuous measurement. It is often used for capillary (microvascular) flow measurements. The disadvantages are the relative (not absolute) measurement values, the limitation of the laser penetration depth, low resolution, longer measurement time, not being a whole field and real time technique.

The laser speckle contrast imaging technique has the advantages of being a real time, high resolution and non-scanning whole field technique. The object of interest is illuminated by the light of a laser source, the illuminated area is imaged by a CCD (Charge Couple Device) camera and the speckle

pattern is captured by the frame grabber and digitized. When an object moves, the speckle pattern will also change. One of the most important applications is the study of the fluctuations caused by blood flow. The frequency spectrum of the fluctuations depends on the blood velocity. A fully digital and real-time technique has been developed (Briers et al. 1996), called LASCA (LAser Speckle Contrast Analysis), based on the first order spatial statistics of time integrated speckle (Jayanthy et al., 2011; Webster, 2009; Puers, 2013).

1.6 modelling and controlling of biosystems

A biosystem is a complex assemblage of interacting physical, chemical, and biological processes. Many of these processes are inherently nonlinear, with considerable uncertainty about both their nature and their interconnections. In other words, a living system is a Complex, Individual, Time variant and Dynamic (CITD-) system. To predict the biological response of such a living system on a certain process input, a model can be developed. The model is able to predict the response of the system output(s) on time instant *t* based on the measured input(s) until time instant *t-k* and assumed input(s) from *t-k+1* until *t* and measured output(s) until time instant *t-k.* Different types of models can be distinguished, among which static versus dynamic models, deterministic versus stochastic models and mechanistic versus data-based models. A deterministic model describes the system output exactly, while a stochastic model describes the system output as a mean with a certain variance. A mechanistic model, also called a white box model, is based on a priori knowledge of the system, while a data-based model, also called a black box model, describes the system based on (dynamic) measurements on the system; the model parameters usually have no physical or biological meaning. A comparison of both model properties is listed in table 7. Grey box models are a combination of both modelling approaches where the most parametrically efficient model structure is determined by the black box approach and the model is interpreted in a physically or physiologically meaningful manner based on the nature of the system under study and the biological, chemical, physical and/or socio-economic laws that are likely to control its behaviour. Linear, time invariant system can be described by a model in the transfer function form, as represented in figure 13. Online modelling of biological responses allows estimating the model parameters in real-time by using a prediction horizon.

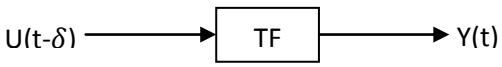

Figure 13: Schematic representation transfer function

	White box	Black box
Application	General	Specific
Fit of steady state	Good	Moderate
Extrapolation	Good	Weak
Interpolation	Good	Excellent
Complexity of model	High	Low
Cost of development	High	Low
Time of development	Long	Short

Table 7: properties white box vs black box model

Model based predictive control uses the model of the system to predict the output. The predicted output is then used to calculate the optimal input to reach the desired output. This procedure is repeated on every instant of time. This approach is illustrated in figure 14. The cost function contains a term which describes the difference between the desired output and the predicted output and a term describing the change of the control input. The goal is to minimize this cost function since this implicates little variance between the desired and predicted output and small input changes. The whole system is summarised in figure 15.

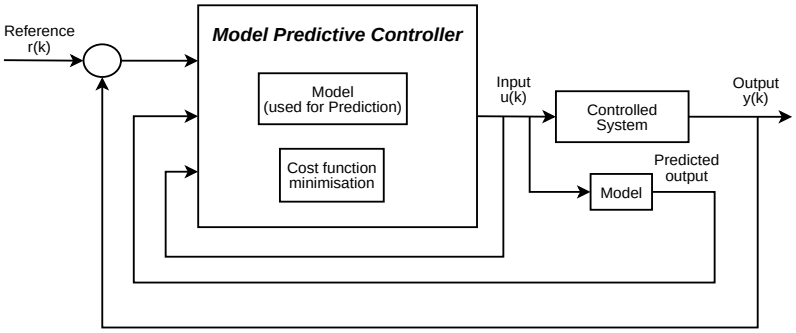

Figure 14: block diagram working controller: The input, output and reference are fed to the model predictive controller. The cost function is minimized in a way the desired output can be reached.

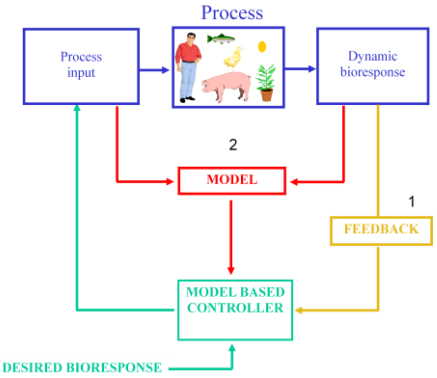

Figure 15: block diagram modelling and controlling of living system: the dynamic bioresponse on a process input is modeled. Based on this model, the controller determines the process input to approach the desired bioresponse. The obtained response is then compared to the desired response by a feedback system

2. Materials and Methods

2.1. Introduction

The experimental work done during the course of this study was based on previous studies performed at the University of Antwerp where a new research platform has been developed, using active cooling of the fingers in order to reduce the blood flow in fingers and nail bed (Steckel et al., 2013).

2.2. Description of the active cooling system

The experimental measurements were performed with the onycholysis device (Figure 16) which is capable to cool all five of the fingers of the left hand by an active cooling system, hence maintaining a low temperature over long periods of time, with high reproducibility. The main advantage of this device over the Elasto-Gel® frozen gloves is the constant temperature that can be applied by the device, while the temperature at the inside of the gloves is all but constant, and the gloves warm up rapidly during the application. Other advantages are the possibility of a specific temperature choice, higher tolerance levels, less discomfort for the patients and less intensive follow-up needed by the nursing staff (on the long term).

The active cooling system works by using five finger-modules each provided by four Peltier elements.

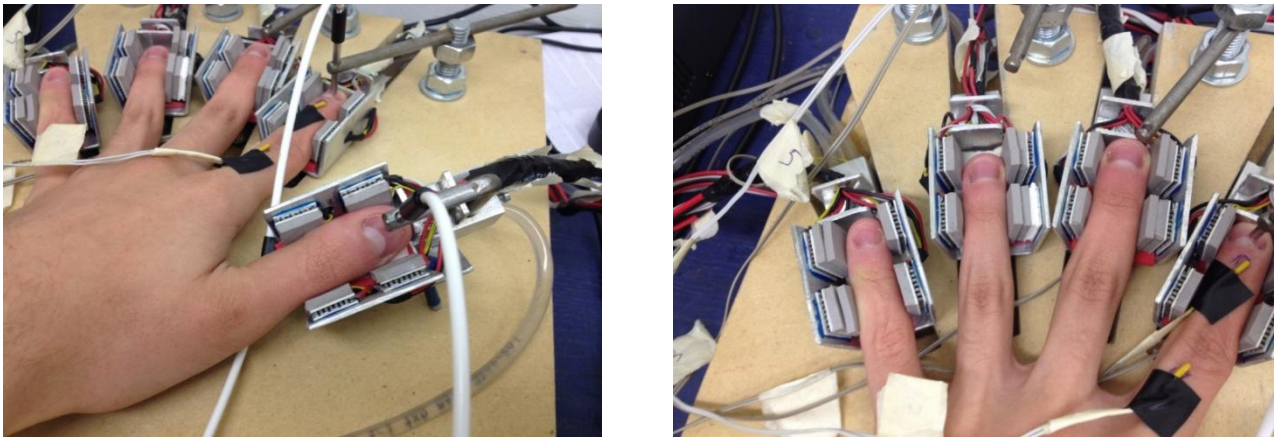

Figure 16: Set-up of the onycholysis device

The Peltier elements are located at the side of the finger modules and make contact with the fingers at both sides of the fingers (2-by-2). Two Peltiers are always connected (two at the fingertip and two behind the first phalanx) in series and are controlled by a steering, so each duo of Peltiers is steered by the same motor steering module. Also, each Peltier element is provided by its own Negative Temperature Coefficient (NTC) temperature sensor to control the steering. A PID controller controls

the amount of electrical power delivered to the Peltier elements, by means of an of-the-shelve proportional motor controller (Figure 17). The temperature measured by the NTC-temperature sensor is fed back to the PID controller, together with a desired temperature. The output of the PID controller is set in a way the error between the desired temperature and the actual temperature is reduced. The PID controllers run on an Arduino processing unit, which allows for swift development and adaptation of the controller software (Steckel et al, 2013).

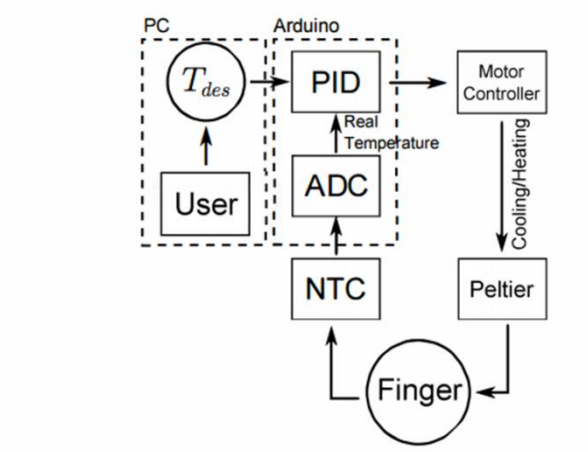

Figure 17: Schematic overview of the control system (Steckel et al., 2013):. A PID controller, implemented on an Arduino controls the electrical power sent to the Peltier element, which proportionally heats or cools the finger, until the desired temperature is reached. The temperature is measured using an NTC and converted from analog to digital by an AD-converter (ADC). The data from the PID controller and the NTC sensor is sent to the PC for further analysis. Two of these control systems are implemented to cool the medial and the proximal region of the finger independently.

The device is provided with five temperature sensors, which allow continuous measurement of the finger skin temperature, and two Laser Doppler blood flow meter moorVMS-LDF2® by Moor Instruments, which measure the response of the blood flow underneath the nail bed in the index finger and the thumb.

A first series of preliminary experiments have been performed on the author himself, to learn working with the equipment and to define the optimal experimental conditions for the larger series of experiments and to agree on the experimental protocol to be presented to the Ethical Committee of the University of Leuven. From these experiments, it has been concluded that the cooling temperature is preferably set at 2 °C; measurements at 6 °C and 10 °C didn't result in enough cooling of the fingers and reduction in blood flow. These findings were in agreement with measurements done at the University of Antwerp last year. Besides, a failure in the equipment has been detected, i.e. 2 out of 4 Peltier elements on the ring finger and on the little finger failed. These elements have been replaced before starting the measurements with the test subjects. However, during the execution of the large series of experiments, again a failure with the elements on the ring finger has

been noticed. Also the measurements on the little finger were not found very reproducible, probably also because it seems more difficult to fix the temperature sensor on the little finger.

2.3. Test subjects

The tests were performed on a homogeneous group of eleven healthy women between the ages of 35 and 55 years (mean = 44,9 years) as given in Table 8. This age interval has been chosen because of the high incidence rates of breast cancer in this group in combination with the fact that chemotherapy is often applied for younger patients (premenopausal women).

Test person (number)	1	2	3	4	5	6	7	8	9	10	11
Age (years)	47	50	35	42	54	39	43	41	44	46	53

Table 8: Ages of the test subjects

The test subjects were in a healthy condition, having no hand injuries and not suffering from perniosis or Raynaud phenomenon. They are all non-smoking subjects, having no (excessive) alcohol starting from the evening before the experiment and having a normal night with normal hours of sleep the night before the experiment.

2.4. Experimental conditions

The onycholysis device consists of a construction on which the left hand can rest; the construction is provided with 5 adjustable holders, so that the equipment can be adjusted for each hand size. Each finger is sandwiched between the four Peltier elements and care is taken that the fingers are properly secured. If the clearance is too large, additional little heat conductive silicone plates are placed between the finger and the Peltier element in order to guarantee the clamping.

Before starting the measurements, the test subjects were seated in the room for at least 30 minutes to acclimatize to the ambient temperature in the room, being 22.38 ± 0.62 °C. For each experiment, the ambient temperature was measured. After placing the fingers in the holders, a temperature of 20 °C was applied with the cooling system during at least 15 minutes, in order to establish similar starting conditions for each experiment and for each test subject.

After this initial period of a quarter of an hour, the actual measurements started. Two series of experiments were performed on each test subject:

- Three measurements with a constant cooling temperature of 2 °C during at least 30 minutes. The cooling liquid is refreshed after every two experiments. This series of tests was carried

out in the morning, on three different days, at the same time as much as possible. Skin temperatures of the five fingers were recorded, as well as the blood flow of the thumb and the index finger. The temperature sensors were located on the underside of each fingertip; the tips of the probes of the Laser-Doppler blood flow meter were placed on the middle of the nail of the thumb and index finger. The results of these measurements and the statistical analysis will be discussed in chapter 3.

- Three measurements with the frozen Elasto-Gel® glove. Before use, the gel filled glove has been refrigerated for at least 4 hours at -18° to -21 °C. The temperature inside the frozen glove was measured before putting on. It was made sure the temperature inside the glove was always between -6°C and -8°C at the start of the experiment. These tests were carried out at three different days, always at noon. The results of these tests and the comparison with the developed onycholysis device will be discussed in chapter 4.

All procedures followed were approved by the Ethical Committee of the University of Leuven. Written informed consent was obtained.

Hence, 65 experiments were carried out[1]. In the figures below, a few sample plots are given of the measurements.

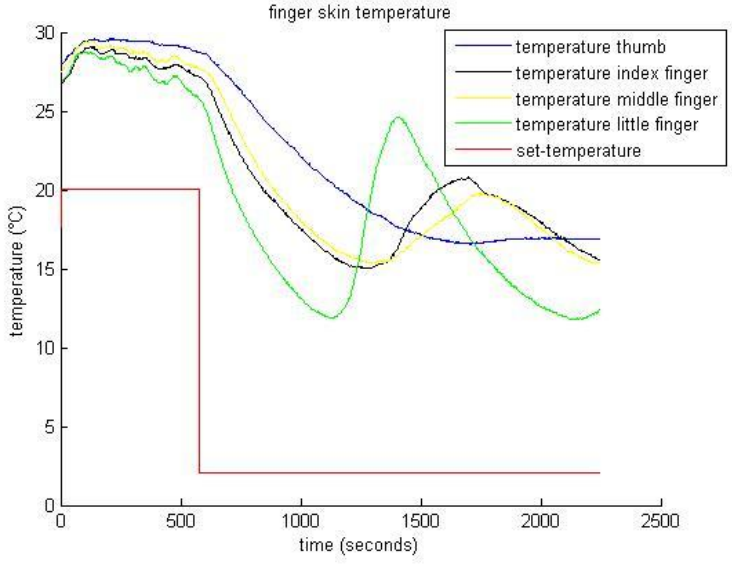

Figure 18: Sample plot of the finger skin temperature as a function of time during cooling at 2 °C (onycholysis device). The CIVD-pattern is clearly visible for all fingers. The ring finger has been left out of consideration because of a deficiency with the cooling of this finger.

[1] One test subject could not tolerate the extreme low temperature of the frozen glove and stopped this series after 2 measurements.

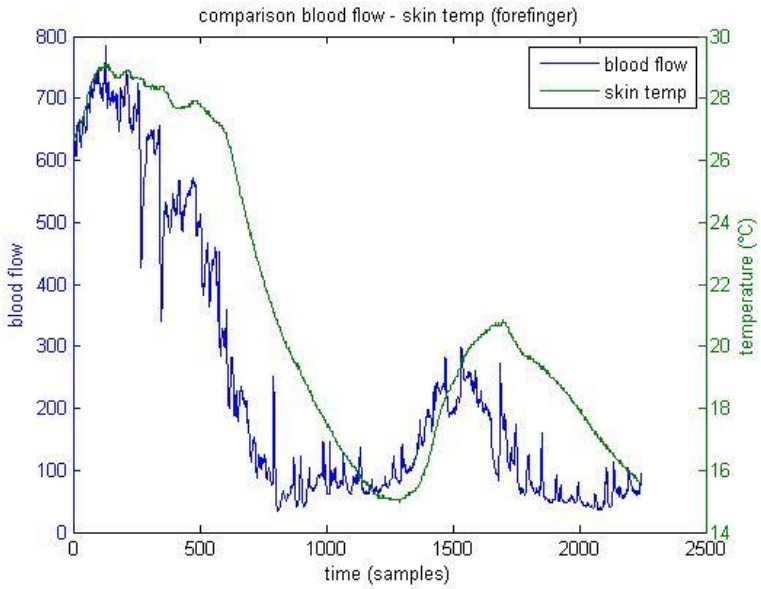

Figure 19: Sample plot of the finger skin temperature and the blood flow measurement as a function of time (onycholysis device). A change is the blood flow is almost immediately followed by a change in the finger skin temperature.

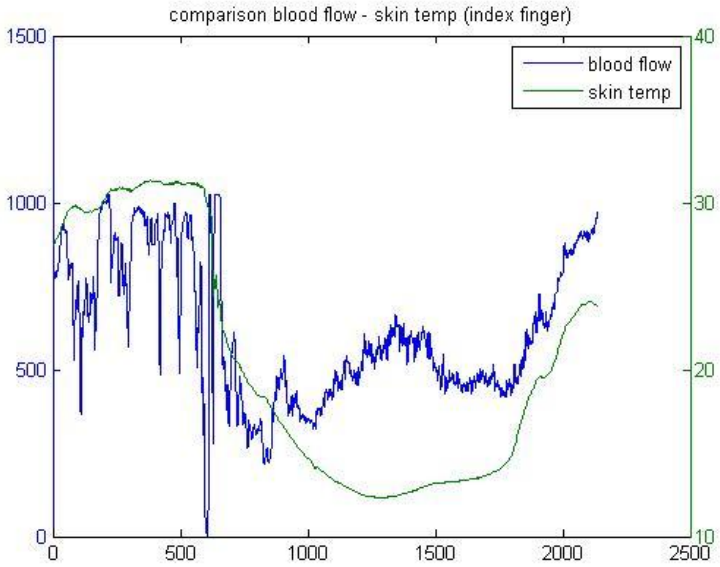

Figure 20: Sample plot of the finger skin temperature and the blood flow measurement as a function of time (frozen glove). The artifacts after about 600 seconds are due to the transition of the hand from the device to the glove. The temperature raise after about 1700 seconds is due to the warming of the glove and possibly a CIVD-reaction.

3. Model identification and model-based controlling

3.1. Introduction

In this chapter, the theoretical background of real-time model-based controlling is briefly described. Next, this theory is applied on the data obtained during the experiments, i.e. a transfer function model is developed for each measurement of the skin temperature and the blood flow as a function of the set temperature set by the device. Based on these models, a PIP-controller is developed that aims to control the finger skin temperature. This is done for all the models of the index fingers of the test persons. At last, the obtained controllers are tested for possible perturbations of the parameters and stability.

3.2. Theoretical basis and Methods used

The model identification and control designing were done using CAPTAIN toolbox. CAPTAIN toolbox is a MATLAB® compatible library for non-stationary time series analysis and forecasting developed by the Centre for Research on Environmental Systems and Statistics (CRES) at the Lancaster University. First the collected data were prepared for modeling using the function **prepz**, which removes the baseline and scales the input. The transfer function for a single-input, single output system is defined as:

$$y_t = \frac{B(z^{-1})}{A(z^{-1})} u_t + \frac{1}{C(z^{-1})} e_t$$

where z^{-1} is the backward shift operator, i.e. $z^{-n} \cdot y(k)$ equals y(k-n) and $z^{-n} \cdot u(k)$ equals u(k-n), etc. Herein, y_i is the i^{th} dependent output variable (in our case, the skin temperature), and u_i the i^{th} independent variable, the set-temperature; e_t is an error term.

This function allows the automatic search over a whole range of different model structures. The Refined Instrumental Variable (RIV) algorithm is used to estimate the model parameters. Here, initial estimates of the system and noise model parameters can be used to define the initial auxiliary model and pre-filter parameters and, as the subsequent recursive estimates of the parameters are obtained, they can be used to update or adapt these parameters. The implementation of the RIV algorithm is based on the following steps:

1. First the number of RIV iterations is set
2. Next, the initial estimates of polynomials $\hat{A}_0(L)$ en $\hat{B}_0(L)$ are found
3. Then, estimates of the noise signal from $\hat{n}_t = y_t - \hat{x}_t$ and $\hat{C}_0(L)$ by least squares method is found

4. Next, values of the pre-filtered variables u_t^*, y_t^* and $\hat{x}_t$ are found based on the estimates in steps 2 and 3
5. At last, steps 2, 3, and 4 are repeated J-1 times using the pre-filtered variables found in step 4

where $\hat{n}_t = y_t - \hat{x}_t = y_t - \frac{\hat{B}(L)}{\hat{A}(L)} u_t$ is an estimation of the noise model.

$\hat{x}_t$ is the vector of instrumental variables, the more highly correlated this vector to the noise free output $x_t = \frac{B(L)}{A(L)} u_t$, the closer the polynomials $\hat{A}_0(L)$ en $\hat{B}_0(L)$ are to the actual, unknown, process parameters and the lower the variance of the eventual RIV estimates. $\hat{x}_t$ also needs to be completely uncorrelated with the noise vector $\hat{n}_t$.

u_t^*, y_t^* and $\hat{x}_t^*$ are the pre-filtered variables, where $u_t^* = \frac{C(L)}{A(L)} u_t$, $y_t^* = \frac{C(L)}{A(L)} y_t$ and $\hat{x}_t^* = \frac{B(L)}{A(L)} u_t^*$

The statistical identification criteria the captain toolbox uses for system identification are the ubiquitous coefficient of determination (R_T^2) , the Akaike Information Criterion (AIC) and the Young Information Criterion (YIC). In the analysis of the model in this work, only R_T^2 and YIC are taken into account. The coefficient of determination and the Young Information Criterion are defined as follows:

$$R_T^2 = 1 - \left(\frac{\frac{1}{N}\sum_{k=1}^{k=N} \hat{e}_k^2}{\frac{1}{N}\sum_{k=1}^{k=N} (y_k - \bar{y}_k)^2} \right) = 1 - \frac{\hat{\sigma}_e{}^2}{\sigma_y^2}, \text{ where the mean value } \bar{y}_k = \frac{1}{N}\sum_{k=1}^{k=N} y_k$$

and

$$YIC = \log\left(\frac{\sum_{k=1}^{k=N} \hat{e}_k^2}{\sum_{k=1}^{k=N} (y_k - \bar{y}_k)^2} \right) + \log\left(\frac{1}{m+n+1} \sum_{i=1}^{i=m+n+1} \frac{\hat{\sigma}_e{}^2 p_{ii}}{\hat{a}_i^2} \right),$$

where:

n + m + 1 is the number of unknown parameters a_i, i = 1,2,..,n and b_j, j = 0,1,…,m in the general transfer function model;

$\hat{e}_k$ the model errors;

p_{ii} is the *i*th diagonal element of the covariance matrix **P*** (**=** $E\{\tilde{a}\tilde{a}^T\} = \sigma^2 P$, with $\tilde{a} = \hat{a} - a$ and σ^2 is the variance of discrete-time white noise),

$\hat{\sigma}_e{}^2 p_{ii}$ can be considered as an approximate estimate of the variance of the estimated uncertainty on the *i*th parameter estimate, and

$\hat{a}_i^2$ are the squared elements of the parameter estimate vector $\hat{p}$.

The coefficient of determination is a statistical measure of how well the model explains or fits the data. The more R_T^2 approaches a value of one, the lower the variance of the model residuals $\hat{\sigma}_e{}^2$ are

compared with the variance of the data σ_y^2. On the other hand, R_T^2 tends to zero if the value of $\hat{\sigma}_e{}^2$ is close to the value of σ_y^2. The first term of YIC is also a measure of how well the model explains the data: the more negative this term, the smaller the model residuals. The second term in the formula of YIC provides a measure of over-parameterization of the model. In other words, YIC is used to identify the most appropriate order of the transfer function model. The more negative the value of YIC, the better defined are the parameter estimates and the smaller their standard errors.

The identification and estimation of the single-input, single output transfer function model which can be coupled with the obtained data from the experiments is developed by the function **rivid**. This function gives eight output elements, among which a standard theta matrix, a vector with the obtained evaluation criteria of the model and a vector with the model output errors and their variance. The theta matrix contains information about the transfer function model structure, the estimated parameters and their accuracy. The CAPTAIN toolbox provides the function **getpar** to extract the parameter estimates of the transfer function model.

The identification and estimation of a suitable model and the practical implementation of the final control algorithm which is used in True Digital Control (TDC) is carried out in discrete-time. Only the deterministic version of the model described above is required for TDC:

$$y_k = \frac{b_0 + b_1 z^{-1} + \ldots + b_m z^{-m}}{1 + a_1 z^{-1} + \ldots + a_n z^{-n}} u_k = \frac{B(z^{-1})}{A(z^{-1})} u_k$$

For control system design, it is necessary to convert the transfer function into a Non-Minimal State-Space (NMSS) model:

$x_k = F \cdot x_{k-1} + g \cdot u_{k-1} + d \cdot y_{d,k}$ or $x(k) = F \cdot x(k-1) + g \cdot u(k-1) + d \cdot y_d(k)$

$y_k = h \cdot x_k$ or $y(k) = h \cdot x(k)$

x_k[2] is called the state vector and contains the present and past sampled values of the output variable y_k and the past sampled values of the input variable u_k, together with the integral-of-error $(=z_k)$[3] between the reference or command input $y_{d,k}$ and the sampled output y_k.

The state transition matrix F, input vector g, command input d and output vector h are defined below:

$$\mathbf{F} = \begin{bmatrix} -a_1 & -a_2 & \cdots & -a_{n-1} & -a_n & b_2 & b_3 & \cdots & b_{m-1} & b_m & 0 \\ 1 & 0 & \cdots & 0 & 0 & 0 & 0 & \cdots & 0 & 0 & 0 \\ 0 & 1 & \cdots & 0 & 0 & 0 & 0 & \cdots & 0 & 0 & 0 \\ \vdots & \vdots & \ddots & \vdots & \vdots & \vdots & \vdots & \ddots & \vdots & \vdots & \vdots \\ 0 & 0 & \cdots & 1 & 0 & 0 & 0 & \cdots & 0 & 0 & 0 \\ 0 & 0 & \cdots & 0 & 0 & 0 & 0 & \cdots & 0 & 0 & 0 \\ 0 & 0 & \cdots & 0 & 0 & 1 & 0 & \cdots & 0 & 0 & 0 \\ 0 & 0 & \cdots & 0 & 0 & 0 & 1 & \cdots & 0 & 0 & 0 \\ \vdots & \vdots & \ddots & \vdots & \vdots & \vdots & \vdots & \ddots & \vdots & \vdots & \vdots \\ 0 & 0 & \cdots & 0 & 0 & 0 & 0 & \cdots & 1 & 0 & 0 \\ a_1 & a_2 & \cdots & a_{n-1} & a_n & -b_2 & -b_3 & \cdots & -b_{m-1} & -b_m & 1 \end{bmatrix}$$

$$\mathbf{g} = [b_1 \;\; 0 \;\; 0 \;\; \cdots \;\; 0 \;\; 1 \;\; 0 \;\; 0 \;\; \cdots \;\; 0 \;\; -b_1]^T$$

$$\mathbf{d} = [0 \;\; 0 \;\; 0 \;\; \cdots \;\; 0 \;\; 0 \;\; 0 \;\; 0 \;\; \cdots \;\; 0 \;\; 1]^T$$

$$\mathbf{h} = [1 \;\; 0 \;\; \cdots \;\; 0 \;\; 0 \;\; 0 \;\; 0 \;\; \cdots \;\; 0 \;\; 0 \;\; 0]$$

[2] $x_k = [y_k \;\; y_{k-1} \;\; \ldots \;\; y_{k-n+1} \;\; u_{k-1} \;\; \ldots \;\; u_{k-m+1} \;\; z_k]^T$

[3] $z_k = z_{k-1} + y_{d,k} - y_k$

In this work, there has been chosen to work with a Proportional-Integral-Plus (PIP) control system, which is an extension of the more conventional Proportional-Integral (PI) control system.

The PIP control law associated with the NMSS model takes the standard state variable feedback form:

$u_k = -k \cdot x_k$,

where k is the n+m dimensional SVF control gain vector, i.e.

$k = [f_0\ f_1\ \dots\ f_{n-1}\ g_1\ \dots\ g_{m-1}\ -k_I]$,

where f_0 and k_I are the proportional and integral actions respectively.

The control input is defined as follows:

$$u_k = -f_0 y_k - f_1 y_{k-1} - \dots - f_{n-1} y_{k-n+1} - g_1 u_{k-1} - \dots - g_{m-1} u_{k-m+1} + k_I z_k$$

The proportional action f_0 and the integral action k_I, which are also present in the PI-controller, are enhanced by the higher order input and feedback compensators $G(z^{-1})$ and $F_1(z^{-1})$, respectively:

$$G(z^{-1}) = 1 + g_1 z^{-1} + \dots + g_{m-1} z^{-m+1}$$

$$F_1(z^{-1}) = f_1 z^{-1} + \dots + f_{n-1} z^{-n+1}$$

Especially when the process has either second order or higher dynamics, or pure time delays greater than one sampling interval, the PIP-controller shows a different response from the more conventional PI-controller. The block diagram of the PIP-controller is shown in figure 20.

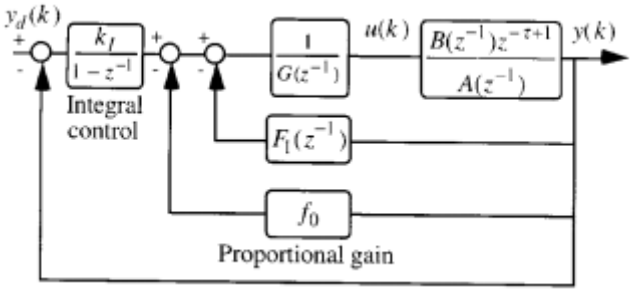

Figure 20: Block diagram of the PIP-controller

The closed loop transfer function can then be obtained directly from the block diagram and takes the form:

$$y_k = \frac{k_I \cdot B(z^{-1})}{(f_0 + F_1(z^{-1})) \cdot (G(z^{-1})A(z^{-1}) + F(z^{-1})B(z^{-1})) + k_I B(z^{-1})}\ y_{d,k}$$

To tune the control gain k_I, pole assignment is one of the ways that can be used. A discrete time system can be considered as stable if its output is bounded for any bounded input. The condition for stability in such a system is that all the poles lie in the unity circle of the complex z-plane, i.e. the

poles have a magnitude less than 1. The position of the poles in the complex z-plane is very important since they determine the speed of response and any overshoot or oscillations.

A root locus procedure produces a graph where the poles are represented for all values of k_I. When the values of the poles are outside the unity circle, the system is unstable for that gain k_I. A normal traject for a root-locus starts at the poles of the open-loop transfer function. After the system breaks at the breakaway point, the poles, which initially move towards each other, separate and travel towards the nearest zero of the transfer function. In MATLAB®, the function **rlocus** plots the root locus of a predefined transfer function. (Pedregal D.J., 2007) (Youssef A., 2011)

3.3. Results and discussion

In this work, the input variable (independent variable) is the set-temperature of the device. The output (dependent variable) is either the finger skin temperature or the blood flow, as illustrated in figure 21. For the blood flow, filtering was required since the blood flow measurements showed a lot of perturbations. For the filtering, a moving average filter was used with window size 20, as illustrated in figure 21. The skin temperature measurements didn't need preprocessing since the obtained graphs were very smooth.

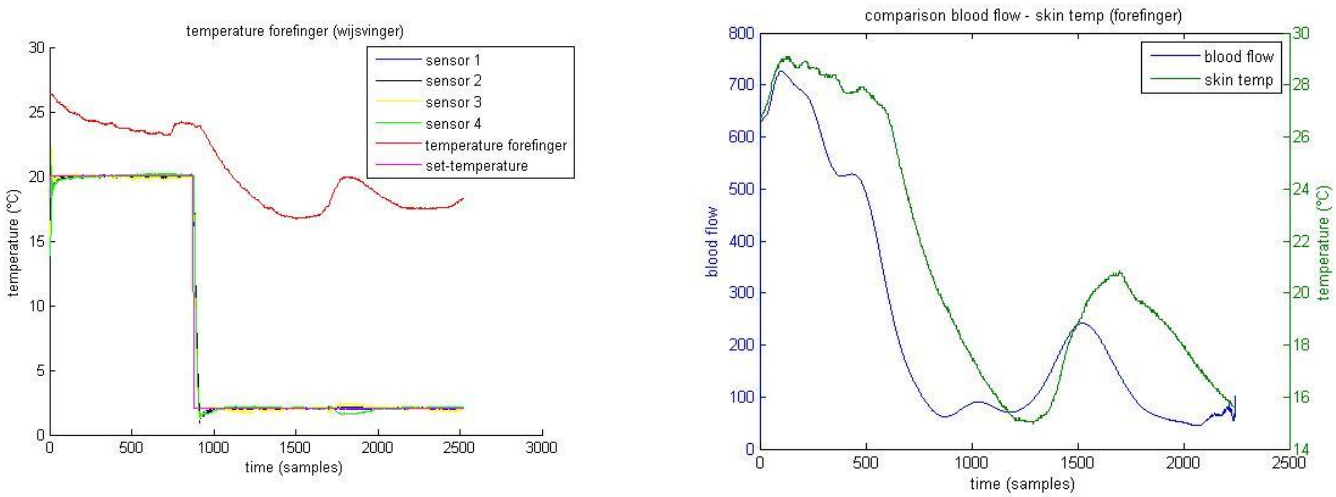

Figure 21: Sample plot of measured data of the finger skin temperature (left) and of the blood flow and skin temperature (right)

From figure 21, the oscillating course of the blood flow and the finger skin temperature can be seen. This proves the theory of the Hunting reaction. It can also be seen that the increase in blood flow precedes the increase in finger skin temperature, which can be an indication that the increase in blood flow causes an increase in finger skin temperature.

Transfer function

A second order discrete time transfer function mode, represented as follows:

$$y_k = \frac{b_1 z^{-1} + \ldots + b_m z^{-m}}{1 + a_1 z^{-1} + a_2 z^{-2}} u_k = \frac{B(z^{-1})}{A(z^{-1})} u_k$$

where y_k is the measured output (finger skin temperature) and u_k is the control input (mean temperature of the Peltier elements), while $A(z^{-1})$ and $B(z^{-1})$ are appropriately defined polynomials in the backward shift operator z^{-1}, was suitable (R^2 = 0.9120 ± 0.1178, YIC = -9.6668 ± 3.2219) to model the dynamic responses of the fingers' skin temperatures on the changes in set-temperature. One test person has been left out of consideration because the Lewis reaction was significantly more profound in her case than for the other test persons. In this case, depending on the experiment, a 1st or 3rd order model was more appropriate.

In figure 22, a plot is shown of the simulated data compared with the generated data from the experiments. This model is generated using the CAPTAIN toolbox in MATLAB®.

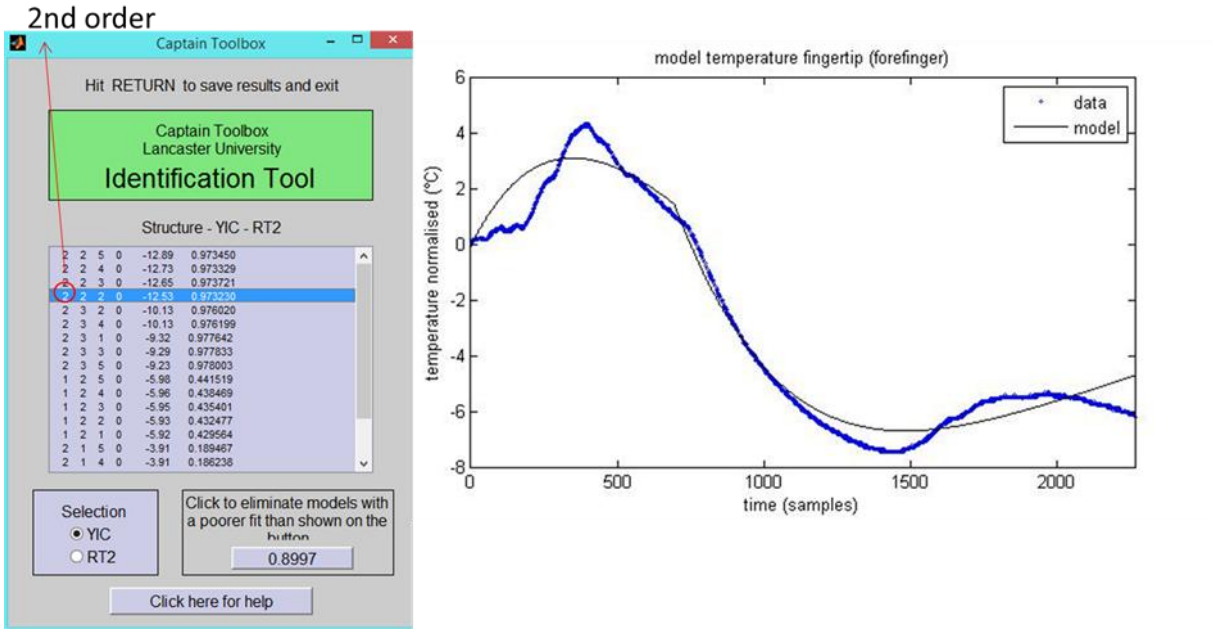

Figure 22: comparison between the simulated and the experimental data. Left it can be seen that a second order TF is suitable. In this example 2 a-parameters, 2 b-parameters and a time-delay of 2 has been chosen.

The models developed for the index finger have been tested for stability and adequate representation of the data, i.e the models are validated. The objective of the validation of a model is to check if the estimated residuals have the standard properties of white noise, i.e. they should behave as a random sequence coming from a Gaussian distribution with zero mean and random variance. To test this, an autocorrelation test of the residuals and a cross-correlation test between residuals and input can be performed. The cross-correlation test can be helpful since the estimation methods for the transfer function assume that the system and noise models are independent of each

other. Therefore, checking the independency of the residuals with respect to the input variables is an important way of validating the model. In other words, if the system model is incorrect, the residuals would be cross-correlated with the inputs. Next to that, an incorrect system model also yields an auto-correlation of the residuals. An auto-correlation of the estimated residuals can also indicate an incorrect noise model. In general, if the cross-correlation function (CCF) lies outside the confidence interval for τ (=time shift) <0, means that there is a feedback from the system output to the system input. On the other hand, if the cross-correlation lies outside the confidence interval for $\tau > 0$, the output of the system is more correlated with the input than described by the model. Values outside the confidence-interval of the auto-correlation function (ACF) can be an indication of a too low model order. A representative auto-correlation of the models for the index finger is given in figure 23. It can be seen that the ACF lies outside the confidence interval for τ = [0; 12]. However, if other values for model order and/or time delay are chosen, similar ACF's are obtained.

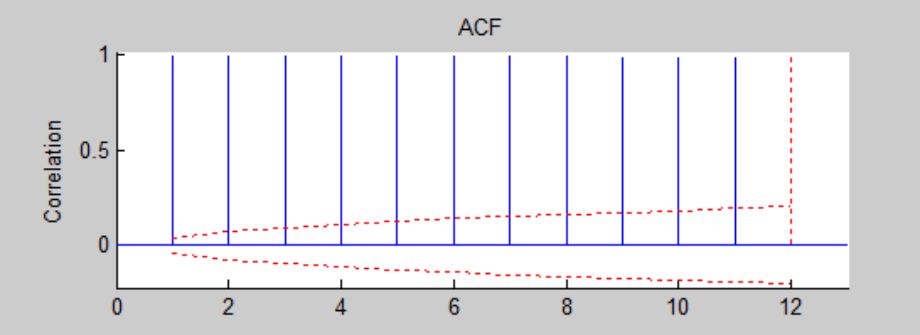

Figure 23: auto-correlation function for model of index finger of test person 3. The autocorrelation values lie outside the confidence interval, which indicates an inadequate noise model.

A representative cross-correlation function is given in figure 24. Also the CCF lies outside the confidence interval, but the absolute values are quite small compared to the auto correlation. Since both ACF and CCF are outside the confidence interval, the noise model and/or the system model are not yet sufficiently adequate. However, the cross-correlation between input and residuals is still acceptable, which justifies the choice for this transfer-function model is this case. Other values for model order and/or time delay gave similar or worse results. A possible reason for this inadequate CCF is noise present in the input.

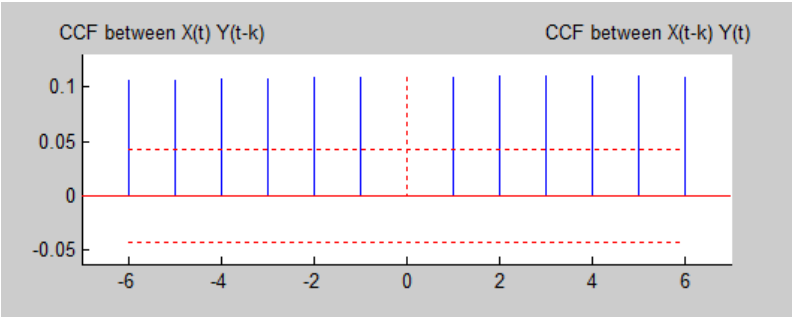

Figure 24: cross-correlation function between the input and noise of the model of index finger of representative test person. The cross-correlation is too high which indicates an inadequate error and/or noise model

The stability of the transfer-function model is tested by calculating the poles of the transfer function. A necessary condition for stability is that the poles lie within the unity circle. In figure 25, the poles of a representative system are plotted in the complex z-plane. It can be seen that, although the poles are close to unity, the poles lie inside the unity circle and so, the condition for stability is satisfied.

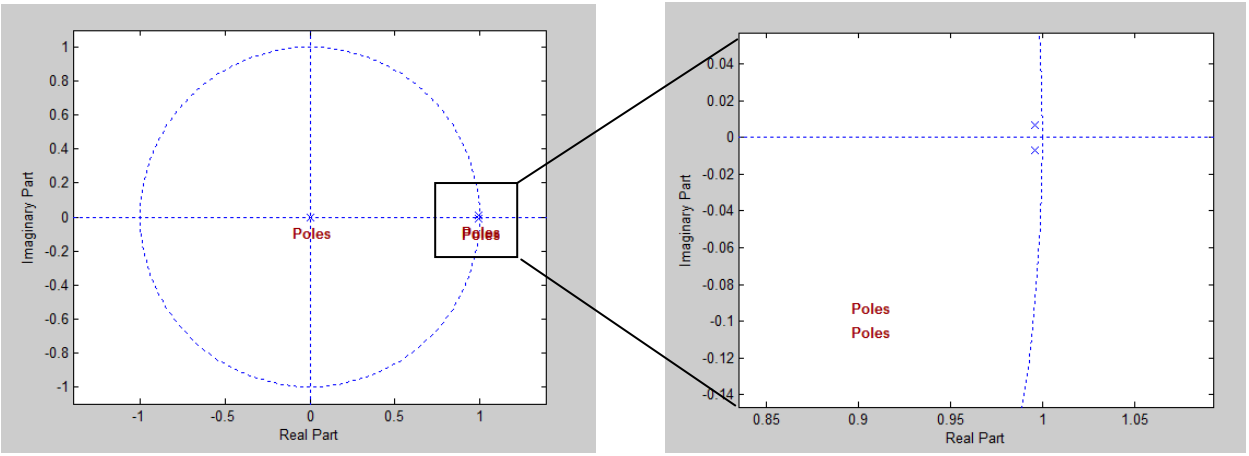

Figure 25: All poles lie inside the unity circle. This confirms the stability of the system

Another validation method is determining the confidence interval for the parameters. In general, it can be said that confidence in model is confirmed if the standard errors are small compared to the absolute values of the (mean values of) the parameters. The decision rule is described as follows:

$$0 \notin [\bar{\theta} \pm 2SE_\theta] \rightarrow \text{confidence in parameter}$$

$$0 \in [\bar{\theta} \pm 2SE_\theta] \rightarrow \text{no confidence in parameter}$$

with $\bar{\theta}$ the mean value of the estimated parameter and SE_θ the standard deviation of for the estimated parameter.

This criterion is satisfied in all cases of the obtained transfer function model.

It can be concluded that the second order discrete TF model is a suitable fit to the data in all cases. The model showed high R_T^2 values (0.80 to 0.9999) in all cases and large negative *YIC* values (-5 to -13), reflecting well defined model parameters estimated with small standard errors. In table ..., the model estimation results obtained for the modelling of the finger tip temperature of the index finger are showed.

R_T^2	*YIC*	Second order TF [2, 3, 1] model parameter estimates
0.9347	-8.5387	a1 = -1.9597 (± 0.3756) a2 = 0.9898 (± 0.2085) b1 = 0.1528 (± 0.0250) b2 = -0.3152 (±0.0586) b3 = 0. 0.1530 (±0.0248)

Table 9: parameter estimates and standard deviations on the parameters for a [2, 3, 1] model. Confidence in the model is confirmed by these values. Also the R_T^2 –and YIC value are satisfactory.

Controller

Based on the model described above, the PIP-controller has been developed. In this work, there has been focused on the development of the controller for only the index finger of the test persons. It could be seen that for all the models, a controller could be found that was suitable. Standard, all the poles had a value of 0.9. When it was noticed that the overshoot was too big or the time response was too large, other values of the poles which seemed more appropriate were chosen. The closer the absolute value of the poles lies to unity, the smaller the overshoot but the larger the time constant. Alternatively, by moving the poles closer towards the origin, the system may be speeded up but the cost of this may be a larger overshoot. In figure 26, previous remarks are illustrated, together with some illustrations of the working of the controller. The response of the controller on a previous determined step-input is plotted. It can be seen that the simulated values follow the desired step input quite well, and that the overshoot/time response are determined by the position of the poles in the complex z-plane.

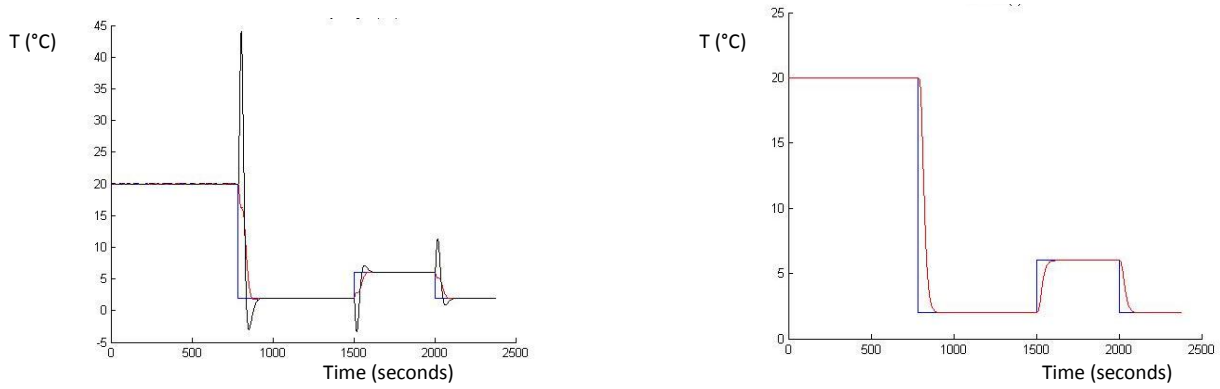

Figure 26: response of PIP-controller on step-input. The simulated values follow desired step-input quite well. The left graph shows a bigger overshoot than the right graph

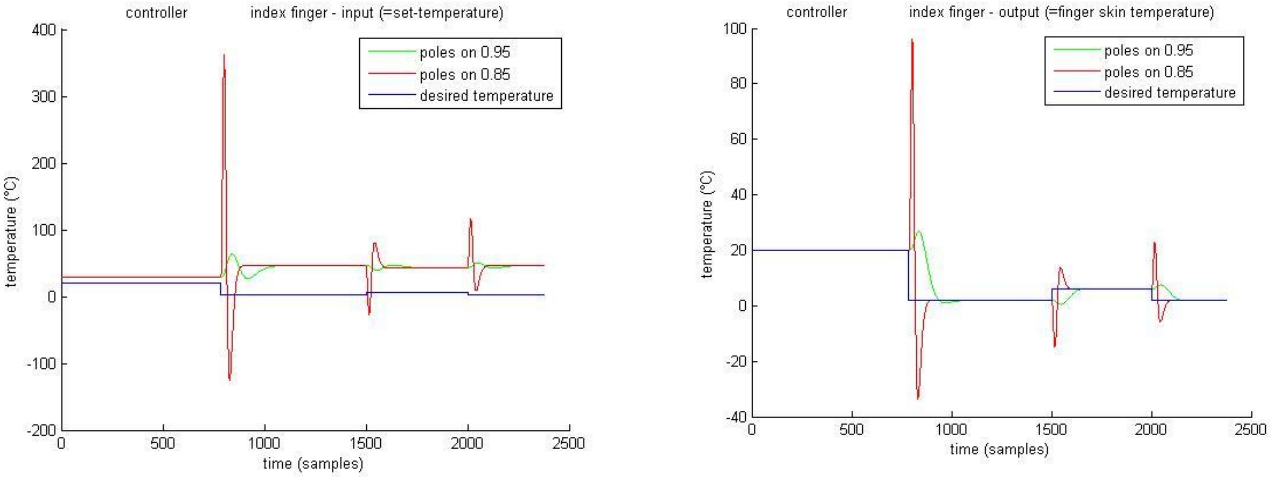

Figure 27: simulated input (left) and simulated output (right) of the PIP-controller for a randomly assigned model. The finger skin temperature (output) is determined by the value of the set temperature (input). The positions of the poles determine the speed of response and the overshoot. There is a trade-off between these two parameters, as can be seen in both graphs.

In figure 27, the simulated input, which corresponds to the set-temperature, needed to control the finger skin temperature, is plotted for the different responses of the controller illustrated in figure 27. It can be seen that for a higher overshoot, higher set-temperatures are needed to reach these extreme values. This is the cost of a faster response but, as illustrated in this example, this is practically impossible to implement in the device since temperatures between -100°C and 400°C have to be reached. So in the final implementation of the device, the response time needed to reach the desired temperature will be longer than optimal avoiding injuries of the patients and to assure the durability of the device.

Robustness of the controller

The robustness of the designed control system is tested by the implementation of a Monte Carlo analysis. The a-and b-parameters of the model are varied between respectively the minimum and maximum a-value and the minimum and maximum b-value obtained for all the parameters of the models generated for all the index fingers of the experiments. In this way, the model parameter (a_1, a_2, b_1 and b_2) perturbations are simulated. Note that there has been chosen for only three b-parameters, namely b_0, b_1 and b_2. This assumption doesn't correspond with the reality since the amount of b-parameters ranges from 2 to 8. In all cases, the value for b_0 in the model was 0, so this value has been chosen fixed and equal to 0. The value of a_1 lies in the range of [-2.6531; -1.9552], the value of a_2 lies between [0.9554; 1.6552], the value of b_1 ranges between [0; 0.2955] and the value of b_2 is between [-0.8823; 0.4945]. For all parameters, 50 values which are equally divided in the ranges described above were chosen. These parameters were then randomly combined to achieve 50 random combinations of the model parameters. In figure 28, the simulations of the finger skin temperature responses to steps in the command input are shown.

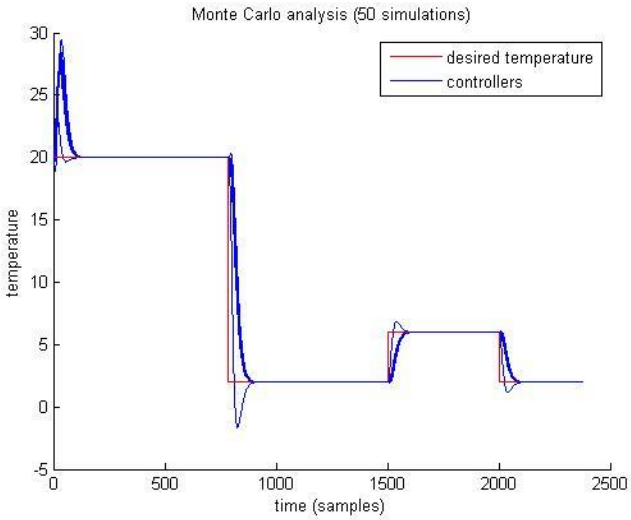

Figure 28: Monte Carlo analysis showing 50 simulations of the finger skin temperature responses to steps in the command input

The Monte Carlo analysis of the controller with 50 simulations shows that the designed controller is robust to unexpected noise that might be associated with the estimated model parameters.

In figure 29, a few examples of the root loci are shown. As stated before, the system is stable when all the poles lie inside the unity circle. The gains are zero at the 'x', which correspond with the poles of the open-loop transfer function and are infinite at the zeros of the transfer function, here represented by 'o'. For many developed models, the range for k_I for which the system is stable is quite narrow. In figure 29, it can be seen that only one pole lies inside the unity circle, which indicates that the system is unstable, i.e. its impulse response is exponentially increasing if time goes to infinite. For other values of the parameters, both poles lie inside the unity circle for a certain range of values for k_I, as illustrated in figure 30. It was derived that the system is stable if the *a1*-parameter lies in the range [-2.2828; -2.2258], the *a2*-parameter lies in the range [1.3267; 1.3838], the b_1-parameter lies in the range [0.1568; 0.1809] and the b_2-parameter lies in the range [-0.1518; -0.0394]. Now, if the b_2-parameter is chosen out of the interval where the system is stable and is combined with values of a_1, a_2 and b_1 that are outside the intervals described above, the system is still stable for a wider range of *a1*-, *a2*- and b_1-parameters. This indicates that the value of the b_2-parameter was the limiting factor for stability. This can be explained by the fact that the value of b_2 was subject to the highest uncertainty since the interval of b_2- parameters of the models was significantly bigger than the intervals of the *a1*-, *a2*- and b_1-parameters.

The lines inside the unity circle are lines of constant damping factors from 0 to 1 and natural frequency lines from 0 to π. If for example an overshoot of less than 5% is required and a rise time of 1 second, the damping ratio[4] needs to be (at least) $\zeta = 0.7$ and the natural frequency has to be greater than ω_n = 1.8. Out of the root locus plots, the possible values for the gain k_I and the poles can then easily be determined. (University of Michigan, 2014) (Smith, 2007)

[4] $\zeta = \sqrt{\frac{\ln(\frac{PO}{100})^2}{\pi^2+\ln(\frac{PO}{100})^2}}$, where PO is percentage overshoot

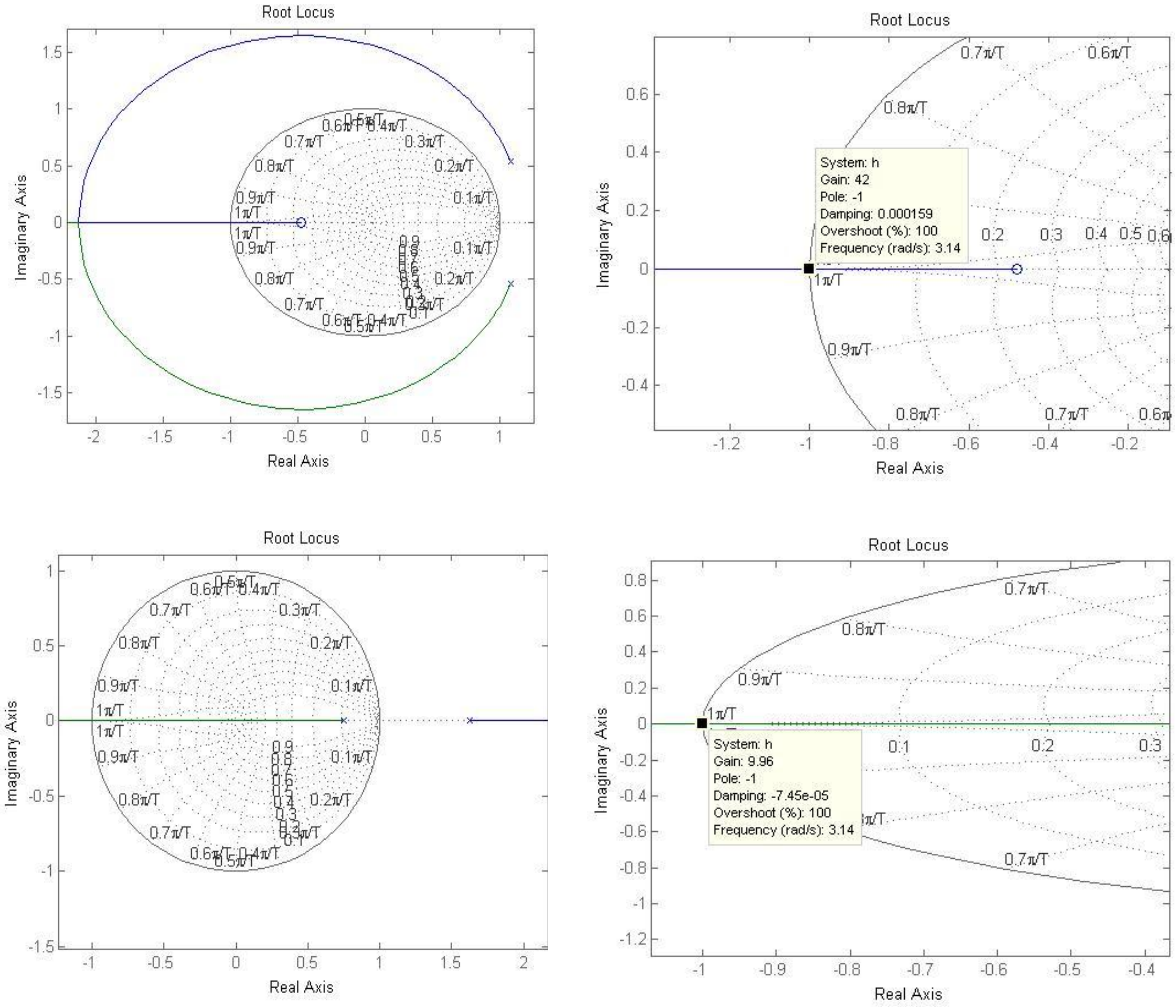

Figure 29: Root locus plot for a1 = -2.1546, = 1.4553, b_1 = 0.2111 and b_2 = 0.1011 (top). Root locus plot for a_1=-2.3825, a_2=1.2268, b_1=0.1146, b_2=-0.3484 (bottom). Both control systems have one pole outside the unity circle, indicating an unstable feedback-system

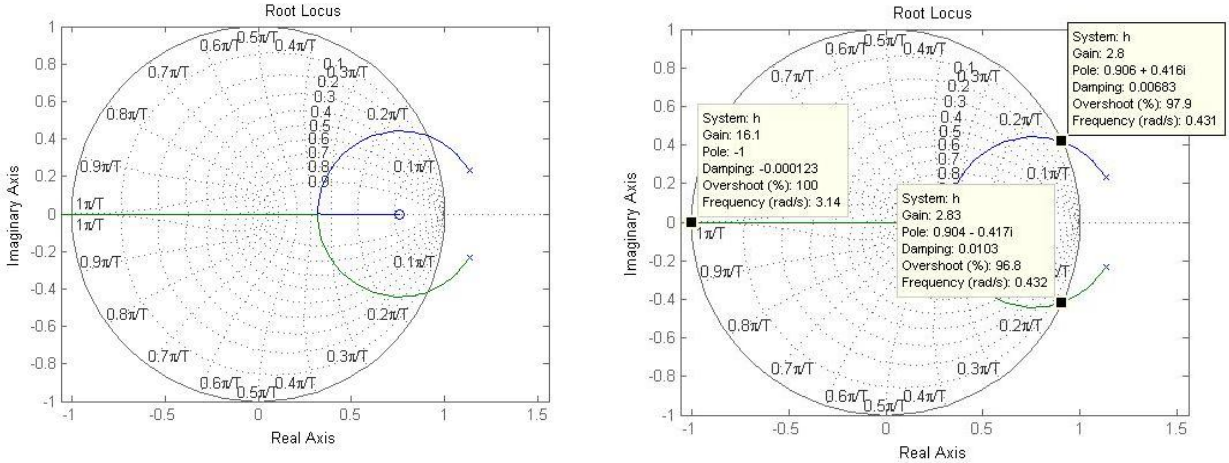

Figure 30: Root locus plot for a_1=-2.2685, a_2=1.3410, b_1=0.1628, b_2=-0.1237. This system has both poles inside the unity circle for k_l 0 and 2.8.

4. Statistical analysis

4.1. Introduction

The statistical analysis of the parameters of the discrete-time transfer function models include both intra- and inter subject analysis. The intra-subject analysis focuses on the variance of the *a1*- and *a2*-model parameters between the different tests and the different fingers of the left hand of the same test person. The inter-person analysis highlights the differences between the same fingers of the different test persons. Both the models developed for the data generated with the device as with the Elasto-Gel® frozen gloves are analysed. At last, the a-parameters of the onycholysis device-models are compared with the a-parameters of the frozen glove-models.

4.2. Material and methods

The model parameters obtained for 10 test persons are subjected to the execution of statistical tests. One test person has been left out of consideration because the Lewis reaction was significantly more profound is her case than for the other test persons. In this case, depending on the experiment, a 1st or 3rd order model was more appropriate. The means and standard deviations of the *a1*- and *a2*-parameters of the thumb, index finger and middle finger are calculated for each test subject, for the models based on the finger skin temperature measurements. This was done by the MATLAB® built-in functions **mean** and **std**. The function **mean** computes the mean μ of a vector A with length N by using the formula:

$$\mu = \frac{1}{N}\sum_{i=1}^{N} A_i.$$

The standard deviations S for a random variable vector A with length N are computed by the formula:

$$S = \sqrt{\frac{1}{N-1}\sum_{i=1}^{N}|A_i - \mu|^2}.$$

The standard deviation is the square root of the variance. A comparison between the a-parameters of the identified models for skin temperature of the different measured fingers of the same person was performed using a two-sample t-test. The test-statistic is given by:

$$t = \frac{\bar{x}-\bar{y}}{\sqrt{\frac{Sx^2}{n}+\frac{Sy^2}{m}}},$$

with $\bar{x}$ and $\bar{y}$ the means of the vector, S_x and S_y the standard deviations and m and n the sample sizes. The null-hypothesis H_0 for this test is that the data in vectors x and y come from independent random samples from normal distributions with equal means and equal but unknown variances. The alternative hypothesis H_a is that the data in x and y come from populations with unequal means. To

test if the means of two normally divided groups are significantly different from each other, a multiple pairwise comparison of the group means can be performed. This test uses Tukey's honestly significant difference criterion to test for significance differences between group means. The 0-hypothesis H_0 for this test is that the means of the compared group are not significantly different from each other. This test is optimal for balanced one-way anova and similar procedures with equal sample sizes. The test is conservative for one-way anova with different sample sizes. The test-statistic is given by:

$$|t| = \frac{|\bar{y}_i - \bar{y}_j|}{\sqrt{MSE(\frac{1}{n_i} + \frac{1}{n_j})}} > \frac{1}{\sqrt{2}} q_{\alpha,k,N-k}$$

where $q_{\alpha,k,N-k}$ is the upper 100*(1 – α)th percentile of the studentized range distribution with parameter k and N – k degrees of freedom, N is the total number of observations and k is the number of groups (treatments or marginal means). It needs to be pointed out that every time a multiple pairwise comparison of the group means was performed, the groups were tested on their normality by a Shapiro-Wilk test.

On the *a*-parameters of the models developed out of the data from the experiments with the Elasto-Gel® frozen gloves, the same statistical analysis and comparisons as described above are performed for the thumb and the index finger.

Also, a comparison between the *a*-parameters of the models developed for experiments with the device and the frozen gloves has been performed. It has been tested if the *a1*- and *a2*-parameters of the models for the device and the glove of the same finger and the same person are significantly different from each other by a two-sample t-test.

At last, the division of the amount of b-parameters and the different time-delays of the different models developed for the finger skin temperature is given[5]. (The MathWorks, 2009)

4.3. Results and discussion

Onycholysis device models

In figure 31, the mean and standard deviation is given for the *a1*- and *a2*-parameters for the index finger for each test person. The mean and standard deviation for the a-parameters of thumb and middle finger are illustrated in appendix A1. The inter-subject values of the mean and standard deviation for these fingers are given in the legend of each figure. It is remarkable that the inter-

[5] NOTE: the bar plots linked to the onycholysis device are coloured green, the bar plots linked to the frozen gloves are coloured blue.

subject standard deviations of the thumb, index finger and middle finger have always almost the same value for both parameters. For both the thumb and the index finger, test person 10 shows a greater standard deviance for both parameters than the other test persons. Also the mean values of the parameters are relatively different from the mean values of the other test persons. Since the environmental conditions were controlled during the tests and the tests were performed at the same time instant, it is hypothesized that other uncontrollable factors, like the amount of sleep before the test, showed great variability before each test for test person 10. For the middle finger, the parameter values of test person 8 are different from the parameter values of the other parameters. The same hypothesis as described above can be applied. A remark on this hypothesis that needs to be made is the question why not all the fingers show the same reaction on different conditions. Another hypothesis that possibly explains the different values of the means for test person 8 and 10 is the fact that every living system reacts differently on the applied cold. A drawback of this hypothesis is that it only explains the rare values of the means but not the greater standard deviations. It needs to be noticed that the deviant values of the parameters are not the result of the presence of outliers and/or bad models, since the parameters are controlled for outliers and the models all had acceptable R^2- and YIC-values.

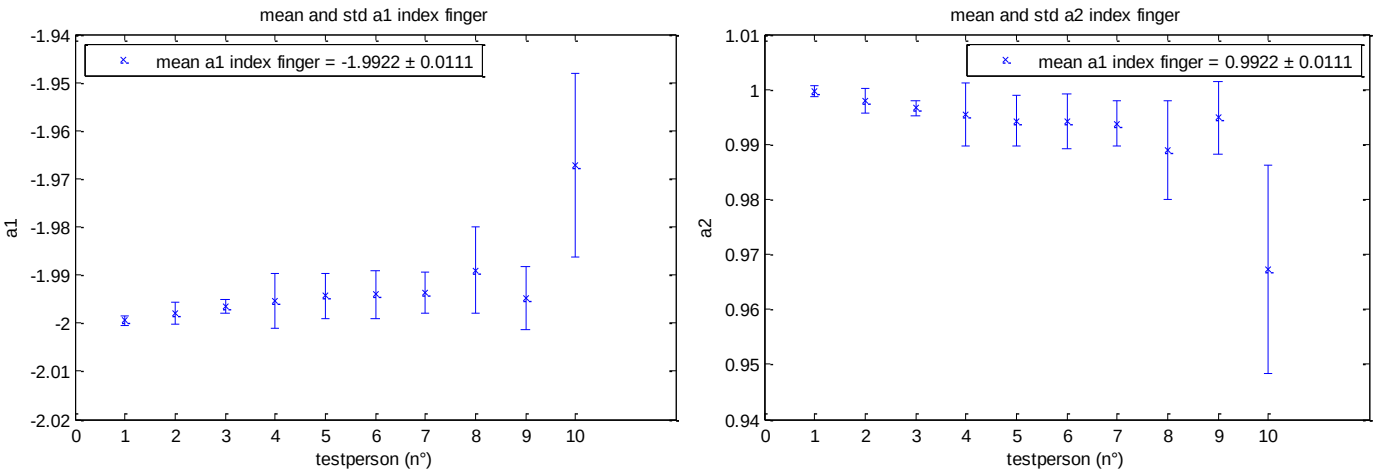

Figure 31: the mean and standard deviation between the different experiments on the *a1*-model parameters (left) and the *a2*-model parameters (right). For both parameters, test person 10 shows a deviation from the other test persons

In figure 32, the within-subject variance between the *a1*- and *a2*-parameters of the different fingers of the left hand is represented for each test person. Test person 6 had the biggest standard deviation between the fingers of the left hand. Since only measurements on the fingers from which it was assured all the measurements were performed correctly were taken into account, the variability can only be attributed to the different reactions of the different fingers to the applied cold.

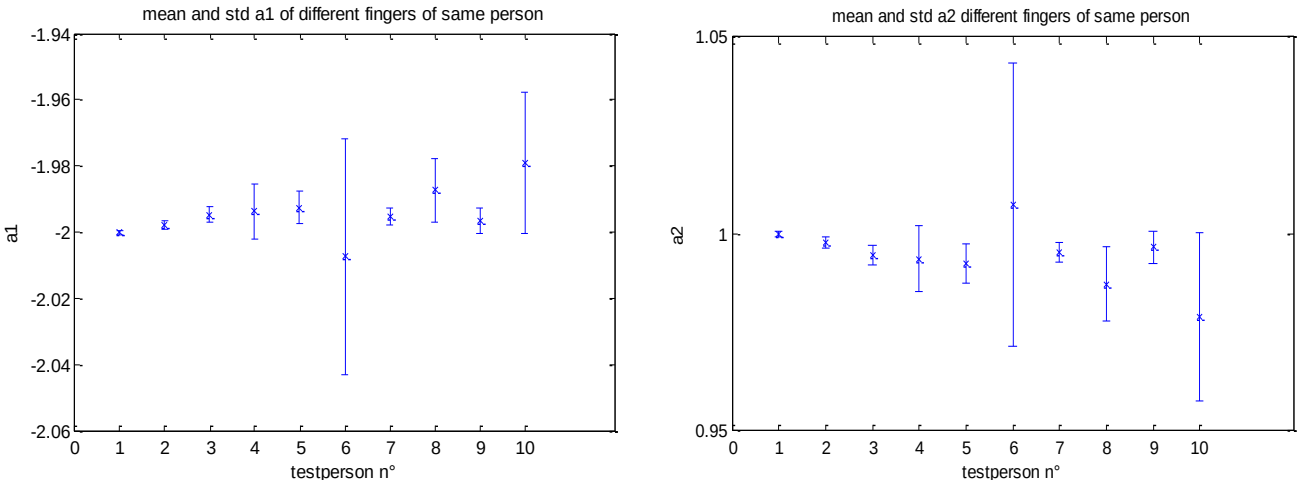

Figure 32: within subject mean and standard deviation of the *a1*-parameters (left) and the *a2*-parameters (right) of different fingers. Test person 6 shows a bigger standard deviance than the other test persons. Also the mean value of the parameters of this test person differs from the other means.

In table 8, the *p*-values resulting from the t-tests comparing the *a1*-parameter of different fingers of the same person are listed for 4 test persons. On a 5% significance level, no significant differences were found between the fingers within-subjects. The tests have been performed on 4 randomly assigned test persons and on test person 6, since figure 31 indicates that this test person showed the greatest variance between the fingers. In figure 33, a graphical representation of the *p*-values of test person 1 is showed. The investigated fingers are represented by bars and the bars are connected with each other by lines. '*', '**' and '***' above the lines indicate significant differences between the connected fingers on respectively a 10%, 5% and 1% significance level. The same representation will be used in the further part of this study. In figure 34, the means of the *a1*- and *a2*-parameters of the same fingers of test person 6 are compared with the means of the *a1*- and *a2*-parameters of the other fingers of test person 6 by a multiple pairwise comparison of the group means.

a1		thumb	index finger	middle finger
test person 1	thumb	1	0.4289	0.0908
	index finger	0.4289	1	0.3013
	middle finger	0.0908	0.3013	1
test person 2	thumb	1	0.2558	0.6973
	index finger	0.2558	1	0.1304
	middle finger	0.6973	0.1304	1
test person 3	thumb	1	0.2244	0.9262
	index finger	0.2244	1	0.2273
	middle finger	0.9262	0.2273	1
test person 4	thumb	1	0.294	0.6261
	index finger	0.294	1	0.4409
	middle finger	0.6261	0.4409	1
test person 6	thumb	1	0.4909	0.4425
	index finger	0.4909	1	0.4468
	middle finger	0.4425	0.4468	1

Table 10: p-values of intra-person *a1*-parameter differences. H_0 is that there are no significant differences between persons. The 0-hypothesis is accepted in all cases on a 5% significance level.

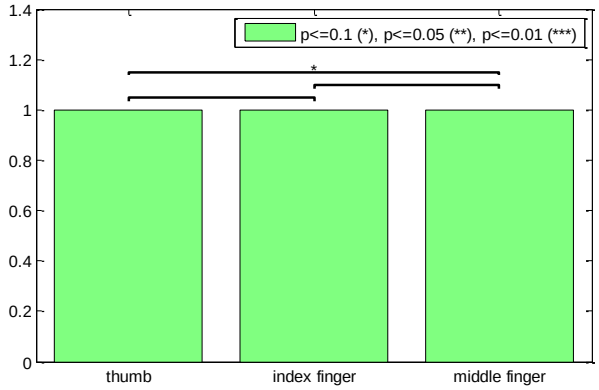

Figure 33: graphical representation *p*-values and significance levels of test person 1.

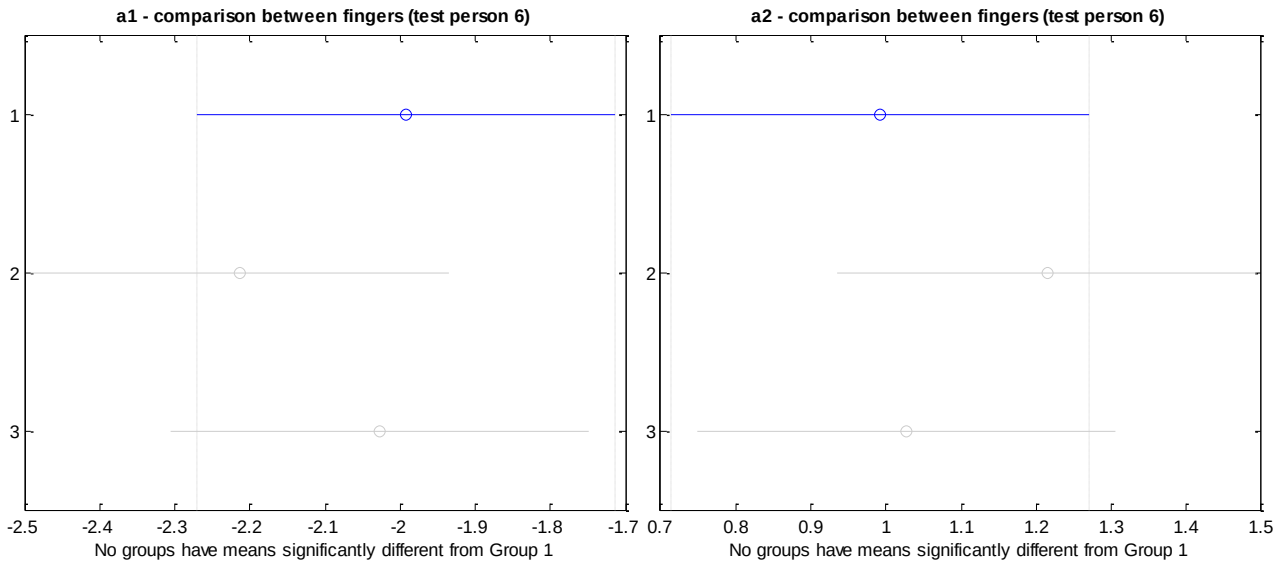

Figure 34: comparison of the means of the *α1*- and *α2*- parameters between fingers (thumb-index finger- middle finger) of test person 6. No significant differences between the means are found.

Other t-tests have been performed to investigate if the differences of the *α*-parameters between the same fingers of different persons are significant. It can be seen in figure 35 (for the index finger) and appendix A1 (for the thumb and the middle finger) that statistical differences can be found between the *α1*-parameters of four randomly assigned test persons. The group means of the *α1*-parameters of the index finger on the other hand don't show significant inter-person differences, as illustrated in figure 36. The multiple comparison of the group means of the thumb and the middle finger are given in appendix A1. The means of the *α1*-parameter of the thumb don't show significant differences, while the group means of a1 of the middle fingers differs significantly from the means of a1 of the middle finger of the other test subjects. This can also be noticed in figure A1.1, where the mean of this parameter is lower than the other means and a very small standard deviation can be seen.

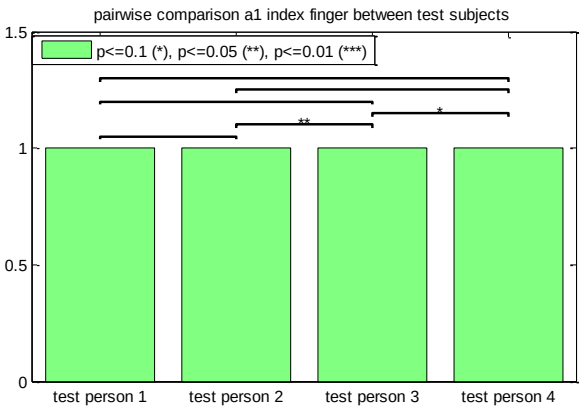

Figure 35: graphical representation p-values and significance levels between test persons 1, 2, 3 and 4. H_0 states that there are no significant differences between the index fingers of the test persons. This is rejected for 2 case on an 10% significance level.

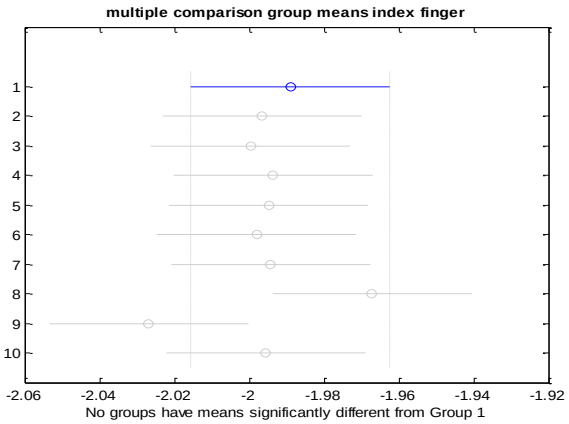

Figure 36: multiple comparison group means of *α1*-parameters of the index finger. No group means differ significantly from each other.

In table 11 and table 12 the division between the amount of b-parameters and the time-delays of all models is given as a function of the finger type. It can be seen that the amount of b-parameters and the time-delays are quite randomly divided between the fingers. No unambiguous conclusions regarding to the development of the transfer function can be drawn here.

# **b-parameters**	b_0, b_1	b_0, b_1, b_2	b_0,…, b_3	b_0,…, b_4	b_0,…, b_5	b_0,…, b_6	b_0,…, b_7	b_0,…, b_8
thumb	12	1	1	4	5	5	1	/
Index finger	4	4	4	7	8	3	/	1
Middle finger	3	3	4	11	7	2	/	/
Ring finger	/	5	2	/	3	2	1	/
Little finger	2	/	3	5	4	5	2	/
+ ------	21	13	14	26	27	17	4	1

Table 11: amount of b-parameters for each finger

Time-delay	1	2	3	4	5
thumb	13	2	1	8	5
Index finger	7	7	5	2	7
Middle finger	5	6	9	8	2
Ring finger	3	/	1	2	2
Little finger	3	1	9	5	7
+ ------	31	16	25	25	23

Table 12: time-delays for each finger

Frozen glove models

Also the a-parameters of the identified transfer function models for the data generated by the experiments with the Elasto-Gel® frozen gloves were subjected to a statistical analysis. In figure 37 the mean and standard deviation of the *a1*- and *a2*-parameters the index finger are shown for each test person. The values for the thumb are illustrated in Appendix A2. This figure indicates the variability between the three experiments performed by each test person and is an indication of the reproducibility of the transfer function model of the parameters. One person has been left out of consideration because she participated on only two experiments with the frozen glove because of cold intolerance. It can be noticed that the standard deviation of both parameters shows great correlation for each test person. In general, the standard deviations are higher compared to models developed for the tests with the onycholysis device. The overall mean and standard deviation of the *a1*- and *a2*-parameters are lower than the a-parameters of the transfer function of the device. The mean of a1 for the thumb is -1.9012 for the gloves models compared to -1.9924 for the device models. The mean of a2 for the frozen glove models is 0.9015 against 0.9924 for the device models for the thumb. The two parameters for the models of the index finger differ in the same order of magnitude between the frozen glove models and the device models. A two-sided t-test confirmed the statistical significance of this finding (e.g. p=0.0212 for the t-test between the *a1*-parameters of the thumb).

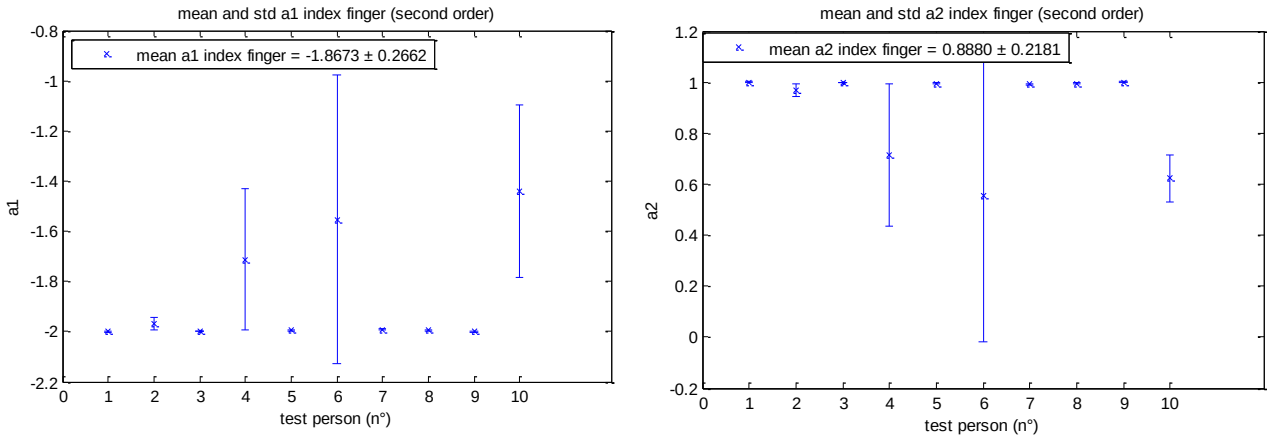

Figure 37: mean and standard deviation a1 (left) and a2 (right) of frozen glove model for each test person. Person 4, 6 and 10 show deviating values for both a1 and a2.

A two-sided t-test has also been performed to investigate the within subject variance of the model a-parameters between the fingers. No significant differences could be found between the index finger and the thumb on both the *a1* and *a2*-parameters, as was also the case for the device-model parameters.

In figure 38, a comparison of the *a1*-parameters of the frozen glove model for the index finger is made between four randomly assigned test subjects by a two-sided t-test. This comparison for the thumb is illustrated in appendix A2. For both the index finger and the thumb, significant differences could be found between the test subjects. This indicates that also for the frozen glove models, the inter-person variance between the a-parameters is higher than the intra-person variance, since for the last one no significant differences could be found. Also a multiple comparison of the means of the *a1*-model parameters for each test person has been performed. No significant differences are discovered between the means of the *a1*-parameters when all the test-persons are compared with each other, as illustrated in figure 39.

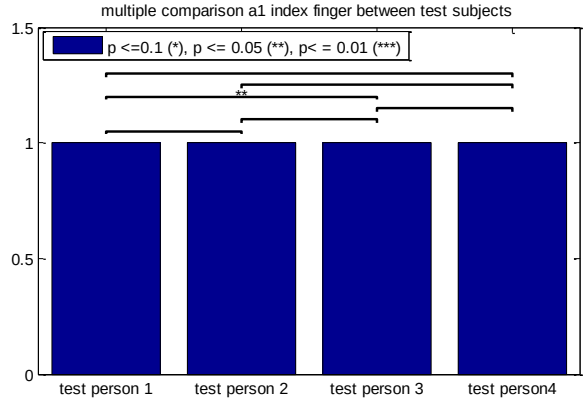

Figure 38: graphical representation p-values and significance levels between test persons 1, 2, 3 and 4. H_0 states that there are no significant differences between the index fingers of the test persons. This is rejected for 1 case on an 5% significance level.

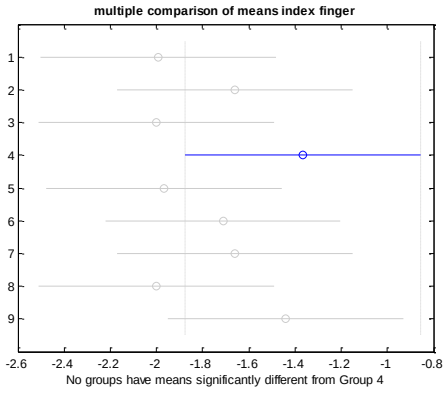

Figure 39: multiple comparison group means of *a1*-parameters of the index finger. No group means differ significantly from each other.

In one case, a first order transfer function model was far more appropriate to describe the finger tip temperature of the thumb during cooling with the Elasto-Gel® frozen glove. For the index finger, a first order model was more suitable in four cases. The mean and standard deviation for the thumb and index finger of the *a1*-parameter are illustrated in figure 40.

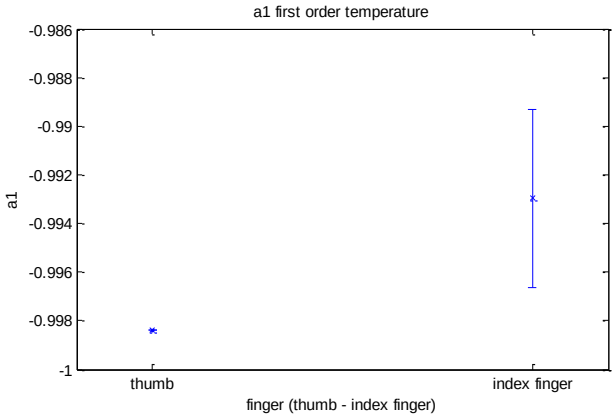

Figure 40: mean and standard deviation thumb and index finger a1 for the first order frozen glove models

In appendix 3, an inter-person comparison of the *a2*-parameters is given for the index finger for both the onycholysis device and the frozen glove models.

At last, a comparison between the a-parameters of the Elasto-Gel® frozen glove and the device has been made for the thumb and the index finger by a two-sampled t-test. The model parameters of the same fingers and the same persons are compared with each other. The *p*-values of this comparison are shown in table 13. Only a few persons showed significantly different model parameters between the models of the device and the glove. It is also remarkable that the *p*-values of both parameters always lie close to each other. This indicates that both parameters show a high correlation.

Test person (n°)	***p*-values**			
	Thumb		Index finger	
	a1	a2	a1	a2
1	0.3182	0.3181	0.6476	0.6498
2	0.9086	0.9222	0.3759	0.3758
3	0.0040	0.0040	0.8851	0.8696
4	0.0334	0.0376	0.1046	0.1045
5	0.3494	0.3254	0.3743	0.3748
6	0.2014	0.2014	0.1126	0.1123
7	0.2616	0.2614	0.1582	0.1585
8	0.4124	0.4127	0.0434	0.0430
9	0.3288	0.3292	0.3373	0.3369
10	0.2795	0.2795	0.2757	0.2756

Table 13: *p*-values for a-parameter comparison between frozen glove model and onycholysis device model for thumb and the index finger of 10 test persons. The H_0-hypothesis states that both the compared parameters come from independent random samples from normal distributions with equal means and equal but unknown variances. This is rejected in only three cases.

5. MECHANISTIC MODEL

5.1. Introduction

As a trial case, a mechanistic model has been developed to calculate the heat transfer and the effect of blood flow on the finger temperature evolution, and applied to the index finger. It was designed using the ANSYS® workbench and the ANSYS Fluent® software. This software contains physical modeling capabilities needed to model flow, turbulence, heat transfer, and reactions for industrial applications.

5.2. Theoretical basis and methods used

For each CFD (Computational Fluid Dynamics) calculation, the analysis is based on solving the mathematical representation of the conservation laws of physics, i.e.:

- The conservation of mass which means that during heat transfer and fluid flow no mass can be created or destroyed.
- Newton's second law: the rate of change of momentum is identical to the sum of the forces acting on the fluid (leading to the Navier-Stokes equation)
- First law of thermodynamics: this means that the rate of change of energy is identical to the net rate of heat added and the net rate of work done.

The laws of physics can be described by differential equations. In a computational analysis technique these governing equations are solved iteratively while using the appropriate boundary conditions for the specific problem analyzed. In the majority of the commercial packages this is done by employing a finite element or finite volume method. For most CFD calculations the latter is preferred as it uses less computational resources and computer processing power. The computational domain is subdivided into a number of contiguous control volumes over which the conservation of the physical properties is calculated using the integral form of the equation.

In an initial step the geometry of the finger was drawn in Designmodeler®, which is the drawing program present in the ANSYS® workbench. The index finger was conceptually designed as a tapered cylinder with a rounded head. On the surface of the finger, positions were designed for the presence of the Peltier elements. The geometry of the finger was meshed using the meshing device of ANSYS®. The mesh consisted out of a structured mesh except near the rounded tip where tetrahedral elements were used. As the mesh consisted of two types of elements the geometry was subdivided in connected volumes in order to enable this type of meshing. As the aim of the model was to

calculate heat transfer, boundary layers were inserted into the mesh allowing a more accurate calculation of the temperature gradient near the surface, as illustrated in figure 41. Also around the Peltier elements the mesh was further refined.

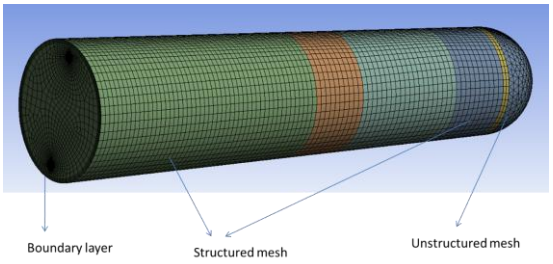

Figure 41: mesh structure on index finger. The unstructured mesh at the tip consisted of tetrahedral elements. The boundary layers at the surfaces allow a more accurate calculation of the temperature gradient near the surface

5.2.1. Temperature profile calculations

Boundary conditions

In an initial calculation, the heat transfer and the finger temperature evolution were calculated using the temperature set points for the Peltier elements as used during the experimental work and illustrated in figure 42. The settings of these experiments were slightly different compared to the earlier described test series, i.e. 100 s at 27°C, 500 s at 15°C and 1.800 s at 6°C. For some calculations the initial step was not applied and the setpoint of 15°C was extended to 600 s, starting at the beginning of the experiment.

The bottom half of the finger was assumed to be isolated as this part of the finger is stuck in the finger module of the device. The upper half of the finger is in contact with the air and here cooling of the finger by natural convection was assumed. At the intersection between the finger and the hand, a constant temperature of 37°C was considered (body temperature). The temperature at the fingertip, corresponding to the temperature measured by the temperature sensor of the device, is calculated, as shown in figure 43.

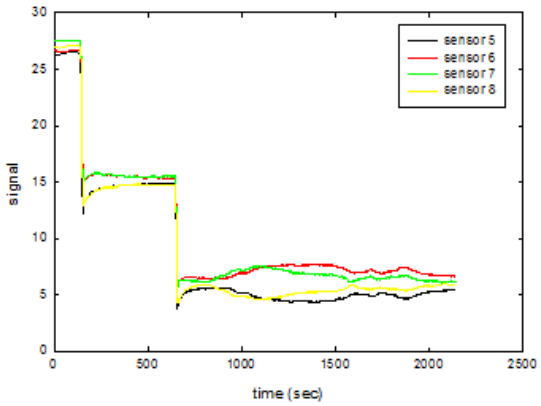

Figure 42: applied temperature profile on index finger

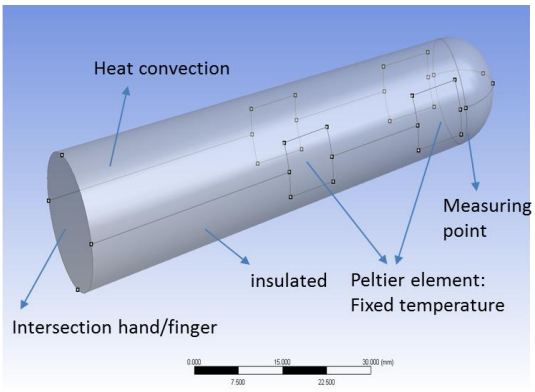

Figure 43: illustration of boundary conditions.

Physical interpretation – boundary conditions.

At the Peltier elements, heat (cold) is transferred to the finger through conduction. The transfer of heat by conduction can be described by Fourier's law, which states that heat flux is proportional to the temperature gradient. The Fourier equation which describes the heat flux through conduction has the following form:

$$\rho \cdot c \cdot \frac{\vartheta T}{\vartheta t} = k \cdot \left(\frac{\vartheta^2 T}{\vartheta x^2} + \frac{\vartheta^2 T}{\vartheta y^2} + \frac{\vartheta^2 T}{\vartheta z^2} \right) + Q$$

or

$$\rho \cdot c \cdot \frac{\vartheta T}{\vartheta t} = k\nabla \cdot \nabla \mathrm{T} + \mathrm{Q}$$

where k = thermal conductivity [W/m °C]

T = temperature [K]

t = time [s]

ρ=density [kg/m³]

c = heat capacity [J/kg °C]

q = heat flux [W/m²]

Q = volumetric heat generation [W/m³]

$\nabla = [\frac{\vartheta}{\vartheta x} \ \frac{\vartheta}{\vartheta y} \ \frac{\vartheta}{\vartheta z}]$

To be able to solve this differential equation, boundary and initial conditions need to be defined. The following possibilities may apply at the boundary *Γ* of the heated/cooled object:

- Fixed temperature (Dirichlet)

  T(x,y,z,t) = T_s at *Γ*, with T_s a known function
- Prescribed surface heat flux (Neumann)

  $k\nabla T \cdot \boldsymbol{n} = -q_s$ at *Γ,* with q_s [W/m²] a known function and **n** outward normal to surface
- Convection boundary condition

  $k\nabla \mathrm{T} \cdot \boldsymbol{n} = h(T_\infty - T)$ at *Γ,* with T_∞ fluid temperature of the surroundings and h the surface heat transfer coefficient [W/m² °C].

The initial condition that is applied is straightforward:

- T(x,y,z,t) = T_0(x,y,z) at t = 0

At the upper half of the finger, the finger makes free contact with the surroundings. It can be assumed that the finger is cooled by free/natural convection. Natural convection is driven by a density difference in the material. The transfer of heat by convection is described by:

$$q_{1-2} = hA(T_1 - T_2)$$

where A = area normal to the direction of heat flow [m²]

q_{1-2} = the heat flow rate from 1-2 [W]

$T_1 - T_2$ = temperature difference between surface and fluid [°C]

h = convective heat transfer coefficient [W/m² °C]

The value of h depends strongly on the type of convection (forced or free convection) and on the geometry of the system. In the case of the index finger, the convective heat transfer coefficient for a cylinder is appropriate, taking into account the similarities between the geometries. To calculate the convective heat transfer coefficient of a horizontal cylinder, the dimensionless Rayleigh number (Ra), Prandtl number (Pr) and Nusselt number (Nu) are required which are respectively calculated as follows:

- $\text{Ra} = \text{Gr} \cdot \text{Pr} = \frac{\beta \cdot \rho^2 \cdot g \cdot L^3 \cdot \Delta T}{\mu^2} \cdot \text{Pr} = \frac{\text{Buoyancy force}}{\text{Viscous force}}$
- $\text{Pr} = \frac{\mu \cdot c_p}{k} = \frac{\mu/\rho}{\alpha} = \frac{\text{Viscous effect}}{\text{Thermal diffusion effect}}$
- $\text{Nu} = \frac{h \cdot L}{k_{fluid}} = \frac{\text{Diffusive resistance}}{\text{Convective resistance}}$

where β = coefficient of thermal expansion [1/K]

g = acceleration due to gravity [m/s²]

L = characteristic length, which is the outside diameter of the cylinder [m]

ρ = density of the flow [kg/m³]

μ = viscosity of the fluid [kg/m·s]

ΔT = temperature gradient [K]

c_p = specific heat [J/kg K]

k = thermal conductivity [W/mK]

α = thermal diffusivity [m²/s]

For a flow over a cylinder, the following correlation is valid:

$$Nu = 0.54 \cdot Ra^{1/4} \text{ for } 10^5 < Ra < 2 \cdot 10^7$$

5.2.2. Modelling the blood flow

In order to calculate the effect of blood flow on the temperature profile a blood channel has been inserted into the index finger. The blood channel was assumed to be U-shaped with inlet and outlet at the intersection between finger and hand. Around the channel, the mesh has been refined gradually. For the Peltier elements the same temperature profile as described above has been used. In order to evaluate the effect on the temperature at the tip of the index finger, different positions of the channel (rotated around the z-axis) and different flow rates have been modeled, as shown in figure 44.

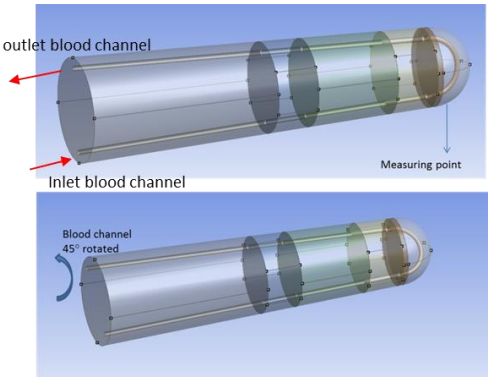

Figure 44: blood channel incorporated in index finger (top). In the bottom figure, the blood channel is rotated around the z-axis by 45°.

The flow of (viscous) fluid can be described by the Navier-Stokes equation. Using this equation, the velocity distribution of blood flow inside a blood channel can be derived. As the flow through the small arteries is assumed to be relatively low combined with a high viscosity, it can be considered as laminar. The geometry is cylindrical. As such the Navier-Stokes equation can be simplified to the Hagen-Poiseuille equation. The boundary condition which is applied is a non-slip condition with a zero velocity at the wall surface of the artery ($v_z|_{r=r0} = 0$). The velocity at a certain radius of a straight cylindrical channel is given by:

$$v_z(r) = -\frac{r^2}{4\eta}\frac{\Delta P}{L}(r_0^2 - r^2)$$

Hence, a parabolic velocity profile is obtained.

The flow rate can then be derived from the equation above:

$$\Phi = \int_0^{r_0} v dA = 2\pi \int_0^{r_0} v_z r dr$$

$$\Phi = \frac{\pi}{8\eta}\frac{\Delta P}{L} r_0^4$$

In this simulation, only a steady flow is considered. However in reality, a more pulsatile (oscillating) flow is obtained. Blood pressure and flow vary with time over the period of heart relaxation and contraction in an oscillatory way. During the systole phase of heart contraction, where the heart chambers contract and blood is ejected into the aorta and the pulmonary artery, the left ventricular pressure rises from 5 to 120 mmHg in about 0.2 seconds and aortic pressure rises from 80 to 120 mmHg. During the diastole, which is the filling phase of the heart, the reverse phenomenon occurs. These pressure and velocity pulses change with distance from the heart. The pulse width broadens and the maximum pressure declines with increasing distance from the heart. Considering the time frame of the heat transfer calculation the flow pattern can be assumed to remain flat and constant. (Nicolaï, B., 2014), (Datta, A. K., 2002)

5.3. Results and discussion

Boundary conditions

Firstly, the physical properties and dimensionless Rayleigh *Ra* and Nusselt *Nu* numbers have to be determined.

Assuming air to be an ideal gas, β can be approximated by 1/T. For an air temperature of 18°C (measured temperature in the testing room) this means that β is:

$$\beta = 1/291K$$

For an ideal gas, ρ is given by $P/(R_gT)$, where P is the pressure and R_g the gas constant. Using tables of thermal properties of gases, the density of air at 18°C can be calculated from linear interpolation:

$$\rho_{291} - \rho_{290} = (\rho_{300} - \rho_{290})/(T_{300}-T_{290}) \cdot (T_{291}-T_{290})$$

The characteristic length of a system for heat transfer can be interpreted as the path of least thermal resistance for the geometry of concern, in this case the length of the finger. The measured length of the finger was 74 mm (=L).

The temperature difference is the difference of temperatures between the bulk fluid and the finger surface. The temperature of the bulk fluid is 18 °C (291 K) and the temperature of the surface of the finger was assumed to be the same as the body temperature, in this case 37°C (310 K).

The viscosity of the fluid, in this case air at 291 K, can also be calculated by linear interpolation using the tables of thermal properties of gases. This approach has also been applied for the thermal diffusivity and the thermal conductivity.

The numeric values for the physical properties are summarized in table 14.

Physical quantity	***value***
β [1/K]	1/291
ρ_{291} [kg/m³]	1.21
g [m/s²]	9.81
L [mm]	74
$\Delta T=T_s-T_f$ [K]	19
μ_{291} [kg/m.s]	$1.79.10^{-5}$
α_{291} [m²/s]	$2.09.10^{-5}$
k_{291} [W/m.K]	0.0255

Table 14: physical properties of air

Using these values of the parameters (table 1), the Rayleigh number can be calculated:

$$Ra = \frac{\beta \cdot \rho^2 \cdot g \cdot L^3 \cdot \Delta T}{\mu^2} \cdot \frac{\mu/\rho}{\alpha} = \frac{\beta \cdot \rho \cdot g \cdot L^3 \cdot \Delta T}{\mu \cdot \alpha} = 8.39 \cdot 10^5$$

Using the calculated Rayleigh number, the Nusselt-number is determined as:

$$Nu = 0.54 \cdot Ra^{1/4} = 16.34$$

Out of the Nusselt number, the convective heat coefficient of a cylinder *h* can be derived:

$$Nu = \frac{h \cdot l}{k_{fluid}} = 16.34 \text{ or } h = \frac{Nu \cdot k_{fluid}}{l} = 5.64 \text{ W/m.K}$$

Material properties

Besides the boundary conditions there is also a need to define the material characteristics. For the calculations carried out here, the physicological properties of the biological materials are summarized in table 15 and 16. These are not absolutely correct and are a simplification of the real values. In order to allow a more in depth study the exact physical properties of all components constituting a hand or a finger need to be determined.

Physical parameter hand substance	*Numerical value*
Thermal conductivity k [W/mK]	0.568
Heat capacity c_p [J/kgK]	3184
Density [kg/m³]	1050

Table 15: physiological properties of hand tissue

Physical properties blood	*Numerical value*
Viscosity (Pa.s)	0.0018
Density (kg/m³)	1060
Heat capacity c_p [J/kgK]	3617
Thermal conductivity [W/mK]	0.57

Table 16: physiological properties of blood

During the calculation the temperature on the fingertip was monitored (transient behavior) at a same position compared to the location of the thermocouple in the experiments.

5.3.1. Calculated temperature profiles without blood flow

In the initial step, a sensitivity analysis on the heat transfer calculation has been carried out without the presence of blood flow. Parameters which have been investigated were the heat transfer coefficient, the position of the Peltier elements relative to the location of the thermocouple, the relative size of the Peltier elements and the initial temperature of the skin.

Without showing all the results of these calculations, figure 45 gives an overview of the effect of some of these variables. The figure shows the measured temperature profile compared to the calculated values. The measured temperature profile shows a stepwise decrease of the temperature resulting from the applied temperature profile.

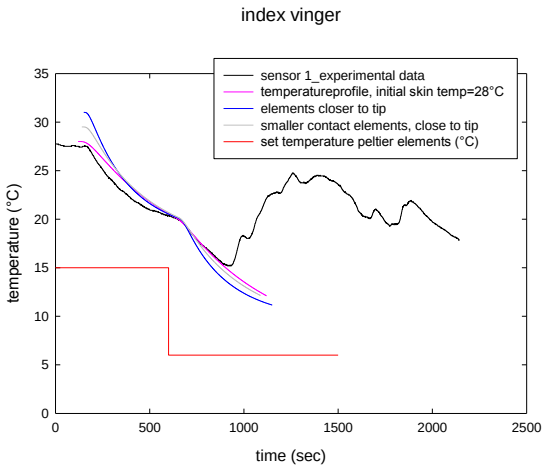

Figure 45: calculated temperature evolution without blood flow. The simulated data approaches the experimental data very good.

The calculated values are in good agreement with the measured values. The best results are obtained when an initial skin temperature is set as the average of the body temperature (37 °C) and the room temperature (18°C). Decreasing the distance between the Peltier elements and the monitoring point leads to a faster drop of the temperature, as can be expected. This is also valid for a larger size of the Peltier elements although to a smaller extent. The exact size of the Peltier element in contact with the finger is difficult to determine as the cooled skin is actually the flatted surface of the finger against the Peltier element, which will actually depends on the diameter of the finger to be modelled.

In the experiments, at a time of 1000 seconds, an increase in temperature is noticed. This is induced by an increase in blood flow through the finger when the temperature drops to a too low value. In order to evaluate this effect, blood flow has been included into the model.

5.3.2. Calculated temperature profiles including blood flow

Figure 46 shows the calculated flow pattern of blood through the artery. The colour scale indicates that the blood flow is parabolic in the straight parts of the tube but a deviation is observed in the U turn, where the blood flow changes in direction. This is even more obvious when plotting the velocity magnitude over the width of the channel which shows a skewed profile in the middle of the U-turn with a higher flow density towards the outside of the artery, as illustrated in figures 46 and 47. It was already mentioned that, in a straight channel the flow is described by the Hagen-Poiseuille equation. However, this is not valid anymore when the flow changes in direction. In the arch, the highest velocity is obtained at the outside of the curvature due to the influence of the centrifugal forces on the blood flow, tending to push the flow outward.

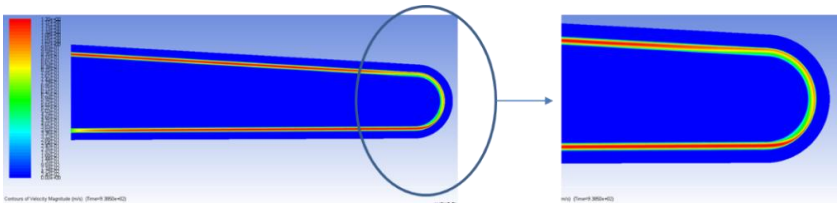

Figure 46: blood flow velocity profile in the artery. A parabolic velocity profile is obtained in the straight parts of the tube. In the U-turn, the velocity is higher at the outside of the artery due to centrifugal forces.

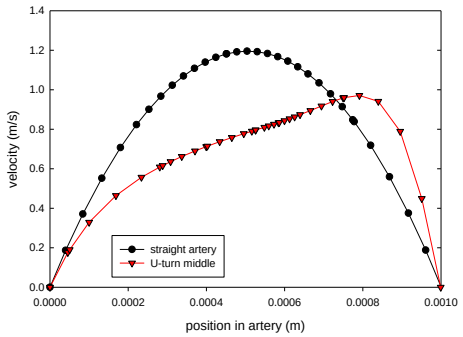

Figure 47: Skewed velocity pattern in U-turn

To describe the motion of blood in the U-turn of the vessel, where also centrifugal forces interact with the blood flow, a more advanced equation is needed. Next to fluid motion in the axial direction, inertial forces push fluid towards the outer wall, generating fluid motion in radial and angular directions. As a reaction of the fluid pushing toward the outer wall of the blood vessel, a secondary force arises that moves fluid away from the wall. The flow in a curvature depends on the internal radius *a* of the blood vessel and the radius of curvature *R*. The Dean number De (W.R. Dean (1927)) is a non-dimensional parameter which determines the nature of secondary flows in curved pipes. It is defined as:

$$De = 2 \cdot \sqrt{\delta} \cdot Re$$

with δ = a/R where a is the internal radius of the pipe and R is the radius of curvature.

$Re = \frac{\bar{u} \cdot a}{\mu}$, the Reynolds number where $\bar{u}$ is the mean axial free stream velocity in the pipe.

In figure 48, the effect of the Dean number on secondary flow pattern can be seen. A low Dean number results in only a slight distortion due to curvature. The contours of constant axial velocity in a cross section are roughly circular, indicating a nearly parabolic velocity profile. On the other hand, a high Dean number results in more skewed iso-velocity contours. In this case, a numerical solution of the Navier-Stokes (Hagen-Poiseuille) equation is required.

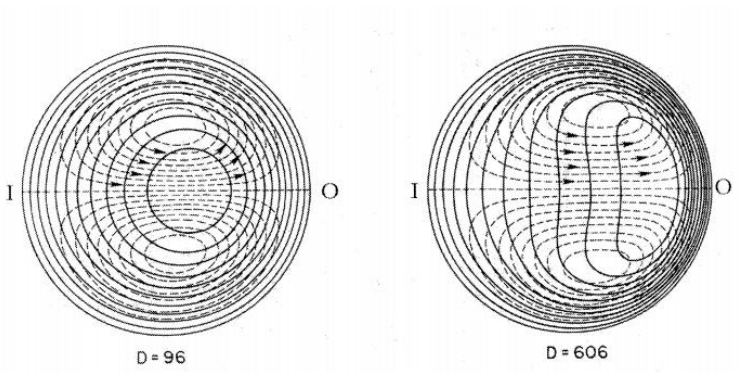

Figure 48: Effect of Dean number on flow pattern. The higher the Dean number, the more profound the secondary flow pattern.

The calculated effect of the blood flow on the temperature is shown in figure 49. The initial skin temperature for these calculations was assumed to be 37°C. This temperature was also assumed as being the blood temperature at the entrance of the artery. The blood flow was initiated at a time of 900 seconds. At a slightly later stage, due to the thermal inertia, an increase in temperature at the fingertip is noticed. The rate of increase not only strongly depends on the exact position of the artery vs the monitoring point but also on the blood flow. Decreasing the distance between the position of

the artery versus the thermocouple position and/or increasing the blood flow increases the rate of change of the temperature monitored.

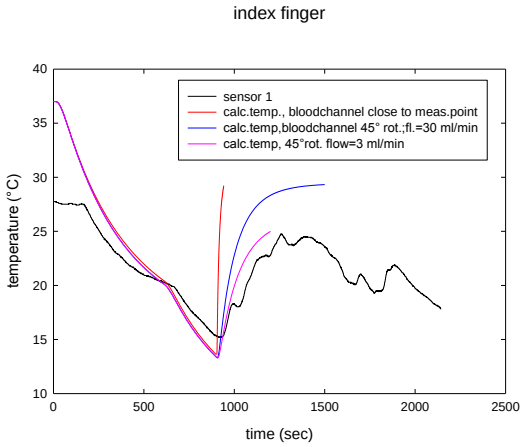

Figure 49: Effect on blood flow on temperature increase. The best simulation was obtained for a flow rate of 3 ml/min and the channel 45° rotated around the z-axis.

In figure 50, the effect of stopping the flow through the artery, in case of a flow of 3 ml/min, is modelled. As can be noticed, when the flow stops, the temperature starts to drop again in a way which is correlating quite well with the experimental results.

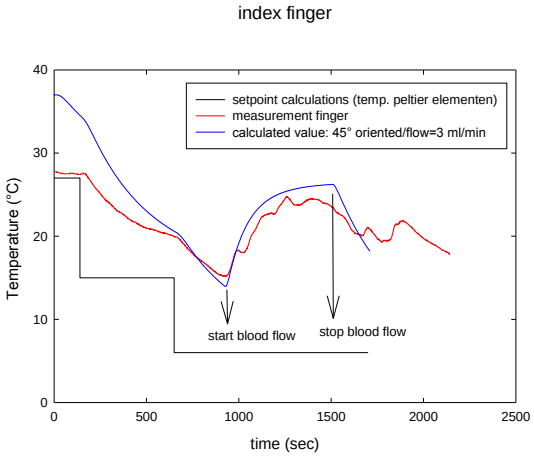

Figure 50: Temperature effect after ceasing the blood flow. The temperature drop correlates well with the experimental results.

The mechanistic model can be considered as a first approach for explaining and monitoring the skin temperature when using the Peltier elements as a cooling device. Phenomenologically, the initial temperature decrease induced by the Peltier cooling, and the subsequent increase resulting from the induced blood flow, followed by another temperature decrease due a reduction in flow can be explained. However, assumptions had to be made on the position and shape of the artery and on the flow rate in order to fit the experimental data. In order to develop a more accurate model, specific knowledge on these parameters has to be acquired. In a more advanced model the blood flow could

be made dependent on the temperature which would enable to model the oscillations in skin temperature as observed in the experimental data.

5.3.3. Heat transfer model for the glove

Next to the heat transfer model for the cooling of the hand induced by the Peltier element and the associated blood flow, also a heat transfer model for the glove system has been developed. The aim of the model is to evaluate which physical phenomena drive or influence the temperature change of the glove. The model as well as the experimental verification demonstrates that the temperature within the glove increases quite fast, even in the absence of a hand inserted in the glove, limiting the time period of the treatment.

For the development of the model, the hand was replaced by an insulating material separating the upper part and the lower half of the glove. The computed data have been compared to experimental data generated using the same set-up as the one which has been modelled.

For the experimental verification of the model a glove was stored in a refrigerator (at -18°C to -21°C) for a number of hours (4 to 6 hours). Subsequently, the glove was placed on the table with an isomo® insert and with a thermocouple positioned between the isomo®® and the glove. In two different experiments, the thermocouple was positioned either between the upper part of the glove (above the isomo®) or the lower part (below the isomo®) and the gel-like substance making up the glove. These experiments allow to separate the effect of conduction and convection on the temperature increase. When the glove is positioned on the table the mean heat transfer mechanism for the lower part consists of conduction of heat from the table diffusing into the glove. At the upper part the glove is mainly surrounded by air, hence the main heat transfer mechanism consists of natural convection. In both cases some heat is also coming from the isomo® but this effect can be neglected due to the limited mass of the insulating material. The experimental set-up is illustrated in figure 51.

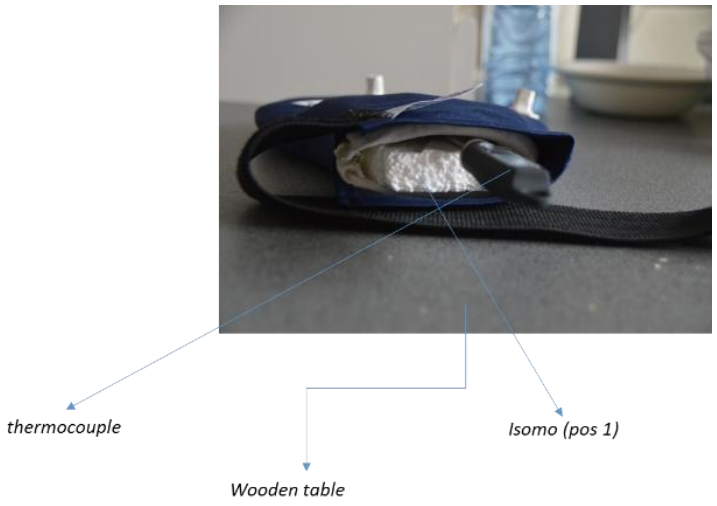

Figure 51: experimental set-up for temperature evolution measurement in the glove

The equations which are to be solved in this model are similar as for the abovementioned model for the finger cooling, except that no blood flow has been considered here. As such this model is limited to solving the heat transfer equation.

The glove itself consists of a thin nylon tissue which protects a crosslinked gel consisting of water (35%) and glycerine (65%). The physical properties used in the calculation for the nylon, the isomo® insert and the gel material are listed in table 17.

Property	Gel	Nylon	wood	isomo®
Specific heat c_p (kJ/kgK)	2.97	1.70	2.31	1.45
Thermal cond. k (W/mK)	0.46	0.25	0.173	0.035
Density (kg/m³)	1170	1150	700	40
Thickness (mm)	9	0.5	36	20

Table 17: physical properties glove material

The meshed model geometry is shown in figure 52. For the calculation it was assumed that the bottom half of the glove remains flat while the upper part follows the shape of the insert. In order to allow a more accurate calculation the mesh size was small with the presence of boundary layers at positions where large temperature gradients are to be expected.

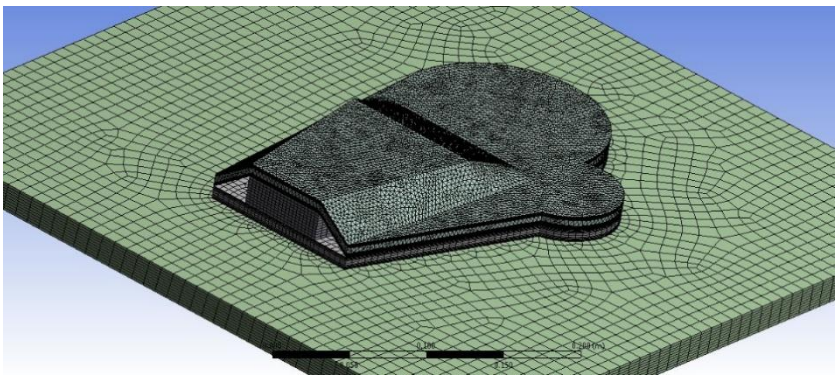

Figure 52: mesh of the glove with insert

In a first model the isomo® insert was omitted and only the glove was considered. Schematically the boundary conditions are illustrated in figure 53. The temperature was calculated at the inside of the glove, at the interface between the upper and the lower part. The heat transfer coefficient h was assumed to be 5 W/mK.

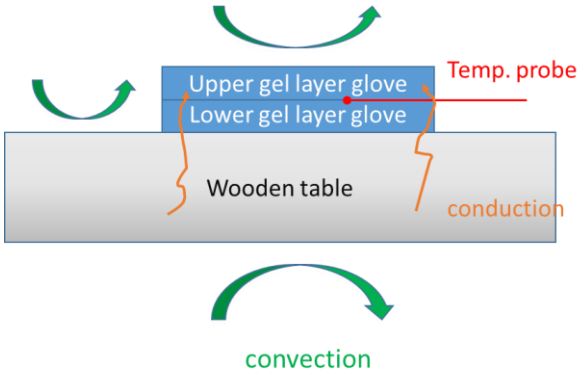

Figure 53: boundary conditions for calculation heat transfer of the glove. The mean heat transfer mechanism for the lower part consists of conduction of heat from the table diffusing into the glove. At the upper part the glove is mainly surrounded by air, hence the main heat transfer mechanism consists of natural convection.

The evolution of the temperature on a cross section of the glove, for an air temperature of 21°C and an initial glove temperature of -13°C is illustrated in figure 54. At the start of the calculation (time =0 min) the glove is cold while the table has a much higher temperature, identical to the temperature of the surrounding air. As the heat transfer process starts it is clear that the glove starts to warm up, clearly driven by a transfer of heat from the table towards the glove, rather than a transfer of heat coming from the surrounding air. This can be derived from the fact that largest colour change occurs at the interface between the table and glove.

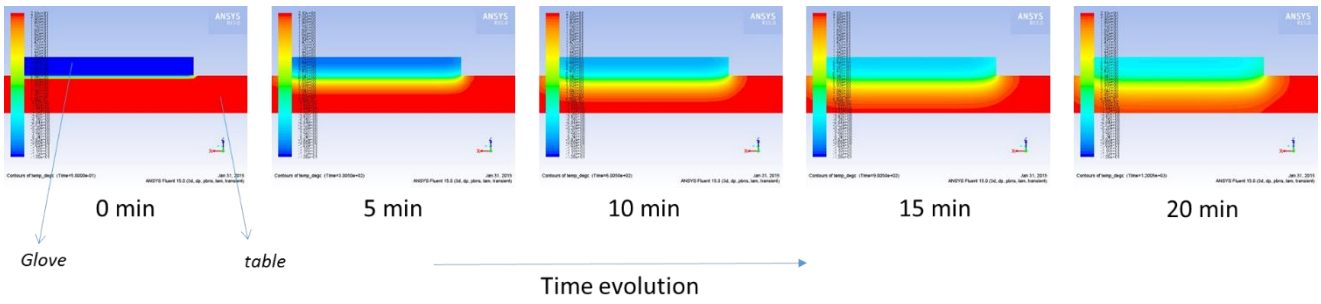

Figure 54: Temperature evolution of the glove supported on a table. Especially conduction induces warming of the glove during the first 20 minutes.

In order to separate both contributions, experiments and model calculations have been carried out, as described above and illustrated in figure 55.

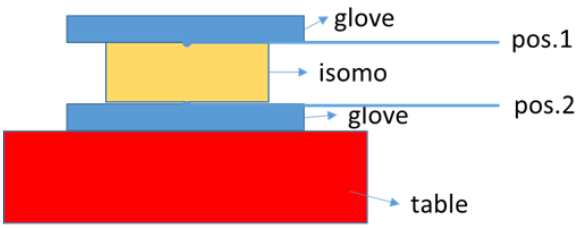

Figure 55: Scheme for experimental set-up for glove with insert

The experimental data show that the temperature evolution strongly depends on the measurement position in the glove, as illustrated in figure 56. The temperature measured below the isomo® insert increases much faster than the temperature measured above the glove, confirming that the heat conduction from the table to the glove is the dominating process determining the temperature change of the glove. After 50 min both temperature curves show a crossover point and the heat convection process becomes more important. The figure also indicates the good correlation between the experimental data and the model calculations. The latter have been carried out for different values of the heat transfer coefficient. As could be expected the calculations carried out for the temperature below the insert are hardly influenced by the heat transfer coefficient as the dominating mechanism is conduction. The temperature values above the insert are strongly influenced by the transfer coefficient. The best correlation between experiment and model are obtained for an h-value of 7 W/MK which is higher than the expected value for natural convection. However the slope of the temperature change shows the best correlation when using an h-value of 5.5 W/mK, which is close to the value for natural convection. Hence, the best correlation between the theoretical prediction and experimental values is achieved when using an h-value of 5.5 W/mK but starting from a slightly higher initial temperature. The latter depends on the storage time of the glove in the refrigerator.

The main conclusion of the modelling work on the glove confirms the experimental observation that the fast initial temperature increase of the glove can be explained by the heat conduction from the supporting table towards the glove while heat convection becomes more important at longer time scales. The value for the time scale decreases when the heat transfer coefficient becomes higher, for instance induced by an air conditioning system.

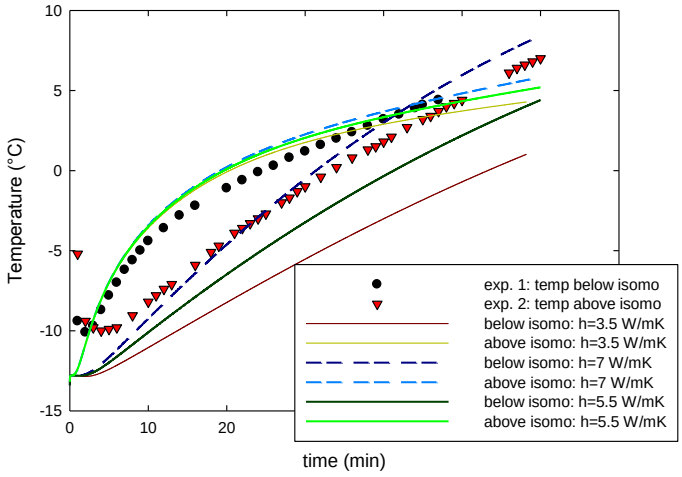

Figure 56: Comparison temperature increase values: model and experimental data. On short term, conduction is the most important mechanism of warming the glove. After about 40 minutes, convection becomes more important.

From both experimental results and the numerical model on the temperature increase of the glove it is obvious that the major mechanism is the heat conduction from the supporting table to the lower part of the glove. The effect of natural convection on the temperature change is much less pronounced.

As such a potential remedy to increase the duration of the treatment might be to position the glove on an actively cooled table which could even induce a cold stream towards the glove. In the latter case this could allow to increase slightly the initial temperature of the glove which could help to keep the treatment more tolerable. (Zarandi, 2000) (Nicolaï, B., 2014) (Holmes, 2015) (Jiyuan et al., 2008)

6. General Conclusion

The ultimate goal of this work was the development of a real-time model-based control system to control the blood flow to the patient's fingers. Experiments were carried out using a Peltier-cooling device, developed at the University of Antwerp, as well as with frozen Elasto-Gel® gloves. A test group of eleven females of 35 – 55 years old participated in the series of experiments. The skin temperature at the tip of the 5 fingers of the left hand has been measured, together with the blood flow in the thumb and index finger. Based on preliminary experiments and on measurements carried out last year at the University of Antwerp, the cooling temperature of the device was set at 2°C, since a significantly more profound effect of cooling is obtained compared to cooling at 6°C and 10°C. The measured temperature profiles all show a typical hunting phenomenon, i.e. a steep decrease in temperature shortly after the cooling has been started, but after a certain time, an increase in temperature is recorded, again followed by a another decrease etc. The blood flow also shows a similar pattern. Moreover, it has been found that the temperature increase occurs with a small delay compared to the increase in blood flow. These phenomena have been observed for both the onycholysis device as well as for the frozen gloves, indicating that this phenomenon cannot easily be avoided. All test subjects reported that the device is much more comfortable and tolerable compared to the gloves, stimulating the further development of the equipment.

For all 65 experiments performed on the group of test subjects, a data-based model has been developed for the finger skin temperature at the fingertip during active cooling. It was found that a second-order transfer function model was suitable (R^2 = 0.9120 ± 0.1178) to model the dynamic responses of the fingers' skin temperatures. Both confidence intervals of the parameters and pole-zero plots validated this model structure. Based on these models, a Proportional-Integral-Plus (PIP-) controller could be developed. This work mainly focuses on the development of the controller for only the index finger of the test-persons, but the algorithm used can easily be applied on the other fingers as well. It has been opted to choose a fixed value for the time delay i.e. 1, and a fixed amount of b-parameters, i.e. 2, since these parameters show a great variability among the different models. This resulted in the following form of the transfer function:

$$TF = \frac{b_1 z^{-1} + b_2 z^{-2}}{1 + a_1 z^{-1} + a_2 z^{-2}}$$

A Monte-Carlo analysis of the designed control system was implemented with 50 simulations for testing the robustness of the developed controller against parameter perturbations. Besides, root-locus plots indicating stability were created. These clearly show the importance of the use of an appropriate model for developing the controller. However, the controller was only stable for a

narrow range of b2-parameters [-0.1518; -0.0394]. Hence, future research will be necessary to develop controllers for other time-delays and/or other amounts of b-parameters to determine stability ranges for the parameters of these transfer functions. The obtained results already show the need for on-line retuning of the model parameters and the consequent retuning of the controller.

Statistical analyses on the parameters of the discrete-time transfer function models, including intra- and inter-subject analyses, have been performed for both the models developed for the data generated with the device and with the Elastogel® frozen gloves. The intra-subject analysis focuses on the variance of the a1- and a2-model parameters between the different tests and the different fingers of the left hand of the same test person. Two-sample t-tests and multiple comparisons of the means using one-way ANOVA don't show significant differences between the experiments and between the fingers for all test persons. This holds for both the Peltier-device and for the glove. The inter-person analyses highlight the differences between the parameters of the models for the same fingers of the different test persons. Statistically significant differences can be found between the a1- and a2-parameters. On the other hand, the means of the a-parameters of the thumb and the index finger don't show significant inter-person differences. This is valid for both the onycholysis device model parameters and the frozen glove model parameters.

At last, the a-parameters of the onycholysis device-models are compared with the a-parameters of the frozen glove-models. Based on the obtained p-values, the H_0 –hypothesis stating that both parameter samples come from distributions with equal means and equal but unknown variances can be rejected. The overall differences of the means of the parameters for different fingers but for the same cooling method are small. This makes it possible to get an estimate of the mean values of the a1- and a2-parameters (respectively 1 and -2) for the device and for the frozen glove (respectively 0.9 and -1.9).

P-values	a1(device) -a1 (frozen glove)	a2(device) – a2(frozen glove)
Thumb	0.0212	0.0066
Index finger	0	6.1388e-04

Table 18: *P*-values comparison *a1*-and *a2*-parameters of onycholysis device- and frozen glove models. The H_0-hypothesis stating that both the compared parameters come from independent random samples from normal distributions with equal means and equal but unknown variances is rejected for all comparisons made.

No significant differences between the a-parameters of the models for the frozen gloves and the index fingers were found within subjects.

As no significant differences are found between fingers of the same person, for the implementation of the device, only one finger of a patient needs to be monitored during active cooling.

Next to the development of a data-based model, also a mechanistic model has been developed for predicting the finger skin temperature. This model should help to get a better physical insight into the phenomena influencing the temperature change of the skin. In a first step, the blood flow inside the finger was assumed to be zero, since vasoconstriction occurs during cooling. Cooling of the fingertip is the result of only conduction at the Peltier-elements and natural convection through the surrounding air. After a certain time period, when the fingertip temperature was assumed to be at its minimum value, blood starts to flow through the finger and this results almost immediately in an increase in the fingertip temperature. An opposite effect is noticed when the blood flow stops again. The results simulated by the mechanistic model describing this phenomenon show a high similarity ($R_T^2 = 0.9757$) with the experimental results.

Besides, also the temperature change of the Elasto-gel® frozen glove has been modelled using a mechanistic approach. It has been shown that, initially in the process, the main physical process contributing to the warming of the glove is heat conduction from the table. This finding can be helpful to prevent early warming up of the gloves by reducing this phenomenon. A potential remedy to increase the duration of the treatment and to make the treatment more tolerable could be to position the glove on an actively cooled table.

In conclusion, it is important to indicate that it is worthwhile to continue working on the developed models since it has been proven that it is possible to develop a controller which adjusts the cooling temperature during the treatment in order to restrict the blood flow as much as possible. To improve the data-based model, it is suggested to collect more data on a more heterogeneous test group, including men, people with different profiles (e.g. people working in cold environments, doing manual labor, …) and to search for an improved blood flow measurement technique.

The statistical analysis shows that, in general, there is a high correlation between the models developed for the same person. The inter-person differences between the transfer function parameters are more significant. Also the cooling method (onycholysis device vs Elastogel® frozen gloves) plays a significant role in the determination of the parameters. Future research should focus on finding a better consistency in the time-delays and the amount of b-parameters since no unambiguous conclusions could be drawn for these factors while they play a major role in the model –and controller development. Besides, also the cost regarding the fit of the data and parameter estimation accuracy of applying a first-order model should be investigated. Yet, a first order model is easier to implement in the control algorithm and as only one a-parameter is present, it reduces the risk of parameter perturbations.

The initial attempts on the mechanistic model already provided a very good insight in the occurring physical phenomena, but further research is needed to determine the exact physical properties. This

should allow to apply the model for predictive calculations. The model for the glove has to be extended to describe the real situation with the hand inserted in the glove. The use of a 3D-scan of the hand should be helpful in this case. In order to further validate the model, it might also be useful to compare the findings of the mechanistic model with scientific research on living organisms, like for example investigating the effect of local cooling on the blood flow by tracer techniques.

Bibliography

BREED, W. P. M., VAN DEN HURK, C. J. G., PEERBOOMS, M., "Presentation, impact and prevention of chemotherapy-induced hair-loss: scalp cooling potentials and limitations*"* in: *Expert Rev. Dermatol*. 2011 (6) nr. 1, pp. 109-125

BRIERS, J. D., WEBSTER, S., Laser speckle contrast analysis (LASCA): "A nonscanning, full field technique for monitoring capillary blood flow" in: *Journal of Biomedical Optics* 1996 (1), pp. 174-179.

CAN, G., AYDINER, A., CAVDAR, I., "Taxane-induced nail changes: Predictors and efficacy of the use of frozen gloves and socks in the prevention of nail toxicity" in: *European Journal of Oncology Nursing* 2012 (16) nr. 3, pp. 270-275

CIASTKO A.R., "Onychomadesis and Kawasaki disease", in: *CMAJ*, 2002 (16), pp. 1069

DAANEN, H. A. M., "Finger cold-induced vasodilation: a review" in: *Eur. J. Appl. Physiol.* 2003 (89), pp. 411 – 426

DAANEN, H. A. M. "Cold-induced vasodilation". *European Journal of Applied Physiology* 2009 (105) nr 4 , pp. 663-664

DAANEN, H. A. M., Layden, J.D., "Reply to A. D. Flouris and S. S. Cheung reply letter regarding "cold-induced vasodilation" ". *European Journal of Applied Physiology* 2010 (108) nr 1, pp. 215-216

DATTA, A. K., (2002), Biological *and Bioenvironmental Heat and Mass Transfer*, CRC Press

DE ALMEIDA, S.M., OSTERNACK, T.M., "Images in clinical medicine. Melanonychia striata" in *The New England journal of medicine*, 2011, (364) nr. 11, pp.e22

FARLEX, I. 2014, denervation hypersensitivity. Retrieved op 12 5, 2014, van The Free Dictionary: http://medical-dictionary.thefreedictionary.com/denervation+hypersensitivity

FERLAY, J., et al., "Cancer incidence and mortality patterns in Europe: Estimates for 40 countries in 2012" in: *European Journal of Cancer* 2013 (49) nr. 6, pp. 1374-1403

FLOURIS, A. D. WESTWOOD, D. A., MEKJAVIC, I. B., CHEUNG, S. S., **"**Effect of body temperature on cold induced vasodilation", *Eur. J. Appl. Physiol*. 2008 (104), pp. 491–499

FLOURIS, A. D., CHEUNG, S. S., "Influence of thermal balance on cold-induced vasodilation" in: *Journal of Applied Physiology* 2009 (106) nr. 4, pp. 1264-1271

FOX, R. H., WYATT H. T., "cold-induced vasodilatation in various areas of the body surface of man", in: *The Journal of physiology*, 1962 (162), 99.289-297

GHETTI, E., PIRACCINI, B. M., TOSTI, A., "Onycholysis and subungual haemorrhages secondary to systemic chemotherapy (paclitaxel)" in: *J. Eur. Acad. Dermatol. Venereol.* 2003 (17) nr. 4, pp. 459-460

GILBAR, P., HAIN, A., PEEREBOOM, V., "Nail toxicity induced by Cancer Chemotherapy" in: *J. Oncol. Pharm. Practice* 2009 (15) nr. 3, pp. 143-155

GILBERT, S., 2014, *Taxanes - Mechanism of Action*. Retrieved op April 2014, 08, van Toxipedia.org: http://www.toxipedia.org/display/toxipedia/Taxanes+-+Mechanism+of+Action

HAYASHI, T., et al, "Phase II Clinical Study of Protection of Nail Change and Skin Toxicity by Using a Frozen Glove in Japanese Patients with Early Breast Cancer Treated by Docetaxel and Cyclophosphamide" in: *J. of Cancer Research* 2009 (69), pp. 1916-1930

HINDS, G., THOMAS, V. D., "Malignancy and Cancer Treatment-Related Hair and Nail changes" in: *Dermatol. Clin.* 2008 (26) nr. 1, pp.59-68

HOFFMAN, R. G., WITTMERS, L. E., "Cold vasodilatation, pain and acclimatization in arctic explorers" in: *Journal of Wilderness Medicine* 1990 (1), pp. 225-234

HOLMES, K. 2015, *Thermal Properties*. Retrieved op 11 25, 2014, van Electro-Thermal Bioinstrumentation Laboratory: http://users.ece.utexas.edu/~valvano/research/Thermal.pdf

HONG, Junshik *et al*., "Nail Toxicity after Treatment with Docetaxel: A Prospective Analysis in Patients with Advanced Non-small Cell Lung Cancer" in: *Jpn J. Clin. Oncol.* 2007 (37) nr. 6, pp. 424–428

HOWSTUFFWORKS, I. D., 2014, *How Blood Works*. Retrieved op 10 22, 2014, van How Stuff Works: http://health.howstuffworks.com/human-body/systems/circulatory/blood2.htm

HUSSAIN, S. *et al.,* "Onycholysis as a complication of systemic chemotherapy: Report of five cases associated with prolonged weekly paclitaxel therapy and review of the literature" in: *Cancer* 2000 (88) nr. 10, pp. 2367-2371

INSTITUTE, N. C., 2006, *Common Terminology Criteria for Adverse Events v3.0 (CTCAE)* , Retrieved 10 22, 2014, from National Cancer Institute: http://ctep.cancer.gov/protocolDevelopment/electronic_applications/docs/ctcaev3.pdf

ISHIGURO, H., et al. "Degree of freezing does not affect efficacy of frozen gloves for prevention of docetaxel-induced nail toxicity in breast cancer patients" in: *Support Care Cancer* 2012 (20) nr. 9, pp. 2017-2024

JAYANTHY, A. K., SUJATHA, N., RAMASUBBA REDDY, M., "Measuring blood flow: techniques and applications – a review" in: *IJRRAS* 2011 (6) nr. 2, pp. 203 – 216

JIYUAN. T., YEOH G., LIU C. (2008), *Computational fluid dynamics: a practical approach*,. Amsterdam Butterworth-Heinemann

KANKERREGISTER, S. (SD), Retrieved op May 08, 2015, van Belgian Cancer Registry: http://www.kankerregister.be/

KRAMER K, SCHULZE W, "Die Kältedilatation der Hautgefäße". *Pflügers Arch* 1948 (250), pp. 141–170,

LEWIS, T., "Observations upon the reactions of the vessels of the human skin to cold" in: *Heart* 1930 (15), pp. 177- 208

LOSSIUS, K., ERIKSEN, M., WALLØE, L., "Fluctuations in blood flow to acral skin in humans: connection with heart rate and blood pressure variability" in: *J. Physiol*. 1993 (460), pp. 641–655

LÜFTNER, D. *et al.*, "Dose-intensified weekly paclitaxel induces multiple nail disorders" in: *Annals of Oncology* 1998 (9), pp. 1139-1140

LUIJKX T., 2013, *Phase contrast imaging*. retrieved 4 28, 2015, van Radiopaedia.org - a collaborative radiology resource: https://who.is/whois/radiopaedia.org

MCCARTHY, A. L., SHABAN, R. Z., GILLESPIE, K., VICK, J., "Cryotherapy for docetaxel-induced hand and nail toxicity: randomised control trial" in: *Support Care Cancer* 2014 (22) nr. 5, pp. 1375-1383

MINISINI, A. M. *et al.*, "Taxane-induced nail changes: incidence, clinical presentation and outcome" in: *Annals of Oncology* 2003 (14), pp. 333-337

MINUTILLI, E. *et al.,* "Paclitaxel-induced nail changes: possible role of its vehicle (Cremophor EL)" in: *Eur. J. Dermatol.* 2006 (16) nr. 6, pp. 693-694

NICOLAÏ, B., Biofluidics – Leuven, KULeuven, Division of Mechatronics, Biostatistics and Sensors (MeBioS), 2014

O'BRIEN, C., "Reproducibility of the cold-induced vasodilation response in the human finger" in: *J. Appl. Physiol.* 2005 (98) nr. 4, pp. 1334-1340

PANAGIOTAKOPOULOS, D., CUPITT, J.M., "Beau's lines", in: *Anaesthesia*, 2000 (55) nr.9, pp.936

PEDREGAL D.J., T. C. (2007). *System Identification, Time Series Analysis and Forecasting. The Captain Toolbox.* Lancaster: Centre for Research on Environmental Systems and Statistics (CRES), Lancaster University.

PIRACCINI, Bianca Maria, ALESSANDRINI, Aurora, "Drug-related nail diseases" in: *Clinics in Dermatology* 2013 (31) nr. 5, pp. 618-626

PIRACCINI, B.M., IORIZZO, M., STARACE, M., TOSTI, A., "Drug-induced Nail Diseases" in: *Dermatol Clin.* 2006 (24) nr. 3, pp. 387-391

PRIESTMAN, T., *Cancer Chemotherapy in Clinical Practice,* Springer, London, 2008 of Dordrecht, 2012

PRODUCTS, A., 2014,Retrieved op 12 5, 2014, van Elastogel: http://www.elastogel.com/

PUERS, R., *Biomedical Measurements and Stimulation,* Syllabus KULeuven, 2013

SAKURAI, M., et al., “Multi-center phase II study of a frozen glove to prevent docetaxel-induced onycholysis and cutaneous toxicity for the breast cancer patients” in: *J. of Cancer research* 2009 (69), pp. 1916-1930

SCOTTE, F., *et al*., “Multicenter study of a Frozen Glove to Prevent Docetaxel-Induced Onycholysis and Cutaneous Toxicity of the Hand” in: *Journal of Clinical Oncology* 2005 (23) nr. 19, pp. 4424–4429

SENDOWSKI, I., SAVOUREY, G., BESNARD, Y., BITTEL, J., “Cold induced vasodilatation and cardiovascular responses in humans during cold water immersion of various upper limb areas”, in: *Eur. J. Appl. Physiol.* 1997 (75), pp. 471–477

SMITH, J. (2007). *introduction to digital filters.* Stanford: Center for Computer Research in Music and Acoustics (CCRMA), Stanford University.

SPAZZAPAN, Simon *et al.*, “Nail Toxicity related to weekly Taxanes: An important issue requiring a change in Common Toxicity Criteria Grading?” in: *Journal of Clinical Oncology* 2002 nog onvolledig

STECKEL, J. *et al*., “A research Platform using Active Local Cooling directed at Minimizing the Blood Flow in Human Fingers” in: *Proceedings of the 7th International Conference on Pervasive Computing Technologies for Healthcare and Workshops* 2013, pp. 81 – 84

KISHNER, S. M. M., CONSUELO, T. L., 2013, *Brachial Plexus Anatomy* . Retrieved op 10 30, 2014, van Medscape: http://emedicine.medscape.com/article/1877731-overview

SWENSON, K., BELL, E.M., NISSEN, J., “Nail Toxicity Associated With Paclitaxel Treatment for Ovarian Cancer” in: *Oncology Nursing Forum* 2014 (40), pp. 17-19

TANAKA, M., “Experimental studies on human reaction to cold. Differences in the vascular hunting reaction to cold according to sex, season, and environmental temperature” in: *Bull. Tokyo Med. Dent. Univ*. 1971 (18), pp. 269–280

THE MATHWORKS, I. 2009, *ANOVA1*. Retrieved op April 2015, 5, van MathWorks: http://www.mathworks.com/help/stats/anova1.html#inputarg_y

THE MATHWORKS, I. 2009, *jbtest*. Retrieved op April 2015, 5, van MathWorks: http://www.mathworks.com/help/stats/jbtest.html

THE MATHWORKS, I. 2009, *multcompare*. Retrieved op April 2015, 5, van MathWorks: http://www.mathworks.com/help/stats/multcompare.html#inputarg_stats

THE MATHWORKS, I. 2009, *Multiple Comparisons*. Retrieved op April 2015, 5, van MathWorks: http://www.mathworks.com/help/stats/multiple-comparisons.html

THE MATHWORKS, I. 2009, *One-Way ANOVA*. Retrieved op April 2015, 5, van MathWorks: http://www.mathworks.com/help/stats/one-way-anova.html

THE MATHWORKS, I. 2009, *qqplot*. Retrieved op April 2015, 5, van MathWorks: http://www.mathworks.com/help/stats/qqplot.html

THE MATHWORKS, I. 2009, *ttest2*. Retrieved op April 2015, 5, van MathWorks: http://www.mathworks.com/help/stats/ttest2.html#btrkaaw

THE MATHWORKS, I. 2009, *One-Way ANOVA*. Retrieved op April 2015, 5, van MathWorks: http://www.mathworks.com/help/stats/one-way-anova.html

TOSTI, A., DANIEL, R., PIRACCINI, B. M., IORIZZO, M., *Color atlas of nails,* Springer, Berlin Heidelberg, 2010

UNIVERSITY OF MICHIGAN, I., 2014, *Introduction: Root Locus Controller Design*. Retrieved op 04 2015, 14, van Control tutorials for Matlab and Simulink: http://ctms.engin.umich.edu/CTMS/index.php?aux=Home

VERWEIJ, J., CLAVEL, M., CHEVALIER, B., "Paclitaxel (Taxol™) and Docetaxel (Taxotere™): Not simply two of a kind" in: *Annals of Oncology* 1994 (5) nr. 6, pp. 495-505

WASNER, G., et al., "Docetaxel-induced nail changes - a neurogenic mechanism: a case report" in: *J. Neurooncol.* 2002 (58) nr. 2, pp. 167-174

WEBSTER, J.G., *Medical Instrumentation – Application and Design*, John Wiley and Sons, 4th Rev. ed., 2009

WILDIERS, H., PARIDAENS, R., "Taxanes in elderly breast cancer patients" in: *Cancer Treat Rev.* 2004 (30) nr. 4, pp. 333-342

WINTHER, D., SAUNTE, D.M., KNAP, M., "Nail changes due to docetaxel - a neglected side effect and nuisance for the patient" in: *Supportive Care In Cancer*, 2007 (15), pp.1191-1197

Youssef A., Exadaktylos, V., Özcan S. E., Berckmans, S. (2011). *Proportional-Integral-Plus (PIP) Control System for Individual Thermal Zones in a Small Ventilated Space.* ASHRAE Transactions.

Zarandi, M. (2000). *Steady and pulsatile flow in curved vessels.* California: California Institute of Technology.

APPENDIX A – Graphs

Content

A1. Parameter graphs thumb and middle finger onycholysis device models
A2. Parameter graphs thumb frozen glove models
A3. Statistical comparison *a2*-parameters (index finger)

A1. Parameter graphs thumb and middle finger onycholysis device models

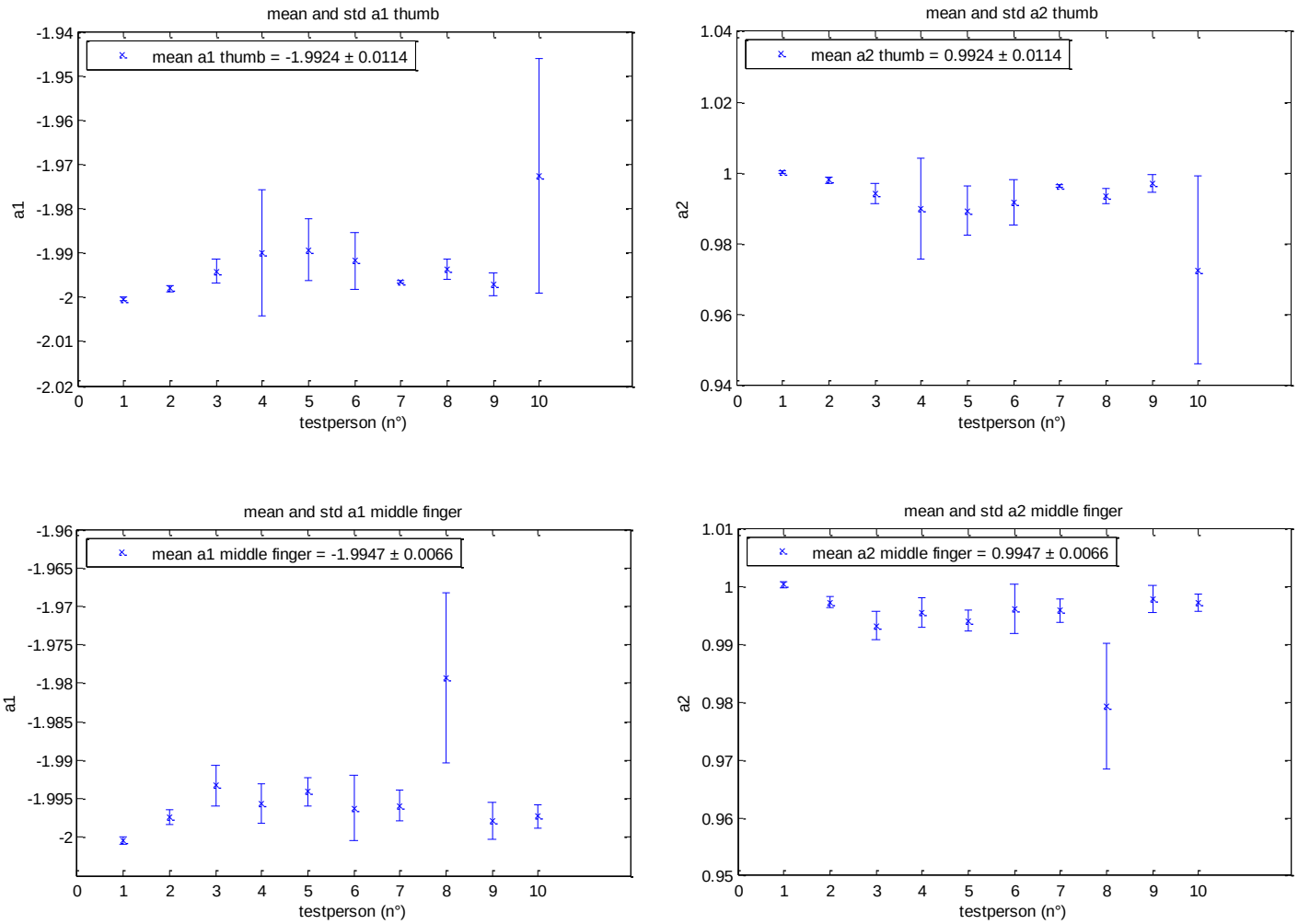

Figure A1.1: **top: the mean and standard deviation between the different experiments on the *a1*-model parameters (left) and the *a2*-model parameters (right) of the thumb. For both parameters, test person 10 shows a deviation from the other test persons bottom: the mean and standard deviation between the different experiments on the *a1*-model parameters (left) and the *a2*-model parameters (right) of the middle finger. For both parameters, test person 8 shows a deviation from the other test persons**

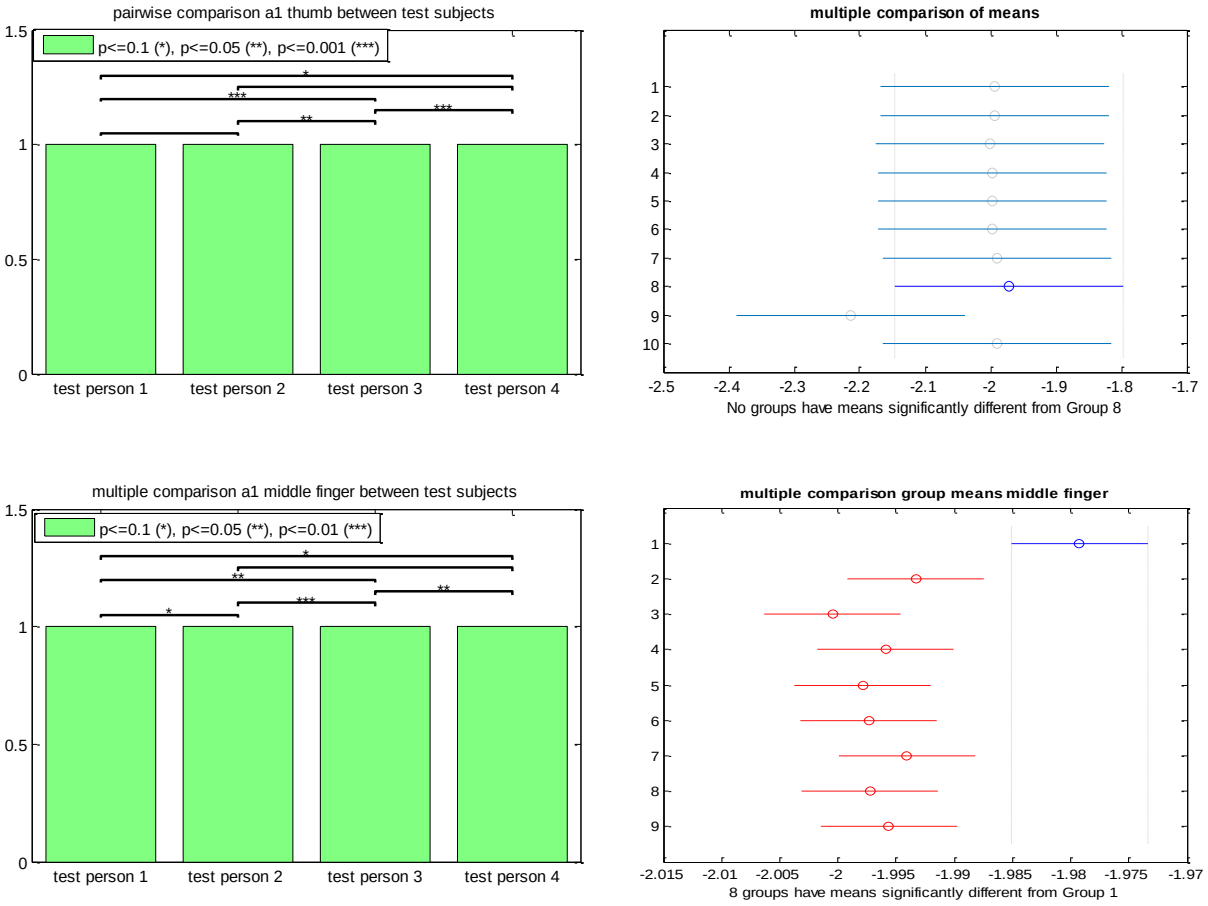

Figure A1.2: graphical representation p-values and significance levels between test persons 1, 2, 3 and 4. H_0 states that there are no significant differences between the *a1*-parameters of the test persons for the tested finger. H_0 is rejected for 4 cases on a 10% or lower significance level for the thumb (top left).
H_0 is rejected for 5 cases on a 10% significance level or lower for the middle finger (bottom left).
The graph right at the top represents the multiple comparison of the group means of *a1*-parameters of the thumb. No group means differ significantly from each other.
The graph right at the bottom represents the multiple comparison of the group means of *a1*-parameters of the middle finger. The mean of the *a1*-parameters differs significantly from the means of a1 from the other test persons.

A2. Parameter graphs thumb frozen glove models

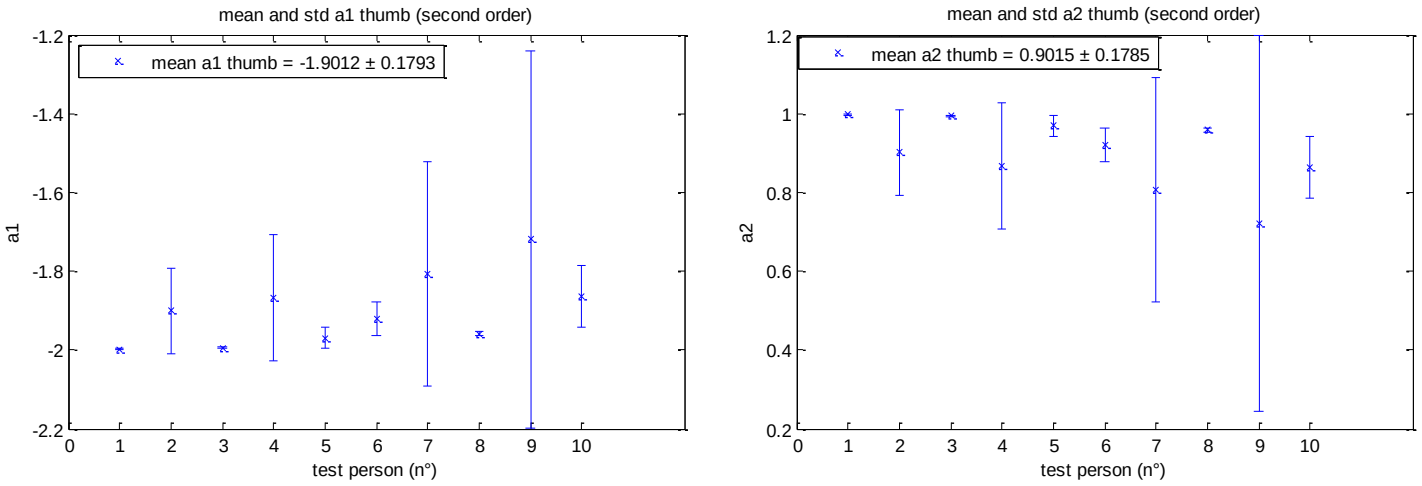

Figure A2.1: **the mean and standard deviation between the different experiments on the *a1*-model parameters (left) and the *a2*-model parameters (right) of the thumb. For both parameters, test persons 2, 4, 7 and 9 show a deviation from the other test persons**

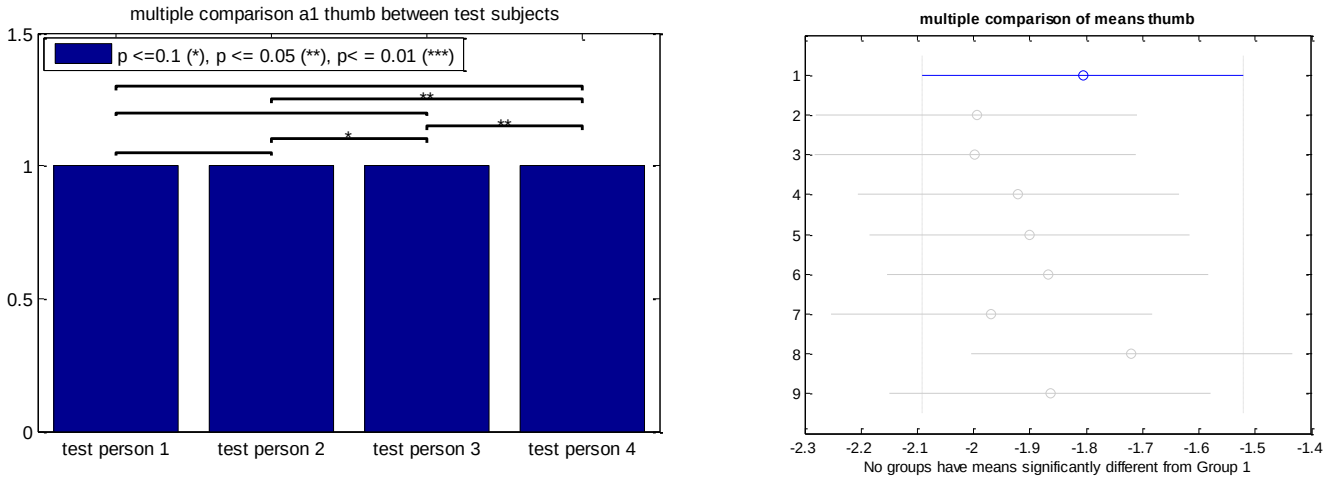

Figure A2.2: **graphical representation p-values and significance levels between test persons 1, 2, 3 and 4. H_0 states that there are no significant differences between the *a1*-parameters of the test persons for the tested finger. H_0 is rejected for 3 cases on a 10% or lower significance level for the thumb (left).**
Multiple comparison group means different test persons. No group means differ significantly from each other (right).

A3. Statistical comparison a2-parameters (index finger)

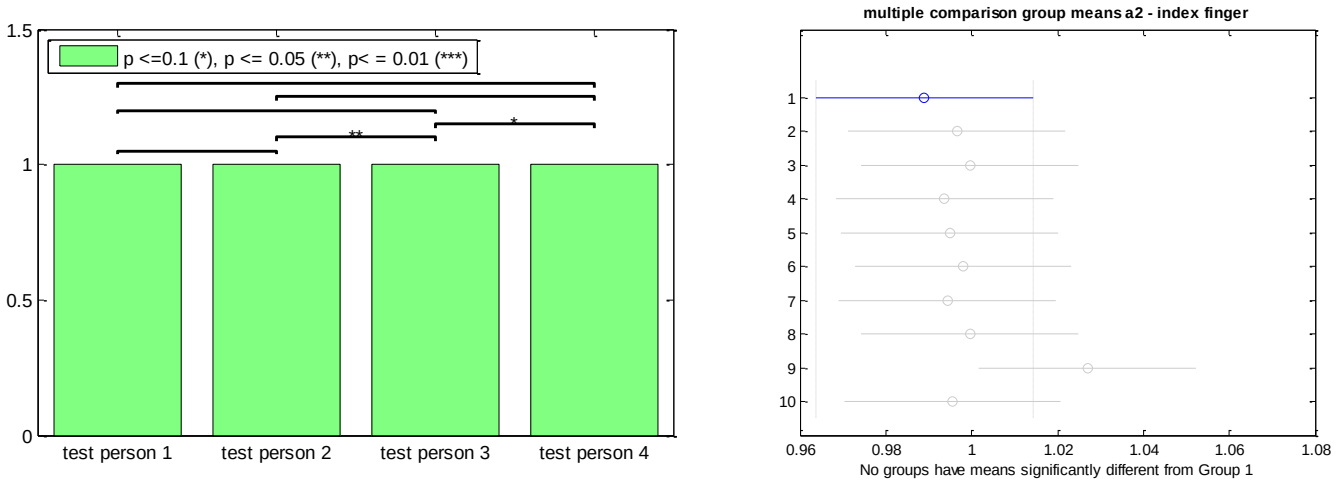

Figure A3.1: **left: graphical representation p-values and significance levels between test persons 1, 2, 3 and 4. H_0 states that there are no significant differences between the *a2*- onycholysis device parameters of the test persons for the tested finger. H_0 is rejected for 2 cases on a 10% or lower significance level for the index finger.**
right: Multiple comparison group means of the index finger for the different test persons. No group means differ significantly from each other.

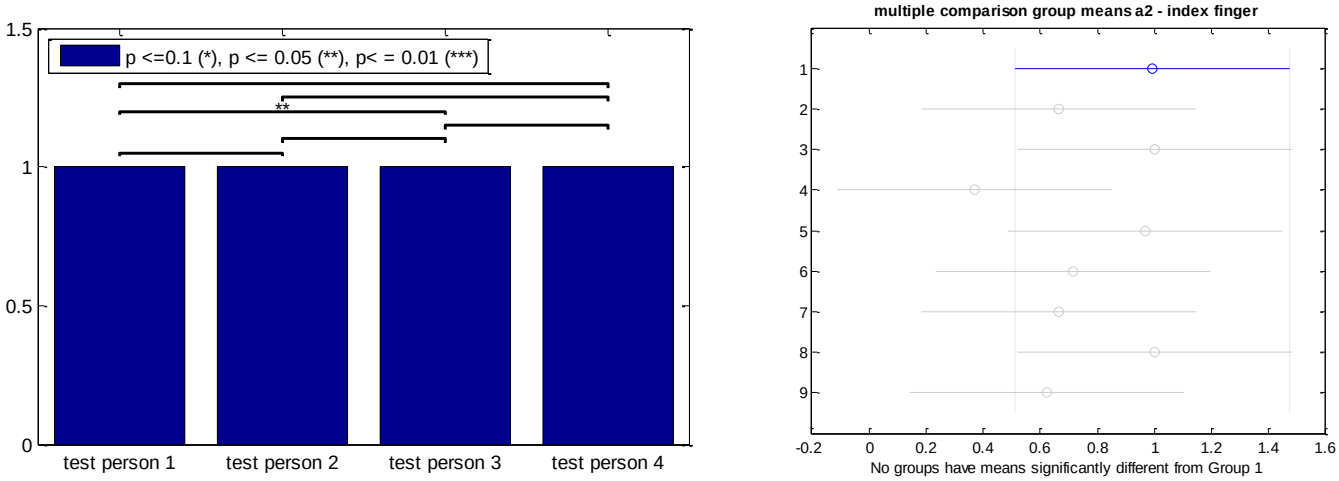

Figure A3.2: **left: graphical representation p-values and significance levels between test persons 1, 2, 3 and 4. H_0 states that there are no significant differences between the *a2*- frozen glove parameters of the test persons for the tested finger. H_0 is rejected for 1 case on a 10% or lower significance level for the index finger.**
right: Multiple comparison group means of the index finger for the different test persons. No group means differ significantly from each other.

Popularised Summary

Worldwide, many people are coping with cancer. In 2012, there were more than 14 million new cases. In Belgium, about one third of men and one quarter of women are affected by cancer before their 75th birthday.

Many patients are treated with chemotherapy to kill the cancer cells, but these drugs also have some adverse side effects. Besides the known side effects like nausea and vomiting, tiredness, hair loss, … also nail toxicity has been reported frequently. This includes changes in nail color, brittleness, and even loss of nails, which can be very painful.

To prevent this nail toxicity, patients have to wear frozen gloves and socks, or have to put their hands and feet in an ice bath. This is very uncomfortable and many patients cannot withstand these extreme cold temperatures. By cooling the fingers (and toes), the aim is to limit the blood flow to the nail bed, and thus limiting the amount of drugs reaching the nail bed.

The aim of this work is to develop another way of cooling the fingers (and toes) which is more comfortable and less painful for the patients. Together with the University of Antwerp, where new equipment has been developed to cool the fingers locally (instead of the whole hand), we tried to define the optimal cooling temperatures and demonstrated that controlled local cooling will be helpful to reduce nail toxicity with as little as possible cold induced burden for the patients.